Universidade do Minho
Escola de Engenharia

Eugénia Cristina Queirós Teixeira

Bacterial cellulose modifications for biomedical applications

October 2022

Bacterial cellulose modifications for biomedical applications
Eugénia Cristina Queirós Teixeira
UMinho | 2022

Universidade do Minho
Escola de Engenharia

Eugénia Cristina Queirós Teixeira

Bacterial cellulose modifications for biomedical applications

Doctoral Thesis
Doctorate in Biomedical Engineering

Work developed under the supervision of
Doctor Francisco Miguel Portela da Gama
and
Doctor Pier Parpot

October 2022

ACKNOWLEDGEMENTS

After this long journey I would like to express my deepest gratitude to all the people who helped me during this work and make this thesis possible. I will start acknowledging my supervisors, Professor Miguel Gama and Prof. Pier Parpot for their help, support, patience and for being so understanding with me. A special thank to Prof. Miguel Gama for giving me the opportunity to develop this research project and, mainly, for never give up on me and encouraging me to keep going.

To the University of Minho, particularly, to Centre of Biological Engineering and all the people that work there and were always available to helping me; a special thank to Joana Azevedo, Patrícia Dias and Carla Magalhães for their essential help on bioreactors. To all the people from LTEB lab for their partnership and continuous availability to listen, to help and to encourage me. All of you were crucial to finish this chapter, particularly, Ana Cristina Rodrigues, Fernando Dourado and also Sara Pinheiro; although she no longer belongs to LTEB group, her contribution was extremely important to part of this work. I also want to thank to Centre of Chemistry and to the excellent people that I met there: Marta Ferreira, Pedro Rocha, Daniela Carvalhal, Vânia Sousa, Luís Lema, Professor Isabel Neves: all of you are a good example to the good people that I met and, in some cases, I had the privilege to work with!

To "my people" at UTAD: my "scientific father" Professor Pedro Tavares who started as my supervisor and stay in my life as my friend! Mariana Fernandes and Lisete Ferrnandes my friends and scientific advisors: thank you both for always supporting me! From UTAD, I cannot forget Professor José Ramiro which is always available for me and also the new good people that this work allowed me to meet: Professor Jose Eduardo Pereira, Professor Justina Prada and Professor Isabel Pires: all of you were an essential support on *in vivo* trials.

I really want to acknowledge all my friends and family for all the support that they gave me in all moments of my life. A special thanks to my "sisters" Sofia Sousa and Cláudia Cardoso which are always there for me and who never let me gave up. To my parents and my brother for being the pillar of my life. Finally, to Nuno which is, simultaneously, my best friend, my husband, my inspiration and my strength. Without your love and support this thesis would never occur. You are the best gift that life has ever gave me. Lastly, I gratefuly acknowledge Fundação Portuguesa para Ciência e Tecnologia (FCT) for the PhD scholarship ref.: PhD Program in Biomedical Engineering'' (ref: NORTE- 08-5369-FSE-000012 opens 4 PhD scholarship position with the financial support of ESF – European Social Fund, under Programa Operacional Regional do Norte - Norte2020.

STATEMENT OF INTEGRITY

I hereby declare having conducted this academic work with integrity. I confirm that I have not used plagiarism or any form of undue use of information or falsification of results along the process leading to its elaboration.

I further declare that I have fully acknowledged the Code of Ethical Conduct of the University of Minho.

BACTERIAL CELLULOSE MODIFICATIONS FOR BIOMEDICAL APPLICATIONS

ABSTRACT

The main goal of this doctoral project is to explore the huge potential of bacterial cellulose (BC) in distinct areas, with particular focus on biomedical field. Specifically, i) the impact of different strains, fermentation time and fermentation medium on the BC properties was assessed; ii) the potential of oxidized BC as a wound dressing was analyzed; iii) exploratory studies on the use of laser technology for the surface patterning of BC were developed.

With regards to the study on the influence of different culture conditions on BC's properties, two strains (ATCC 53582 and ATCC700718), two distinct culture media (HS and MOL medium) and different bioreactors (static and agitated) were used. The time of culture was different in the static (6,15 and 30 days) and agitated (8 days) fermenters. The obtained results allowed to conclude that only slight differences (with no statistical relevance) between static and agitated conditions were observed in what concerns to BC properties. Then, and intending to explore the applicability of BC on biomedical field, BC membranes with hemostatic activity were produced through electrochemical oxidation. After oxidation using tetramethylpiperidine-1-oxyl (TEMPO) radical, the samples were characterized through several techniques. The oxidation degree was evaluated by titration and the obtained values revealed that increased from 4% to 7% and up to 15%, corresponding to an applied charge of 400, 700 and 1200 Coulombs, respectively. *In vitro* and *in vivo* biodegradability of oxidized BC membranes were evaluated and compared with that of Surgicel®, a commercially used hemostatic dressing. The oxidized BC preserved the crystallinity and the 3D nano-fibrillar network, and demonstrated hemostatic activity, although not as effective as that of Surgicel®. *In vivo* assays demonstrated that the oxidized membranes did not induce an inflammatory response, revealing a good biocompatibility. Finally, the surface pattern of BC was achieved through direct design of the laser patterns on wet BC surface. The interaction of the texturized surfaces with fibroblasts (L929) was assessed. The obtained results using XPS and FTIR techniques showed that the use of laser did not chemically modify the BC surface. The biocompatibility of both pristine and modified BC membranes was evaluated using mouse skin fibroblasts cells. SEM results showed that fibroblasts were present in both BC membranes surfaces exhibiting its usual phenotype, and significant differences between both groups in terms of metabolic activity were not detected. These results showed the good biocompatibility of both pristine and modified BC membranes, further work being necessary to exploit the potential of this methodology.

Keywords - Bacterial cellulose; biomedical applications; fermentation; hemostatic materials; surface patterning

MODIFICAÇÕES NA CELULOSE BACTERIANA PARA APLICAÇÕES BIOMÉDICAS

RESUMO

Este projeto de doutoramento pretende explorar o enorme potencial da celulose bacteriana (CB) em variadas áreas, dando particular enfoque à área biomédica. Especificamente, i) foi analisado o impacto de diferentes estirpes, tempo de fermentação e meio de fermentação nas propriedades da CB; ii) foi analisado o potencial da CB oxidada no tratamento de feridas; iii) foram realizados estudos exploratórios com tecnologia laser para a padronização de superfícies de CB.

Relativamente ao estudo da influência de diferentes condições de fermentação nas propriedades da CB, foram testadas duas estirpes (ATCC 53582 e ATCC700718), dois meios de cultura distintos (HS e MOL) e bioreatores (cultura estática e agitada). O tempo de cultura também foi distinto, na cultura estática (6,15 e 30 dias) e agitada (8 dias). Os resultados obtidos permitiram concluir que houve apenas pequenas diferenças (sem relevância estatística) entre a cultura estática e agitadas em termos de propriedades de CB. Seguidamente, e com o objetivo de explorar a aplicabilidade da CB na área biomédica, foram produzidas membranas de CB com atividade hemostática por oxidação eletroquímica. A oxidação foi realizada usando o radical tetrametilpiperidina-1-oxil (TEMPO). O grau de oxidação foi avaliado por titulação, tendo-se obtido valores de 4% para 7% e 15%, correspondendo a uma carga aplicada de 400, 700 e 1200 Coulombs, respetivamente. A biodegradabilidade *in vitro* e *in vivo* das membranas de CB oxidadas foi avaliada e comparada com o Surgicel®, uma compressa comercial usada no tratamento de feridas. A CB oxidada preservou sua a cristalinidade e estrutura nanofibrilar, demonstrando atividade hemostática, embora não tão eficaz quanto o Surgicel®. Os ensaios *in vivo* demonstraram que as membranas oxidadas não induzem resposta inflamatória, revelando boa biocompatibilidade.Finalmente, a modificação da superfície da membrana de CB foi efetuada através da padronização com laser. Os resultados obtidos pelas técnicas de XPS e FTIR mostraram que a utilização do laser não modificou quimicamente a superfície da CB. A biocompatibilidade das membranas de CB foi avaliada usando fibroblastos (L929). Os resultados da microscopia eletrónica de varrimento mostraram que os fibroblastos aderiram em ambas as superfícies exibindo o fenótipo característico, não sendo detetadas diferenças significativas entre os dois grupos em termos de atividade metabólica. Estes resultados mostraram a boa biocompatibilidade das membranas de CB com e sem padronização, sendo necessários estudos adicionais para explorar o potencial desta tecnologia.

Palavras chave - Celulose bacteriana; aplicações biomédicas; fermentação; materiais hemostáticos; padronização da superfície.

LIST OF CONTENTS

LIST OF FIGURES

LIST OF TABLES

LIST OF ABBREVIATIONS

ATR-FTIR – Attenuated Total Reflectance - Fourier Transform Infrared Spectroscopy

BAI – Biomedical-associated infections

BC – Bacterial Cellulose

BCL – Bacterial Cellulose laser

CrI – Crystallinity Index

CSL –Corn Steep Liquor

CV – Cyclic Voltammetry

DDS – Drug Delivey System

DP – Degree of Polymerization

EPS – Extracellular Polymeric Substances

FBGC – Foreign Body Giant Cells

FBR – Foreign Body Reaction/Response

H&E – Hemotoxylin and Eosin stain

HAs – Hemostatic Agents

HS – Hestrin and Schramm medium

HST – Hyperthophic Scar Tissue

IL – Interleukin

K. xylinus – *Komagataeibacter xylinus*

LTS – Laser Texturing Surface

MCP-1 – Monocyte Chemotactic Protein-1

MIP – Macrophage Inflammatory Protein

NMR – Nuclear Magnetic Resonance Spectroscopy

PBS – Phosphate Buffer Saline

PDMS – Polydimethylsiloxane

rcf – Relative Centrifugal Field

RGD – Arginine-Glycine-Aspartic acid

RGDS – Arginine-Glycine-Aspartic acid-Serine

ROS – Reactive Oxygen Species

SEM – Scanning Electron Microscope

TE – Tissue Engineering

TEM – Transmission Electron Microscopy

TEMPO – 2,2,6,6-Tetramethylpiperidine-1-oxyl radical

TGF – Transforming Growth Factor

vvm – volume of air per volume of reactor per minute

XPS – X-ray Photoelectron Spectroscopy

XRD –X-ray Diffraction

Remarks:

In general, the International System of Units (SI) was used in this work. Sometimes multiples and sub-multiples of the SI units were also used, as well as other non-SI units but allowed by SI, such as the use of liter to express volume. Some units not recognized by the SI were also used to express some variables, such as the volume percent (% v/v), and mass per volume percent (% m/v) to denote the composition of some solutions, the revolutions per minute (rpm) to indicate the agitation rates and the volume of air per volume of reactor per minute (vvm) to designate the aeration rates, due to the usual use in fermentation technology area.

Chapter 1

Introduction

In this first chapter, the context and motivation that supported this thesis are explained; the objectives of the work are delineated, and the content of this manuscript is outlined for the reader. Finally, the scientific dissemination outcomes of the performed work (research papers and communications in science meetings) are reported.

1.1 - Context and Motivation

Given its superior technical properties, bacterial cellulose (BC) has a broad range of applications, such as in the food and cosmetic industries. Beyond this, and with particular interest to this work, the application of BC on biomedical field is also possible and widely explored.

BC represents an alternative source of cellulose with good mechanical properties, high crystallinity, high degree of polymerization and high-water content. It is also biocompatible, hydrophilic and non-toxic, exhibiting high purity, since unlike plant cellulose it does not have any hemicelluloses, pectin and lignin (1–3). BC can be produced under static and agitated conditions. Depending on the culture method, the resulting macroscopic morphology, microstructure, and properties are different. Having this in consideration, the choice of the fermentative technique is related with the final application of BC. Comparing both methods, static culture is the most used process, due to its simplicity. Since the BC is produced at the air-medium interface, one of the main challenge on a bioreactor design is to ensure a higher air-medium surface (4,5). However, this fermentation technique is characterized by the high cost, low rate of production and some issues are described related to delivery of oxygen, being the reason why agitated fermentation has been proposed. With agitated fermentation it could be possible to produce BC with different features. Instead of a one-piece membrane obtained in static conditions, pellets or irregular masses and fibrous suspensions are obtained with different sizes that could vary from 10 μm to 10 nm in diameter, bearing several shapes, from spherical or ellipsoidal, to stellate. These new features are consequence of the rotation speed, culture time and the additives used in the culture medium (6). The appearance of agitated culture intended to overcome the issue related to the delivery of oxygen by increasing the oxygen transfer. However, this increase on oxygen transfer generates non-cellulose producing mutants that are often related with lower levels of BC production, limiting its up-scaling. Nevertheless, some bioreactor cultures seem to be able to produce high levels of BC. However, this implies higher operational complexity. Therefore, the simpler static culture has been frequently used to obtain BC despite the long cultivation time required.

As previously mentioned, the fermentation method affects the resulting BC properties. Thus, it seems crucial to study that influence through the evaluation of different parameters, such as: distinct bacterial strains, different times of culture and, of course, different fermentation methods.

BC and other natural polymers are extensively applied in biomedical field due to their special properties. In this field, BC has been explored for wound healing applications and also for tissue

engineering and drug delivery. Taking this into account, in this doctoral project two distinct applications on biomedical field are envisaged. The first one is related with the possible application of BC as a hemostatic dressing.

Hemostasis is the first stage of wound healing process. It is ascribed to the ability of the body to control the flow of blood when a vascular injury occurs. Thus, hemostasis includes the production of blood clot and its consequent dissolution followed by the repair of the injured tissue. It has a complex interplay of four key elements: the vascular endothelium, platelets, the coagulation pathway and fibrinolysis (7). Different hemostatic approaches may be applied according to the type of injury. Surgicel®, made by Ethicon Inc. of Johnson & Johnson, is a bio-absorbable material widely applied for intraoperative hemostasis and prevent adhesion in surgery. This material act as a mesh for platelet adhesion and aggregation, helping the formation of an artificial clot, while its negative charge is likely to activate the secondary hemostasis as well (8,9). Nevertheless, some issues were reported associated with the use of Surgicel®. One example of these issues is the case in which a patient was diagnosed with intracranial hemorrhage (10). Aiming to overcome the reported Surgicel® issues, in this work the production of a new hemostatic material based on BC is aimed, using electrochemical methods. It is also hypothesized that surface oxidation may lead to a substantial improvement of the BC biodegradability.

Finally, the surface modification of the BC topography, as a means to improve its biocompatibility as an implantable biomaterial, will be tested. When implanted in the human body, biomaterials contact with surrounding tissues and induce a host response. The nature of this reaction determines the biocompatibility of the biomaterial. The human immune system is composed by the innate and adaptive systems that plays an important role in reacting against any foreign materials. Indeed, the implantation of any biomaterial may trigger a reaction of the immune system called Foreign Body Reaction/Response (FBR) that induce the formation of a capsule of dense fibrous tissue surrounding the implant, which eventually cause its loss of functionality. Thus, host reactions will determine the success of integration and biological performance of the biomaterial (11,12). Related with FBR, the biomaterial-associated infections (BAI) is another critical issue to address when a biomaterial is implanted. BAI take advantage on the presence of a substrate for opportunistic pathogen colonization, which culminates into an inflammatory response. In fact, the combination between FBR and bacteria creates a dysregulated immune niche more susceptible to bacterial adhesion and infection (13). Thus, it is essential the development of new approaches targeting BAI in order to avoid the possible biomaterial failure. Considering this, the modification of the biomaterial surface could contribute to solve this problem since

after implantation, biomaterial surface is the stage where interactions between the material and cells occurs. Hence, topographical features at micro and nanometer scales offer a promising new methodology to control cell-surface interactions. One example of this new methodology is the laser surface texturing which is based on the direct treatment of a surface using a laser beam. It is characterized by its high reproducibility, and it can be performed through the production of a regular or irregular patterns of bumps, dimples, and (linear or non-linear) grooves. Furthermore, it modifies the surface roughness and chemistry in several materials without using toxic substances. Also, it is a high processing-speed methodology with a low risk of surface contamination due to the absence of direct contact during the process (14). Thus, in this work, it is also aimed to pattern wet BC membranes using a CO_2 laser and evaluate the influence of this treatment not only on BC properties but also on fibroblasts (L929) adhesion. With this technique, here developed only at exploratory level, it is expected to overcome the above issues related with biomaterial implantation.

1.2 - OBJECTIVES

The work developed in this doctoral project and presented in this manuscript aims not only to increase the existing knowledge related with BC but also to develop new and improved applications for BC, especially on biomedical field.

The main objectives of this work are the following:

- Understand the influence of fermentation conditions on BC properties in order to envision new applications for this material, with special focus on biomedical field. To achieve that different parameters will be tested: distinct strains, different times of culture and the influence of static and agitated fermentation;
- In order to overcome some critical issues reported regarded to the use of Surgicel®, this work aim at producing BC membranes with hemostatic activity. For that, we carried out the electrochemical oxidation of BC membranes with the tetramethylpiperidine-1-oxyl (TEMPO) radical;
- Finally, an exploratory study was performed intending to improve the interaction of BC with biological tissues through surface laser patterning.

In this perspective, this project aims at presenting the ground basis for the development of innovative bacterial cellulose products with excellent technological properties that meet emerging needs.

1.3 - THESIS OUTLINE

This thesis is divided into 6 main chapters, in which **chapter 4** was published as research paper in a scientific journal.

Chapter 2 *- Literature Review*, is a scientific state-of-the-art review on the subject of the present thesis. The main BC properties that make it an astonishing material to be applied in different fields are discussed.

Chapter 3 *– The influence of different fermentation conditions on bacterial cellulose properties.* reports the effect of using different bacterial stains, different fermentation methods, different culture media and times of culture on the BC properties.

Chapter 4 *– Hemostatic oxidized bacterial cellulose membranes:* present the new properties acquired by BC after oxidation through electrochemical methods.

Chapter 5 *– Laser patterning of bacterial cellulose membranes surface and its influence on cell adhesion:* a preliminary study on BC surface modification through laser pattering and its influence on fibroblasts adhesion.

Chapter 6 *– Conclusions and future work*, a final overview of the thesis is performed, highlighting the main findings and conclusions, and adding some suggestions for the future work with BC modifications, especially for biomedical applications.

1.4 - DISSEMINATION AND COMMUNICATIONS

The experimental work exhibited in this thesis was partially published in international journals, as well as communications in national and international science meetings. The scientific output originated from this work is listed below.

Publications in peer-reviewed journals

- Queirós, E.C., Pinheiro, S. P., Pereira, J. E., Prada, J., Pires, I., Dourado, F., Parpot, P., Gama, M., (2021). Hemostatic dressings made of oxidized bacterial nanocellulose membranes. Polysaccharides. 2(1), 80-99. https://doi.org/10.3390/polysaccharides2010006.
- Queirós, E.C., Rodrigues A.C., Dourado, F., Gama, M., (2021). Effect of culturing conditions on the properties of the bacterial nanocellulose. In preparation.

Conference Poster

- E. C. Queirós., S. P. Pinheiro., J. E. Pereira., J. Prada., I. Pires., P. Parpot., M. Gama (2019) " Synthesis and characterization of oxidized bacterial cellulose through electrochemical methods: its biodegradability and potential as hemostatic material", 4th International Symposium on Bacterial Nanocellulose, Porto - Portugal, October, 2019.
- E. C. Queirós., S. P. Pinheiro., J. E. Pereira., J. Prada., I. Pires., P. Parpot., M. Gama (2019) " Synthesis and characterization of oxidized bacterial cellulose through electrochemical methods: its biodegradability and potential as hemostatic material",30th Annual Conference of the European Society for Biomaterials together with the 26th Annual Conference of the German Society for Biomaterials, Dresden - Germany, September, 2019.
- E. C. Queirós., S. P. Pinheiro., P. Parpot., M. Gama (2018) "The potential of bacterial cellulose as hemostatic material", CHEMPOR2018, Aveiro - Portugal, October, 2018.
- S. P. Pinheiro., E. C. Queirós., V. Carvalho., Gama, M., P. Parpot. (2017) "Development of hemostatic materials made of electrochemically oxidized bacterial cellulose", CEB Annual Meeting, Braga - Portugal, July, 2017.

1.5 - REFERENCES

1. Eslahi N, Mahmoodi A, Mahmoudi N, Zandi N, Simchi A. Processing and Properties of Nanofibrous Bacterial Cellulose-Containing Polymer Composites: A Review of Recent Advances for Biomedical Applications. 2019;60(1):144–70.
2. Gorgieva S, Trček J. Bacterial Cellulose: Production, Modification and Perspectives in Biomedical Applications. Nanomaterials. 2019;9(10).
3. R P, CR L, PL A, RG S. Bacterial cellulose: a versatile biopolymer for wound dressing applications. Microb Biotechnol. 2019;12(4):586–610.
4. Chawla PR, Bajaj IB, Survase SA, Singhal RS. Microbial cellulose: Fermentative production and applications. Food Technol Biotechnol. 2009;47(2):107–24.
5. Parte FGB, Santoso SP, Chou C-C, Verma V, Wang H-T, Ismadji S, et al. Current progress on the production, modification, and applications of bacterial cellulose. 2020;40(3):397–414.
6. Wang J, Tavakoli J, Tang Y. Bacterial cellulose production, properties and applications with

different culture methods – A review. Carbohydr Polym. 2019;219:63–76.

7. JM S, J A, H D. The hemostatic system. Curr Med Chem. 2004;11(17):2245–60.

8. C A, GH A, T O. Tissue reaction to three subcutaneously implanted local hemostatic agents. Br J Oral Maxillofac Surg. 1997;35(2):129–32.

9. Wang H, Chen P. Surgicel® (oxidized regenerated cellulose) granuloma mimicking local recurrent gastrointestinal stromal tumor: A case report. Oncol Lett. 2013;5(5):1497–500.

10. B L, H Y, M C, Y L, J Y. Surgicel application in intracranial hemorrhage surgery contributed to giant-cell granuloma in a patient with hypertension: case report and review of the literature. World J Surg Onco. 2014;12(1).

11. R K, F J. The pathology of the foreign body reaction against biomaterials. J Biomed Mater Res A . 2017;105(3):927–40.

12. Jewell CM, Collier JH. Biomaterial interactions with the immune system. Biomater Sci. 2019;7(3):713–4.

13. S Z, C B, M R. Host tissue as a niche for biomaterial-associated infection. Future Microbiol. 2010;5(8):1149–51.

14. Riveiro A, Maçon ALB, del Val J, Comesaña R, Pou J. Laser Surface Texturing of Polymers for Biomedical Applications. Front Phys. 2018:16.

Chapter 2

Literature Review

This chapter provides a brief overview about the most relevant aspects related with bacterial cellulose properties and its broad applicability in different fields. Also, the evidences associated to BC biosynthesis/production and its possible chemical modification that increase and improve BC's features to be applied mainly on biomedical field will be present.

2.1 – BACTERIAL CELLULOSE: BIOSYNTHESIS AND PROPERTIES

Cellulose is essentially synthesized by plants, but it can be also synthesized by bacteria, algae and fungi. Cellulose is present in cotton, wood, hemp, and other plant-based materials and it is almost an unlimited organic polymer resource on earth. However, bacterial cellulose (BC) arises as an alternative source with great potential for some specific applications, given its superior technical properties. In particular, the high purity (it does not has lignin and hemicelluloses) and ability to absorb a very high amount of water makes it an exceptional source of cellulose (1,2).

BC can be produced by different types of organisms, including several bacterial gender: *Aerobacter, Acetobacter, Achromobacter, Agrobacterium, Alcaligenes, Azotobacter, Pseudomonas, Rhizobium, Sarcina,* and *Zoogloea* (3). All of them are able to produce BC with different structures and biological roles (table 2.1) (4) *Komagataeibacter xylinus* species, (5) formerly known as *Glucanoacetobacter xylinus*, being the most efficient producer.

Table 2.1. Bacterial sources of BC with distinct structures and biological roles (4).

	Gender	Biological role
Fibril structure	*Aerobacter*	Flocculation in wastewater
	Agrobacterium	Attachment to plants
	Alcaligenes	Flocculation in wastewater
	A.hansenii	Maintenance in aerobic environment
	Rhizobium	Attachment to plants
Ribbon structure	*Acetobacter*	Maintenance of aerobic environment
	Achromobacter	Flocculation in wastewater
3D network nanofiber	*Glucanoacetobacter*	Maintenance of aerobic environment
Amourphous/not defined	*Pseudomonas*	Flocculation in wastewater
	Sarcina	Not defined

Zoogloea	Not defined

The cultivation method and the used bioreactor will determine the production of different shapes, such as membranes, hollow tubes, pellets or thin fibrous materials. *Komagataeibacter* is a Gram-negative, acetic acid and strictly aerobic bacteria which exhibits rod-shape, and lives mainly in fruits and vegetables in decomposition. They are able to use carbon sources such as glucose, glycerol, sucrose, fructose, mannitol among others, at temperatures and pH in the range 25-30^{o}C and 3-7 pH, respectively, but exhibiting distinct properties and yields (6). In static culture, the bacteria produces BC as extracellular pellicles that has a nanofibrillar structure, one side displaying a denser surface, while the other exhibits a gelatinous layer (7,8). Furthermore, the bacteria produce cellulose as a film at the liquid-air interface, which allows it to remain close to the oxygen supply. The cellulose film also acts as a physical barrier protecting the bacteria against UV radiation, keeping an hygroscopic and moisturized environment (6). BC can also be produced in stirred tanks. However, this type of cultivation method results in lower volumetric BC productivity and yield than static conditions, in addition to raising operational issues. Moreover, higher rotation speed lead to a lower BC production (9).

The synthesis of BC is a complex process that involves different catalytic and regulatory proteins. It is an aerobic process that is directly connected with cellular catabolism. Nevertheless, the process does not affect other anabolic processes like protein synthesis (10). BC synthesis begins with the isomerization of a glucose 6-phosphate molecule into glucose 1-phosphate, which is an intermediary that reacts with UTP producing uridine-di-phosphoglucose (UDP-glucose), a precursor for BC synthesis. After that, the bacteria polymerize glucose residues into linear (1,4) D-glucan chains in a reaction catalyzed by cellulose synthase A (which is activated by cyclic-di-GMP) (Fig. 2.1). The obtained chains are excreted across the cell wall through extrusion pores forming a ribbon-like structure composed of hundreds and thousands of individual chains, producing an ultra-thin 3D network of interconnected nanofibers (11,12).

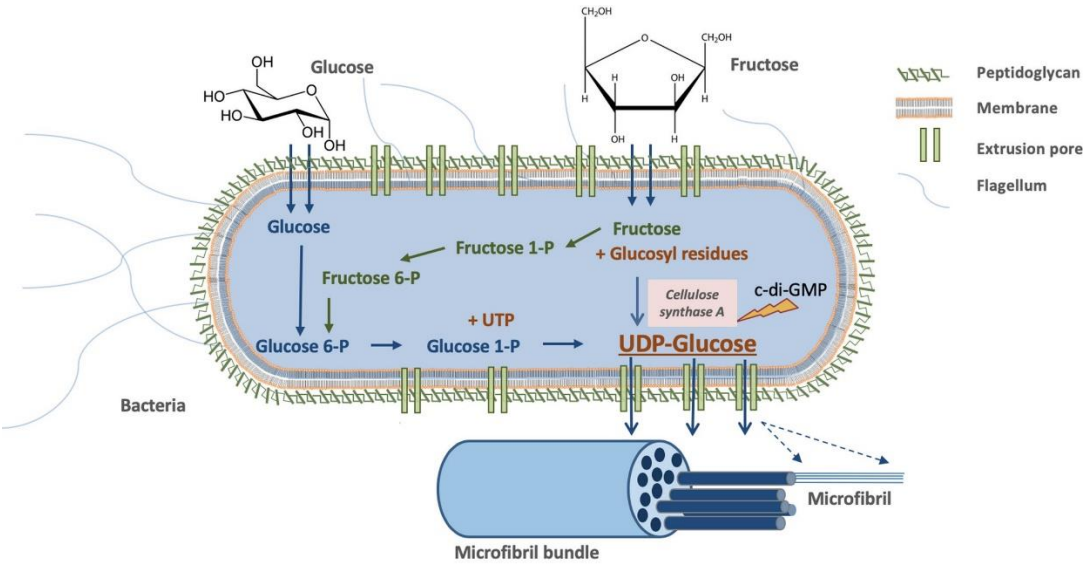

Figure 2.1. Schematic representation of the BC biosynthesis [Adapted from (12)].

The produced nano-fibrils (1.5 nm width) bind each other creating the cellulosic nanoribbons, parallel to the bacterium cells longitudinal axis (40 to 70 nm width) (13). Thus, BC is a high molecular weight homopolymer with glucopyranose units connected by (1,4)-glycosidic links (14) (Fig. 2.2), bearing primary and secondary alcohol functions and an acetal group. The center of this acetal group is occupied by the C1 carbon, the anomeric carbon. The cellulose chain has a pendant hydroxyl group on one side and an hemiacetal group on the other. Thus, β-D-glucopyranose rings displays a chair conformation where the hydroxyl groups are positioned in equatorial position which is essential to allow intramolecular H-bonding between two successive rings, *i.e.*, from O(3´)-H hydroxyl to the O(5) ring oxygen and from O(2)-H hydroxyl to the O(6´) hydroxyl (3).

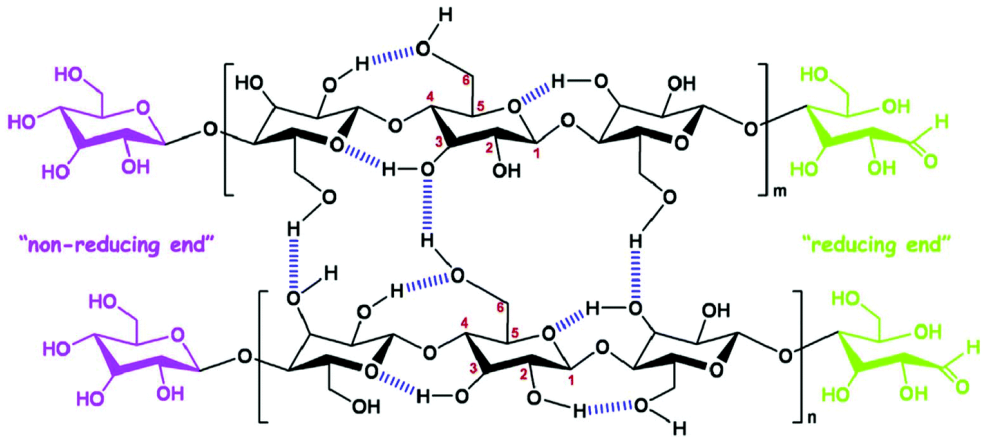

Figure 2.2. Schematic illustration of the chemical structure of BC and its intra and inter molecular hydrogen bonds [Adapted from (14)].

Hydroxyls groups present in cellulose are equatorially positioned, which allows new connections with adjacent chains, producing one structure stabilized with hydrogen bonds. These hydrogen bonds yield a rigid crystalline structure with hydrophilic surface, but a hydrophobic core, which creates insoluble cellulose. The size of the cellulose molecule is determined by the degree of polymerization (DP) which refers the number of glucose units present in a chain (15).

Native cellulose presents not only good mechanical stability but also high crystallinity (up to 90%), where the crystal is made up from meta-stable cellulose I. In fact, there are different polymorphs of crystalline cellulose (I, II, III, IV), each one being defined by its unit cell parameters. Cellulose I, also named "natural" cellulose, is the crystalline cellulose produced by several organisms like plants, algae and bacteria, among others. Cellulose I contain two coexisting phases: a triclinic structure (Iα) and a monoclinic one (Iβ) (16) (Fig. 2.3), present in distinct proportions, depending on its origin. The first one is the major polymorph for most algae and bacteria, while the second one is dominant for higher plant cell wall cellulose and in tunicates (17).

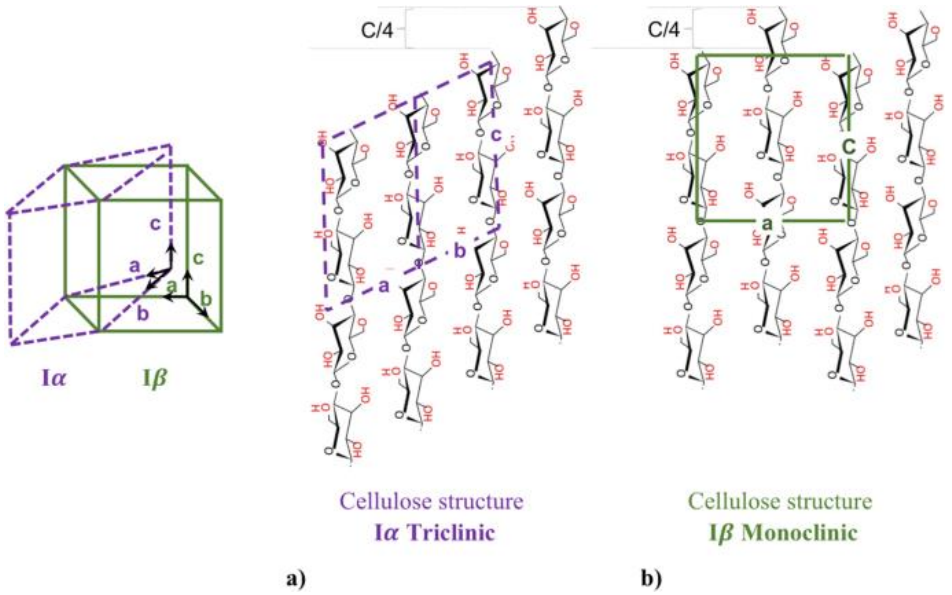

Figure 2.3. Cellulose crystal structure: a) Iα triclinic structure and b) Iβ monoclinic structure [Adapted from (16)].

The chains of BC are thus packed into cellulose Iα, cellulose Iβ and also amorphous domains. The main difference between Iα and Iβ regards their intra and inter-unit H-bonding network, being the inter-unit H-bonding also different for cellulose II. This type of polymorph is thermodynamically more stable than cellulose I, being obtained through the regeneration or mercerization of cellulose I. Indeed, cellulose I and II exhibited distinct conformation of the polysaccharide chain since the former is parallel and the later anti-parallel, which determines changes on the mechanical properties of the material, specifically a decrease on Young's modulus from 27 GPa (cellulose I) to 21 GPa (cellulose II) (3). On the other hand, cellulose III can be obtained by swelling cellulose I or II with amines or liquid ammonia, while cellulose IV is classically formed by annealing of cellulose II or III in glycerol (18).

BC has great mechanical properties (Young's modulus around 15-35 GPa and tensile strength of 200-300 MPa), high degree of polymerization (up to 8000) and high water content - up to 200 times its dry weight (5). It is a biocompatible, hydrophilic and non-toxic material that exhibits high purity since unlike plant cellulose it does not have any hemicelluloses, pectin and lignin. Many studies demonstrate that BC does not trigger a foreign body reaction. Helenius et al. (2006) assessed the *in vivo* biocompatibility through subcutaneous implantation in rats for 1, 4 and 12 weeks. The chronic inflammation, foreign body responses, cell ingrowth and angiogenesis were evaluated through histology, immunohistochemistry and electron microscopy. The obtained results showed that there were no macroscopic and microscopic evidences of inflammation around the implants. Also, there were no signs

of fibrotic capsule or giant cells and BC was well integrated into the host tissue and did not induce any chronic inflammatory reactions (19). Pértile et al. (2013) also showed the good biocompatibility of BC in a long-term *in vivo* study. The BC samples were implanted in mice and it was showed that a mild and benign inflammatory reaction occurred, which decreased along time and did not induce a foreign body reaction. Furthermore, there were no signs of chronic inflammatory reaction or encapsulation, while formation of new blood vessels around and inside (in the periphery) the implants were observed (20). Zhou et al. (2019) showed that the *in situ* incorporation of a carboxymethyl group on BC surface increased the cell affinity and viability. Also, after implantation, the tissue reaction revealed that carboxymethylation considerably increased the biocompatibility, since a lower inflammatory reaction was observed (21). More recently, Zhang et al. (2020) evaluated the *in vitro* biocompatibility of a BC scaffold for corneal stroma replacement, through the cultured of rabbit corneal epithelial and stromal cells on the BC scaffold, during a 3-month follow-up. The obtained results showed that BC supported cell adhesion, proliferation and differentiation. On the other hand, *in vivo* tests further confirmed the good biocompatibility and stability of BC in rabbit cornea, making BC an attractive option for tissue engineering of corneal stroma (22). Summing up, BC has a huge potential to be applied in several fields. In biomedicine, BC has been suggested as wound dressing material, as a replacement for skin, cartilage, bone and blood vessels, performing as a scaffold in tissue engineering strategies and also as a drug delivery system (12,23). Nevertheless, and beyond biocompatibility, biodegradation is one other desirable requirement for many applications in biomedical field. The modification of BC in order to increase and improve its biodegradability has been attempted. BC may be chemically modified through its hydroxyl groups. Thus, an improved biodegradation may be achieved through the oxidation, making BC reabsorbable by the organism. Besides this, after oxidation BC displays other characteristics such as hemostatic features, thus being a suitable raw material for some applications as a medical device (24,25). The potential of BC in the food and cosmetic industries has also been extensively reported, in particular as a thickener and stabilizer of oil in water emulsions (26,27).

2.2 – Culture methods for BC production

A previously mentioned, BC can be produced under static and agitated conditions. Depending on the culture method, the resulting macroscopic morphology, microstructure, and properties are different (4). In 1954, Hestrin and Schramm developed a culture medium to produce BC, commonly named as HS medium, that became widely used for researchers and producers. The medium is composed by 2%

glucose (main carbon source), 0.5% peptone, 0.5% yeast extract, 0.27% anhydrous disodium phosphate, 0.115% citric acid monohydrate and adjusted to pH 6 (28). The production costs are high, due to the low volumetric productivity, making critical the development of new approaches that solve this problem. In fact, long cultivation times requiring large amounts of culture medium and low production yields are some of the difficulties in the conventional production of BC. In order to answer these problems, different fermentation parameters have been studied such as pH control, carbon sources (sugarcane, molasses, sucrose and rotten fruit), the bacteria strain, oxygen delivery and the bioreactor design (29–31). Recently, another strategy applied by the researchers is related with the use of agro industrial wastes to create a culture media showing an increase of cellulose production with lower costs. Furthermore, the addition of inducers to activate the energy metabolism in the microorganism and/or reduce the formation of metabolic by-products is another tested cultivation strategy (6).

The choice of the fermentative technique, i.e. static or agitated, is related with the final application of BC, since the physical, mechanical and morphological features are dependent of the culture process. Static culture for BC production is the most common technique due to its simplicity. This method is characterized by the cultivation in shallow bottles or trays containing the liquid growth medium. The culture can be performed for several days or weeks after inoculation and fermentation at 25º-30ºC and a pH of 3-7. During the cultivation, the formation of a floating layer of a gelatinous BC pellicle occurs on the interface, being the BC production directly related to the surface area of the air-liquid interface. The BC pellicle is visible at the surface of the liquid about 2 days after the beginning of the culture and its thickness increases with the culture time (4,31). In order to solve the high cost, low rate of production and the delivery of oxygen ascribed to the static culture, the agitated conditions have been proposed. In fact, in static conditions the delivery of oxygen occurs only at the interface; however, very high oxygen supply achieved in a stirred tank has also a negative influence, since it may lead to a decrease of BC production due to the selection of non-producing mutants. Indeed, in some works using agitated conditions a lower productivity as compared to that achieved in static ones was justified by the appearance of a non-cellulose producing mutant and the genetic instability of bacteria under dynamic conditions (32,33). Thus, the decrease on BC production is consequence of cellulose-negative mutants (Cel-), which become more frequent than the producing cells (Cel+). Furthermore, although not increasing the BC yield, dynamic conditions may allow the production of BC with different characteristics. Instead of a one-piece membrane obtained in static conditions, pellets or irregular masses and fibrous suspensions are obtained than can vary in size from 10 μm to 10 nm in diameter, bearing various shapes, from spherical or ellipsoidal, to stellate. These parameters are related with the rotating speed, culture time and also with the additives

used in the culture medium (4). According to Hu *et al.* (2010), in agitated culture, the rotation speed is a key parameter in the formation of sphere-like BC. The authors tested four rotational speeds obtaining spheres with distinct sizes. In fact, when the applied rotational speed was less than 100 rpm it was difficult to find any sphere-like BC particles and irregular shapes was obtained. In opposition, the spherical shape appeared at 125 rpm with a size around 8 mm. Moreover, the increase of the rotational speed to 150 rpm produced a different shape exhibiting a tail-like feature with a decrease around 2.5 mm on its size. For speeds above 200 rpm, the formation of sphere-like BC was inhibited and some interconnected BC particles were observed, with a diameter around 1 mm. Additionally, high rotational speed did not increase the amount of produced BC (34). A layered structure is observed in microstructure of the sphere-like BC, where denser fibers and bacteria are present, while the interior region is hollow (4).

The agitated culture was proposed aiming to increase not only the oxygen transfer rate but also the mass transfer rate through the induction of a low shear stress. Nevertheless, as mentioned above this type of culture is also responsible to produce non-cellulose mutant that are often related with lower levels of BC production limiting its up-scaling. However, some bioreactor cultures seem to be responsible to produce high levels of BC. Since the BC is produced at the air-medium interface, one of the main challenge on a bioreactor design is to ensure a higher air-medium surface. Figure 2.4 depicts the stirred tank, the rotating disk and airlift bioreactors which are some examples of different configurations used for BC production (4,31,32).

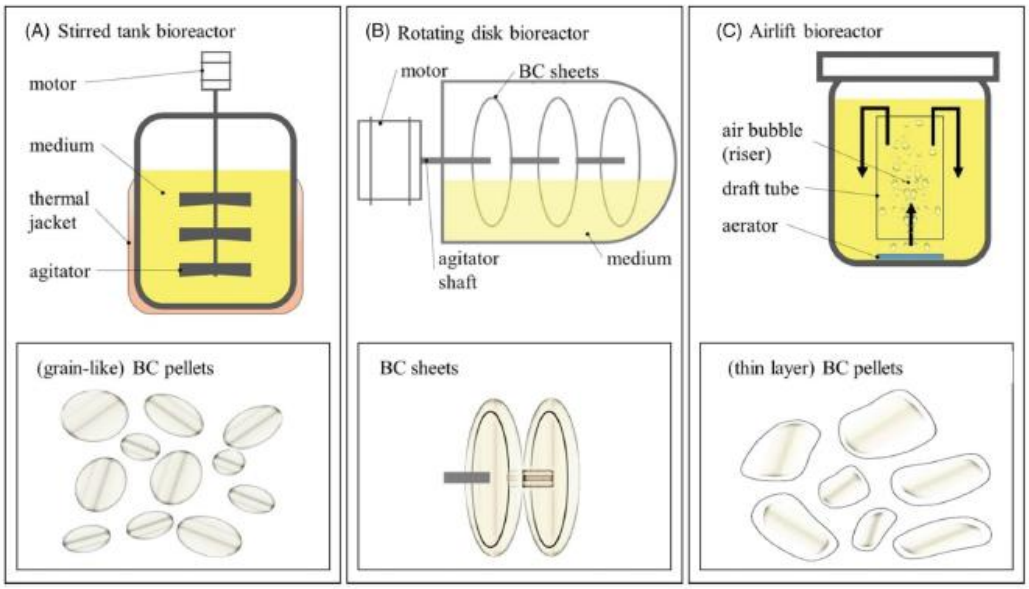

Figure 2.4. The different bioreactors design and the correspondent obtained BC's shape. A) stirred tank bioreactor producing BC pellets; b) rotating disk bioreactor producing BC sheets and c) airlift bioreactor producing thin layer BC pellets [Adapted from (31)].

The stirred tank allows high levels of mass transfer but requires high energy consumption. The agitated conditions bring about operational issues related to the increased viscosity, difficulty in properly mixing the system as the concentration of BC increases, which makes the operation at large scale highly complex. On the other hand, airlift bioreactor not only reduce the energy demand but also is able to produce lower shear stress when compared with stirred tank bioreactors, as agitation is achieved through the supply of an appropriate amount of air or oxygen. In the case of rotating disk bioreactor, the disks are partially submerged in the culture medium while the other half is exposed to the atmosphere. As the disks rotate continuously, the bacteria adsorbed at the surface of the disks alternatively contacts the atmosphere and liquid media all over the time, supplying nutrients and oxygen. Thus, the BC film grows on the surface of the disks (32). Using this bioreactor design, several types of solids and fibers can be added directly to the medium being incorporated on the forming BC layer, improving its properties. The main goal of this bioreactor is to achieve BC with a more homogeneous structure. However, the yield is not considerably higher when compared with the one obtained from the static culture (4).

To sum up, the main drawback in agitated cultures is the production of cellulose-negative mutants and operational complexity. Consequently, the simpler static culture has been frequently used to obtain BC despite the long cultivation time required.

2.3 – BIOMEDICAL AND COSMETIC APPLICATIONS OF BC

Natural polymers are extensively applied in biomedical field due to their special properties. BC has mainly been studied for wound healing applications, as artificial skin and blood vessels and also for tissue engineering and drug delivery, as briefly reviewed ahead.

2.3.1 – Drug delivery systems

Drug Delivery Systems (DDS) intents to achieve a targeted therapeutic action, minimizing the side effects and allowing the control on the effective drug concentration over long periods of time. They include several approaches, formulations, technologies and systems especially developed to transport medicines inside the body in a safely manner and efficiently achieve their desired therapeutic effects. Contrary to the conventional systems for the administration of drugs, which generally exhibited side effects due to a systemic, nonspecific bio-distribution and uncontrolled drug release characteristics, the modern DDS allow the reduction on the dosage frequency and maintain the drug concentration at target tissues for a longer period of time (35).

The superior properties of BC in the design of DDS has been demonstrated. Specifically, on transdermal drug delivery, the use of BC prevents moisture evaporation and maintain the contact with the injured area, which helps the localized drug delivery to the target site (36). BC membranes for transdermal delivery using different drugs has been widely studied by the group of Freire and Silvestre, from the University of Aveiro. The studied drugs included lidocaine (37), ibuprofen (38), caffeine (39) and diclofenac (40). In all studies, the first step was the partial removal of water by squeezing the BC membrane, which is then loaded by absorption of a solution with the selected drug. Glycerol is also impregnated, yielding plasticizing effects and helping the penetration of the drugs across the *stratum corneum*. The authors showed SEM results demonstrating that the drugs were homogeneously distributed on the BC membranes. All the drugs were tested for *in vitro* skin permeation and compared with conventional formulations. The results demonstrated that the drugs had slower permeation rates when compared to conventional formulations, which represents a benefit when a long-term release is required. More recently, the same authors investigated the long-term storage stability of BC membranes loaded

with the same drugs, using accelerated testing conditions at different temperatures and relative humidity. All the systems were relatively stable with no significant structural and morphological changes or variations in the drug release profile. These results showed the potential of BC for dermal delivery systems (41). Given its 3D network, BC allows the encapsulation of other drugs and can act as drug carrier. Müller et al. (2013) studied the applicability of BC as DDS for proteins using serum albumin as model drug. Albumin loading on never-dried and freeze-dried BC was compared, both formulations showing a dependency of concentration, temperature, time and pre-swelling. It was shown that loading and release of the protein were governed by diffusion and swelling controlled mechanisms, similarly to the behavior of the most conventional hydrogels. Moreover, drug loading was higher for never-dried BC gels comparing with freeze-dried BC, which might be explained by the structural changes in the BC network during freeze-drying. However, both formulations exhibited potential as suitable DDS (42). Another study performed by Moritz et al. (2014) showed the incorporation of octenidine in BC aiming to develop a ready-to-use system for wound treatment. The drug loading and release, mechanical characteristics, biocompatibility and antimicrobial efficacy were assessed. The resulting material exhibited improved healing and superior material properties, combined with an efficient infection control and minimized unwanted side effects. Moreover, octenidine loaded BC had comparable release profiles to already marketed products and was stable for up to 6 months storage without losing their physicochemical and biological features (43). Recently, Li et al. (2019) explored the potential of BC for oral delivery of melatonin. In order to prepare BC nanofiber suspensions, BC was previously hydrolyzed by sulfuric acid followed by the oxidation and the melatonin-loaded BC nanofiber suspension was prepared by emulsion solvent evaporation method. The obtained results showed that the new formulation had good thermodynamic stability and melatonin was uniformly distributed in the BC nanofibers suspension. *In vitro* release studies revealed that this formulation exhibited faster dissolution rate and much higher cumulative release rate and bioavailability than the commercially available melatonin formulation (44).

2.3.2 – Tissue Engineering

Tissue engineering (TE) is another field where BC potential application has been widely studied. TE is an interdisciplinary field, merging knowledge from both engineering and life sciences, aiming at developing new bio-based implants to repair or replace and restore function of damaged tissues or organs (45,46). Several works describe the use of BC in TE. For instance, a novel BC-alginate composite scaffold obtained by freeze drying was tested by Kirdponpattara et al. (2015). In this work, BC-alginate scaffold showed a stable structure in both water and phosphate buffer saline (PBS), exhibiting highly

interconnected pores and good swelling ability demonstrating no cytotoxicity against L929 mouse fibroblast cells. Furthermore, for long-term culture, BC-alginate composite scaffolds were able to support cell attachment, spreading, and proliferation on the surface. However, under static conditions, the cell migration and growth inside the scaffolds were limited, due to insufficient porosity. All the obtained results indicated that this new scaffold facilitate diffusion, cell proliferation and tissue generation for TE applications (47). In other study, a highly porous and biocompatible regenerated BC-gelatin composite scaffold was produced. This scaffold exhibited interconnected pores, high porosity and rapid swelling, which ensure nutrient exchange ability during practical applications. Additionally, it allowed the adhesion and proliferation of fibroblasts and penetration up to a depth of 200 μm after 7 days of culture. It also enhanced the expression of metalloproteases which revealed that extended cell culture might lead to extracellular matrix production inside the scaffold (48). Osorio et al. (2019) modified the BC 3D surface in order to develop a novel approach to biomimic soft extracellular matrix chemistry using fibroblasts to immobilize adhesion proteins such as collagen and fibronectin. These proteins were responsible for activating the integrin adhesion pathways, generating a stronger cell adhesion to the biomaterial. Higher cell adhesion was observed, revealing that this approach was able to biomimic the chemical surface of soft extracellular matrix (49). BC membranes were also used by Klinthoopthamrong et al. (2020) to produce an active non-resorbable guided tissue regeneration membrane conjugated with plant-derived recombinant human osteopontin (p-rhOPN). Initially, BC was grafted with poly-acrylic acid brushes in order to introduce multiple carboxyl groups on BC surface providing an anchoring site for p-rhOPN conjugation. This process did not influence the mechanical strength and fibrous structure of BC and full coverage for p-rhOPN was obtained. It was also confirmed by different assays that the biological functions of p-rhOPN was preserved after surface immobilization and could enhance bone tissue regeneration. This new strategy potentially promote human periodontal ligament stem cells adhesion and osteogenic differentiation to a greater extent than BC alone (50).

2.3.3 – Cosmetics

The application of BC in skin treatments, essentially as facial masks, is known for a long time. Amnuaikit et al. (2011) evaluated the effects of BC masks in humans and their satisfaction with the product. The obtained results allowed to conclude that a single application of the BC masks enhanced moisture uptake by facial skin and the patient expressed satisfaction with the product (51). Pacheco et al. (2018) used cosmetic masks based on BC membranes to incorporate two different active cosmetics. One of them was composed by oat, rosemary, calendula extracts and hydroviton. The other one was

composed by propolis extract at 30% of polypropylene glycol. The results revealed that the loading of the BC membranes with both active cosmetics did not modify its pristine nanofibrilar structure and could be used as support for sustained release. The sensory tests indicated high scores for skin adhesion and mask handling and the release of formulations from BC membranes demonstrated altogether, an appropriated system for cosmetic application (52). Another work driven by Perugini et al. (2020) studied the effect of different cosmetics (anti-aging, lifting, and cell renewal) on skin moisturizing, color, viscoelastic properties, skin surface smoothness, wrinkle reduction, dermal homogeneity and stratum corneum renewal. A significant decrease on skin roughness and wrinkle breadth was observed, as well as a significant improvement on dermis homogeneity and firmness after two months of treatment with "anti-aging" BC-based masks. Moreover, after one month of treatment it was observed that: i) when BC-based "lifting" masks were used there was a substantial improvement on skin firmness and elasticity and, ii) the use of "cell-renewal" purifying and regenerating BC-based masks promoted the production of new skin cells through a mild exfoliating action, which improved the *stratum corneum* cohesion. These findings showed the effective tailored system to release into the skin different active components (53). Amorim et. al. (2020) also presented a biomaterial entitled BioMask based on BC and enriched with natural propolis, aiming to help in the healing of inflammations caused by acne. The incorporation of the natural propolis did not change the nanofibrilar structure of BC and enabled superior mechanical properties, suggesting that it could be applied as a vehicle for releasing active components in a more efficient way. This work showed that the combination of natural biodegradable polymers with natural active extracts might provide new biotechnological products that address the needs of the world market, which pursues safer and environmentally friendly alternatives (54).

2.3.4 – Artificial vessels

BC can be synthesized with different shapes, generating an ideal substrate for cell attachment and proliferation, thus making it a good candidate to develop artificial vessels, as shown by Klemm *et al.* (2001;2009). In these works, the authors designed a material called BActerial SYnthesized Cellulose (BASYC®). This new tubular product was shaped directly during the cultivation and applied as artificial blood vessel, since it exhibited enough moldability and similar mechanical properties. It was implanted in the carotid arteries of rats and pigs, revealing long-term stability while maintaining the bypass unobstructed for 3 months. In fact, in a first work, the BC implants were placed on an artificial defect of the carotid artery of rats for 1 year. The results revealed the formation of neointima and ingrowth of active fibroblasts. In a second work, the grafts were implanted into carotid arteries of pigs and remove after 3

months. The obtained results indicated that novel BC engineering technique produced stable vascular tubes, confirming the highly attractive approach to *in vivo* tissue engineered blood vessels (55,56). Andrade et al. (2010) functionalized BC with chimeric peptides containing a cellulose-binding module and adhesion peptides in order to improve the adhesion of human microvascular endothelial cells (HMEC) to BC. The study revealed that the presence of adhesion sequences significantly increased the HMEC attachment to BC surface and also stimulated angiogenesis. Therefore, the use of recombinant peptides containing the adhesion sequences allowed to control the interaction of this material with cells through its high affinity and specificity for cellulose surfaces (57). Several different materials were used to functionalized and improve BC properties. One example is poly (vinyl alcohol) (PVA). This material was responsible for enhanced tensile strength and improved water permeability of BC, which is important to maintain their long-term integrity (58). Similar results were obtained by Leitão et al. (2016) which also proved the good properties of BC for this application. The novel approach developed by these authors also exhibited a dense, malleable, and mechanically strong tubular BC prosthesis. Preliminary *in vivo* studies revealed the presence of neo-vessels and endothelial cells on the luminal surface of the graft (59). In other work, BC was modified through the deposition of chitosan into the fibril network. Furthermore, heparin was also chemically grafted into the BC tubes aiming to improve the anticoagulation and endothelialization performance. The strength at break increased but burst pressure slightly decreased with the novel methodology. However, and as aimed, the anticoagulation and endothelialization performance was improved remarkably with the presence of both chitosan and heparin, revealing the great potential to be applied as small-diameter vascular prosthesis (60).

2.3.5 – Wound healing dressings and artificial skin

Wound healing is a dynamic biological process that leads to the tissue regeneration of wounded tissue. It includes the participation of several cellular and matrix components encompassing four different stages: i) coagulation (immediately after injury), ii) inflammation (starting shortly after injury) during which swelling occurs, iii) cell proliferation, where new tissue and blood vessels are formed and, finally, iv) the maturation phase, where the remodeling of new tissue occurs (Fig. 2.5). Actually, there is a significant overlap between all these phases and the entire healing process could take months to be complete (61).

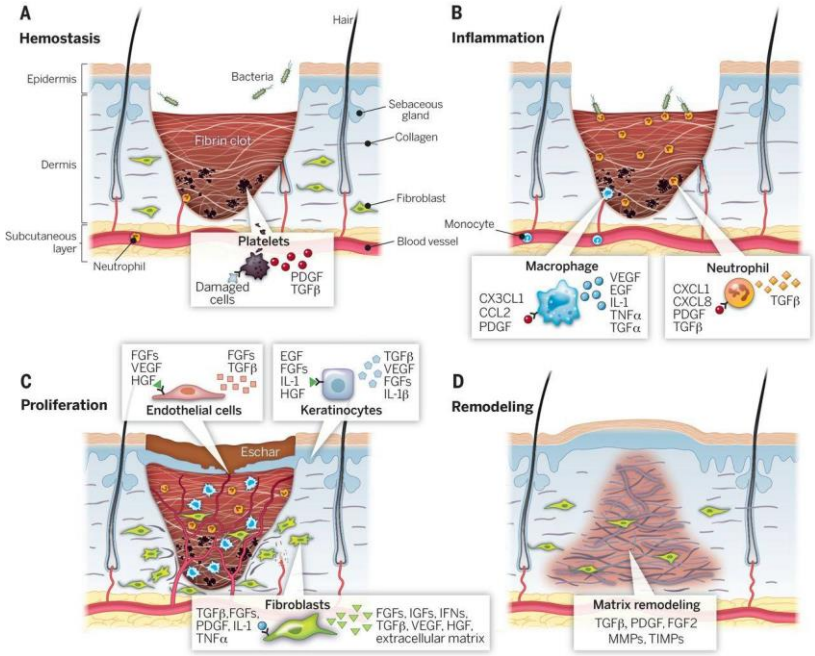

Figure 2.5. The distinct stages of wound healing: a) hemostasis; b) inflammation; c) proliferation and d) remodeling [Adapted from (73)].

As previously mentioned, coagulation occurs immediately after the injury and the main goal is to prevent the exsanguination. Nevertheless, there are some works that include this phase on the inflammation process. The inflammation phase begins immediately after injury and the elements of the coagulation cascade, inflammatory pathways and immune system (all interconnected) are required to prevent ongoing blood and fluid losses, infections and also to remove dead and devitalized (dying) tissues. Hemostasis is achieved through the formation of a platelet plug followed by a fibrin matrix which will be the anchorage point to the infiltrating cells. Neutrophils are the first recruited cells responding to the activation of complement, the degranulation of platelets and also the products of bacterial degradation. Monocytes appear 2-3 days after the injury and differentiate into macrophages. On the early inflammation phase hypoxia occurs (ischemic environment) along with fibrin matrix formation. On the other hand, the main goal of proliferative phase is to repair the injured tissue area and to establish an immune barrier against invading microorganisms. It is characterized by cellular proliferation and migration of different cell types. It begins with the migration of keratinocytes to the injured dermis and new blood vessels start to form in a process called as angiogenesis. This process involves endothelial cellular proliferation, rupture and rearrangement of the basal membrane, migration and association in tubular structures which are the new blood vessels. At the end of the proliferative phase, the fibroblasts are stimulated by macrophages and some of them differentiate into myofibroblasts which are contractile cells. Both fibroblasts and myofibroblasts interact and produce extracellular matrix, essentially in the form of collagen, forming the

mature scar. Finally, 2-3 weeks after the injury and lasting for a year or more, occurs the third phase (maturation) where remodeling process happens. Here, all the processes activated after injury will decrease its activity and stop. The involved cells such as macrophages and myofibroblasts undergo into apoptosis or abandon the wound, leaving a mass that holds some cells, but it is mostly composed by collagen and other extracellular matrix proteins. The epithelial-mesenchymal interactions regulate not only skin integrity but also hemostasis. Additionally, after 6-12 months, it occurs the remodeling of the acellular matrix from a mainly type III collagen to mostly type I collagen. This process is governed by metalloproteinases that are secreted by fibroblasts, macrophages and also by endothelial cells (62,63).

In clinical applications, BC is widely applied as a wound dressing, due to its biocompatibility and ability to retain water. BC wound dressings are highly porous and hydrophilic, so they can absorb exudates and also perform as drug delivery systems, delivering antibiotics or other medicine into the wound. These dressings are easy to remove without causing pain to the patient, because they are not adhesive (64). There are several studies showing that BC is very effective material as wound dressing. Kwak et al. (2015) evaluated over a period of 15 days the skin regeneration and angiogenesis in burn injury skin on Sprague Dawley rats. Their findings showed that the wound severity was lower overtime in BC treated groups comparing to the control gauze treatment. Moreover, the epidermis and dermis thickness as well as the number of blood vessels was superior in that group. There was also a significant decrease in the number of infiltrated mast cells, vascular endothelial growth factor and in angiopoietin-1 expression on the BC membranes treated group. With these results, it could be concluded that the BC membranes may accelerate the wound healing process without inducing any negative systemic effects (65). Pandey et al. (2016) studied the physical properties and cytotoxicity of hydrogel composed of BC and polyacrylamide as a dressing material to cover partial-thickness burn wounds in Sprague Dawley rats. BC membranes presented a highly porous structure and swelling features that makes it appropriate for wound dressing applications. It was non-irritant and had a significant effect on wound contraction when compared to the non-treated group. The *in vivo* results also showed that the hydrogel with BC enhanced epithelization and accelerated the fibroblast proliferation without any signs of local inflammatory response (66). Another study evaluated the antimicrobial efficiency of BC wound dressing functionalized with Ɛ-poly-L-lysine. This functionalization induced an inhibition on *S. epidermidis* growth but did not affect the improved cytocompatibility to cultured human fibroblasts, as compared to native BC (67). Loh et al. (2018) developed a BC/acrylic acid (BC/AA) hydrogel cell carrier containing human keratinocytes and human fibroblasts for full-thickness wound healing. The obtained results revealed that BC/AA hydrogel exhibited a very good cell attachment and viability, allowing the cell transfer when applied onto the skin.

Furthermore, both the hydrogel alone and with cells accelerated wound healing compared to the untreated groups, suggesting the potential application of BC/AA hydrogel with double function, *i.e.*, as a cell carrier and as wound dressing (68). More recently, Ciecholewska-Jusko et al. (2020) performed an *in vitro* evaluation of a novel *ex situ* modification of BC which improves its ability to absorb water after drying (over 5 times higher when compared to the unmodified BC). *Ex situ* modification was achieved through crosslinking BC with citric acid aiming to prevent the collapse of BC structure after the evaporation of water from interfibrillar spaces under dehydrated conditions. With this modification, it was possible to improve the ability to absorb water but also to reduce the water release rate over 6 times when compared to unmodified BC. Moreover, crosslinked BC exhibited 1.5x higher water absorption capacity than the current commercial dressings dedicated to highly exuding wounds, while cytotoxicity effects against L929 fibroblasts was not observed. These findings indicated that the developed method is very promising on the design of innovative dressings applied to chronic wound management (69).

In addition to wound healing, BC may be also applied as artificial skin. Skin is the largest organ of the body and act as barrier against exogenous components, pathogens and mechanical stress. Damage on skin is responsible for water loss and the invasion of bacteria. Thus, a quick regeneration or repair after any injury is mandatory (70,71).

Dressings used as skin substitutes are produced with several combinations of synthetic and/or biologic components. These dressings intents to close the wound and replace the functions of the skin, both temporarily and permanently. Skin substitutes provide reconstructive solutions since they are able to increase the dermal component of the healed wound, reduce the inflammatory response, reduce or remove inhibitory factors and provide a safe coverage (72). There is no ideal skin substitute, however there are some strategies such as autografts, allografts and xenografts that are commonly applied. Grafts corresponds to a viable tissue or a collection of viable cells which are harvested from the donor to a recipient in order to reconstruct it. Autografts arise as the gold standard since they provide minimum immunological rejection, since these grafts are harvested from one site to another within the same individual. In the case of allografts, the donor and recipient are different individuals of the same species, i.e., derived from cadavers. This kind of grafts has some disadvantages such as the immunological rejection and disease transmission. Finally, it could be possible to use xenografts, which are obtained from different species. However, xenografts have disadvantages similar to allografts (73). Nowadays, there is a huge diversity of skin substitutes commercially available. They exhibit mechanical properties and anatomic features with high similarity to the tissue that they intend to replace. When implanted into

the body they gradually degrade, leaving behind a matrix of connective tissue with suitable structural and mechanical properties. Despite their great potential for the treatment of chronic wounds and third-degree burns, skin substitutes are still limited by their high cost, risk of infection and the possibility of create a second wound in the case of harvesting patient's own cells to aid wound healing (74).

BC, with its suitable properties and clinical performance, arises as an important material for wound care as artificial skin and also as a wound dressing. Considering this, in wound care, there are some commercially available materials made from BC which are present on table 2.2.

Table 2.2. Commercially available materials produced from BC [Adapted from (75)].

Product	Application
BioFill®	Temporary skin substitute
BioProcess®	Skin transplant, treatment of burns, ulcers, and decubitus
NexFill®	Dry bandage for burns and wounds
Membracell®	Temporary skin substitute
Cellumed®	Treatment of large surface wounds in horses
Nanoderm™	Wound dressing for acute and chronic wounds
Suprasorb® X	Hydrobalance wound dressing for non-infected and low exudate wounds
Suprasorb® X + PHMB	Antimicrobial Hydrobalance wound dressing containing 0.3% of polyhexamethylene biguanide for wounds with risk of infection
DermaFill™	Translucent wound dressing
CELMAT® Wound/Eye/Face	Hydrated wound dressing

CELMAT® Wound/Eye/Face H	Hydrated wound dressing with sodium hyaluronate
CELMAT® Wound/Eye/Face P	Hydrated and antiseptic wound dressing with polyhexanide

In fact, BC is able to preserve the moist environment which is important for the re-epithelization process and also bears other properties, such as: i) exudates retention ability; ii) high mechanical strength at wet state; iii) liquid/gas permeability; iv) small risk of irritation due to its high purity; and v) simple wound inspection due to its transparency (75).

2.3.5.1 – Hemostasis

Uncontrollable bleeding is an important cause of several associated deaths on emergency and hospital settings. Hemostasis arises as the primary body response to fight hemorrhage. It includes the production of blood clot and its consequent dissolution followed by the repair of the injured tissue. As referred above, hemostasis occurs through the complex interplay of four key elements: the vascular endothelium, platelets, the coagulation pathway and fibrinolysis. Thus, the hemostatic system can be divided in primary hemostasis, secondary hemostasis and fibrinolysis (76). Briefly, primary hemostasis describes the cellular interaction of platelets and the formation of the platelet plug at the injured vessel wall. On the other hand, the secondary hemostasis is ascribed to the deposition of insoluble fibrin, which is generated by the proteolytic coagulation cascade. This stage is initiated, amplified and prolonged in a sequence of activations of coagulation proteins and regulated by different positive and negative feedback mechanisms. The fibrinolytic system represents the tertiary hemostasis and regulates the disruption of blood clots restoring the blood flow (77,78).

In more detail, immediately after the injury of endothelium the primary hemostasis begins. This step is characterized by vasoconstriction, platelet adhesion and the formation of a soft platelet plug. A local contraction of the vascular smooth muscle occurs and the blood flow decrease, promoting platelet adhesion and activation. Circulating von Willebrand factor (vWF) act as a bridge between endothelial collagen and platelet surface receptors, the glycoprotein complex I being the main receptor for vWF. The adhesion of platelets to collagen activate signals that are responsible to promote the increase of cytosolic Ca^{2+} levels. Calcium ions bind the phospholipids providing a surface for the assembly of several

coagulation factors which are released after platelets activation. These factors include: serotonin, prostaglandin and thromboxane, that stimulate further platelet aggregation. These substances are also important for the maintenance of local vasoconstriction (77,79,80). Figure 2.6 depicts the different steps of platelet adhesion, activation and aggregation.

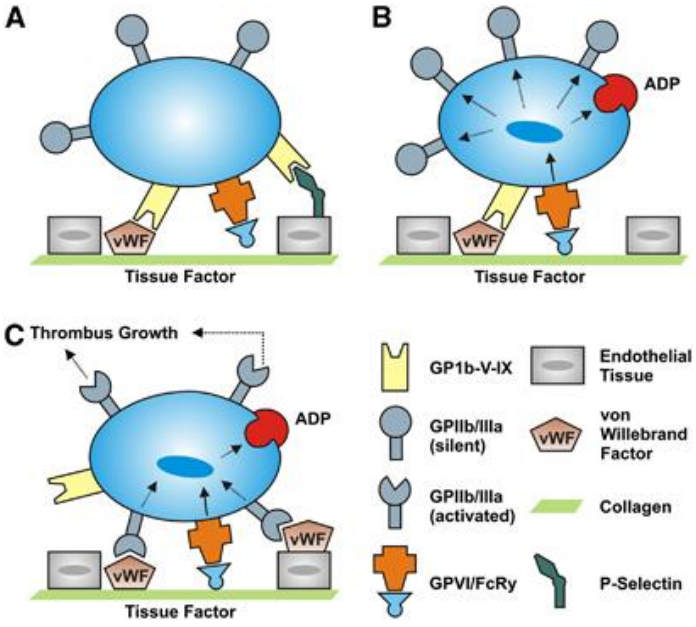

Figure 2.6. The different stages on platelet adhesion, activation and aggregation [Adapted from (81)].

As above mentioned, (Fig. 2.6a) the initial adhesion of platelets is mediated through the binding of glycoprotein ((GP)Ib-V-IX) to the vWF domain on endothelial cells. Then, the binding of P-Selectin follows, enhancing the platelet recruitment and the interactions between the glycoprotein (GPVI) and collagen stabilize the thrombus (Fig. 2.6b). After that, the secretion of platelet agonists like adenosine diphosphate (ADP) promotes the cellular activation. This phase is also characterized by the transformation of the GPIIb/IIIa receptors into a high affinity state. Finally, (Fig. 2.6c) the platelet activation via integrin-fibrinogen ends with platelet aggregation and following the thrombus growth (81).

The secondary hemostasis consists of the cascade of coagulation that leads to the cleavage of soluble fibrinogen by thrombin, forming the fibrin clot. The coagulation cascade involves plasma proteins, calcium ions and blood platelets. Traditionally, coagulation cascade is classified into intrinsic and extrinsic pathways, both of which converge on factor X activation (Fig. 2.7). Produced by liver, the coagulation factors circulate in an inactive way until the coagulation cascade is initiated. Then, a series of sequential and dependent coagulation factor activation reactions occurs. The plasma clotting system is started by

two different mechanisms: the tissue factor pathway and the contact pathway (or extrinsic and intrinsic, respectively).

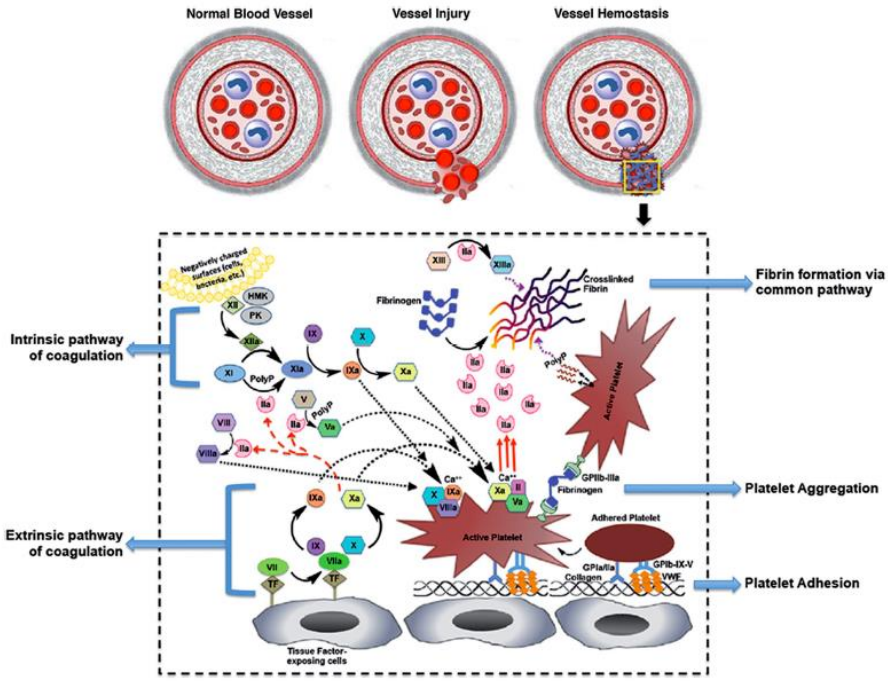

Figure 2.7. Illustration of blood vessel hemostatic mechanism [Adapted from (84)].

Both pathways converge resulting in the formation of a fibrin clot which strengthens the primary platelet plug. In the intrinsic pathway, exogenous material with negative charge activates factor XII (FXII). This induces a downstream proteolytic activation of other coagulation factors until the factor X (FX) is activated. In more detail, the intrinsic pathway occurs ultimately through thrombin activation by FXII. It is activated when FXII, PK (proteins prekallikrein) and HK (high-molecular weight kininogen) assemble on a suitable surface or polymer. Activated FXI will activated FIX, which then acts with its cofactor (FVIII) to form tenase complex on a phospholipid surface to activate FX. In turn, the extrinsic pathway initiates when trauma of the vasculature expose tissue factor. This event will activate coagulation factor VII (FVIII) in the presence of calcium ions, promoting the conversion of FX to FXa. Thus, both pathways converge at the production of FXa. In the final common pathway FX with FV transforms the prothrombin (FII) into thrombin, which converts fibrinogen (FI) to fibrin. Fibrin is stabilized by FXIIIa (activated by thrombin), which cross-links the fibrin monomers producing a stable clot (79,82–84).

Finally, the fibrinolytic system intents to dissolve blood clots along the process of wound healing and also prevents the formation of blood clots in healthy blood vessels. This is a concurrently running system whose activation occurs during the coagulation cascade, aiming to limit the size of the clot. It is composed by three serine proteases existing as zymogens (i.e., proenzymes in the blood). Thus, fibrinolysis is an enzymatic process whereby plasmin dissolves the fibrin clot into fibrin degradation products. This enzyme is produced by the protease tissue-type plasminogen activator (tPA) and urokinase-type plasminogen activator (uPA) released from vascular endothelium (77,79).

2.3.5.2 – Topical hemostatic agents

Hemorrhagic episodes are inevitable during a surgery procedure. Massive bleeding is controlled using standard surgical techniques like stitches, ligatures or clips. However, when diffuse bleeding occurs or the natural physiologic hemostasis is not enough to control hemorrhagic episodes, it is pivotal the use of hemostatic materials. Topical hemostatic agents (HAs) are a useful tool to supplement the coagulation system when the conventional procedures do not effectively control bleeding. Furthermore, the ideal HAs should exhibit high hemostatic action, low tissue reactivity, biodegradability, low cost, and specificity for different situations. There is no single ideal hemostatic agent meeting all these requirements, being imperative the careful choice of the suitable product for a given operative environment (85,86). HAs can be broadly divided into active and non-active (Fig. 2.8), distinguished by having or not physiologically active substances that may interfere on the blood clotting process. However, there are some HAs that reveal characteristics of both groups and they are called as flowable HAs (87).

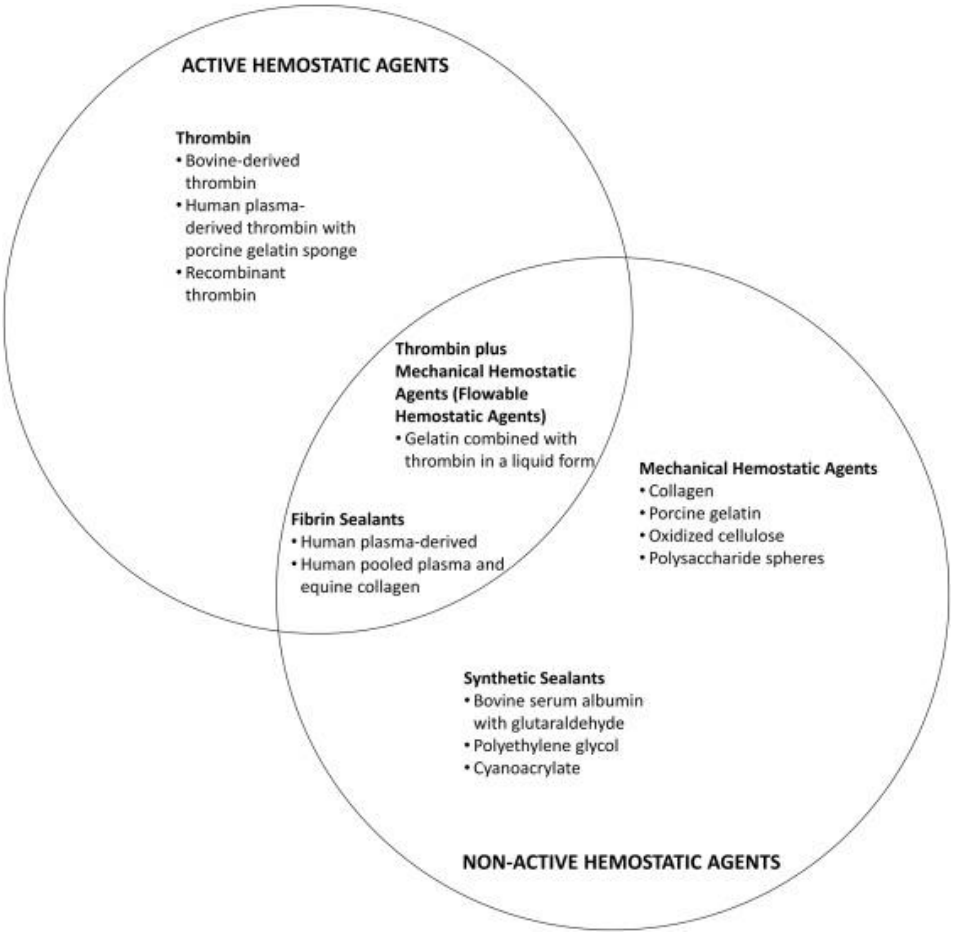

Figure 2.8. Available topical hemostatic agents [Adapted from (87)].

Active HAs include thrombin, alone or in combination with other mechanical HAs, such as gelatin sponge. They provide high concentrations of thrombin, converting fibrinogen into fibrin at the bleeding site, forming a clot. On the other hand, and as previously mentioned, the non-active HAs do not intrinsically contain thrombin or other biologically active components, being composed only by the mechanical hemostatic agents and synthetic sealants. The former is characterized by the ability to produce a physical matrix that provides a barrier over the bleeding site and include oxidized cellulose, gelatins, and polysaccharides spheres. This type of HAs should be left in place until clot formation and then gently removed to avoid disruption and re-bleeding. The synthetic sealants are essentially applied to prevent suture hole bleeding in cardiac and vascular procedures, acting as adhesives and forming a watertight barrier over the bleeding sites. Finally, combining features of the mechanical and active HAs, arise the flowable HAs. This kind of HAs are able to block blood flow and actively convert fibrinogen in blood into fibrin at the bleeding site. They are divided into bovine collagen combined with human pooled-

plasma thrombin, and animal source gelatin combined with recombinant human thrombin, bovine, or human pooled-plasma thrombin. After application, flowable agents required the reconstitution of thrombin, which is mixed with a gelatin matrix. The final product displays a foam-like consistency being delivered through a blunt-nosed or blending applicator to the target site, expanding up to 20% over 10 minutes after application. In postponed applications, the product might be stored during 3 hours after the mixing process is completed. The excess of the product must be clean through saline irrigation without any risk of clot disruption. Both clot and the remaining product could stay *in situ,* both being resorbed in 6-8 weeks (87–89).

2.3.5.3 – Polysaccharide-based hemostatic materials

The previous section introduced the different available types of topical HAs. There are several different hemostatic strategies that may be selected according to the injury type (90). Polysaccharides are natural polymers composed of sugar building blocks that allow chemical and physical modification. There are several works describing the use of polysaccharide-based materials as topical HAs, tissue adhesives and sealants. Beyond others polysaccharides, chitosan and cellulose are widely applied in this field (83). Chitosan based hemostatic agents have been investigated due to its positive charge which is, in fact, a double-edged sword in this area. Usually, it accelerates red blood cell adhesion, platelet adhesion and activation, while, at the same time, it inhibits the activation of the contact system. Thus, and in order to improve its hemostatic efficacy, its modification is required. HemCon®, Celox® and Colgel® are some examples of chitosan-based HAs (91–93).

Cellulose, specially, oxidized cellulose (OxCell)-based HAs are also commonly used. When applied into the bleeding site, OxCell is able to absorb the blood and entrap different components such as blood proteins, platelets and red blood cells. This leads to an increase of the blood coagulation factors concentration accelerating the blood coagulation process until the clot formation. This phenomenon produces a gel-like "pseudo-clot" that can act as a barrier to block the blood flow. Furthermore, the coagulation process is induced by the negatively charged carboxylic groups on OxCell surface through the activation of the coagulation factor XII (94–96). Oxycel® and Surgicel® are some examples of OC-based HAs available as woven and nonwoven, respectively (86,92,97). Surgicel® made by Ethicon Inc. of Johnson & Johnson Medical Limited is a bio-absorbable material widely applied for intraoperative hemostasis and adhesion prevention in surgery. Surgicel® seems to act as a mesh for platelets adhesion and aggregation, helping on the formation of an artificial clot, while its negative charge is likely to activate

the secondary hemostasis as well. It is advisable to remove Surgicel® when the hemostasis is achieved. However, the most common procedure is to left it *in situ* to reabsorb spontaneously, usually without any secondary effects. If left *in situ*, the material become gelatinous in 24 to 48 hours, while the complete degradation should occur between 4 and 6 weeks (86,92,98). Nevertheless, there are different reported cases describing the presence of Surgicel® residues and several problems are ascribed to its use. One of such cases was the presence of a recurrent gastrointestinal stromal tumor four months after surgical resection, that was ascribed to the intra-abdominal foreign-body granuloma caused by the presence of Surgicel® residues (99). Another case reported the formation of a foreign body reaction, contributing to the development of an intracranial giant-cell granuloma. In this case, the patient was diagnosed with intracranial hemorrhage which was assigned to the use of Surgicel® (100,101). Other reports concerned the use of Surgicel® in thoracotomy in order to control hemorrhage. However, it passed through the intervertebral foramen causing spinal cord compression (102,103). Considering all the problems associated to the available materials, it is important to improve and/or develop new hemostatic dressings. In this context, other cellulose-based materials have been broadly explored and several modifications have been tested to increase its hemostatic potential. Vosmanska et al. (2014) modified OxCell with inert argon plasma which caused significant changes on chemical composition of the surface layers, as well as changes in morphology of those layers. The plasma treatment yielded a more acidic material owing to higher content of hydroxyl and carboxyl groups, which caused larger inhibition zones against *E. coli* and *S. epidermidis*, thus showing an improvement on antibacterial properties. The modification using inert argon plasma also improved the required properties for hemostatic function ascribed to oxidized cellulose (104). On the other hand, the functionalization of OxCell with chitosan is also widely described in the literature. Oxidized cellulose-chitosan sponges may be prepared by lyophilization, showing better hemostatic effect on hepatic trauma when compared to oxidized cellulose alone. Besides this, the proposed material revealed greater biodegradability and biocompatibility, suggesting its potential as a surgical hemostat (105). Cheng et al. (2019) developed a *N, O*-carboxymethyl chitosan/oxidized regenerated cellulose (*N, O*-CS/ORC) composite gauze. This material was degradable and had excellent antimicrobial activity against *S. aureus* and *E. coli*, which is important to prevent wound infection. Moreover, when tested in a rat model with abdominal wall defect and cecum abrasion, it revealed to be effective to prevent the formation of peritoneal adhesion (106). Another study developed by Demirekin et al. (2015) proposed a novel oxidized regenerated cellulose powder using two different metal ions (sodium and potassium). The materials showed bactericidal activity against *S. aureus* and *in vivo* studies with rats

indicated that powder materials performed a quick blood coagulation and did not damage the tissue at the application area (96).

2.3.5.4 – Oxidation of BC

Different methods have been tested to chemically modify BC membranes, being the surface acetylation, alkali, sulfuric acid and phosphorylation treatments some of the applied methods (25). The chemical modification at the C1 and C4 positions of the glucopyranose ring usually promotes degradation, resulting in a considerable decrease of crystallinity through the reduction of microfibril length and the loss of the exclusive mechanical behavior of BC (107). Beyond the previously mentioned methods, chemical modification of BC can be also achieved through oxidation. Generally, this method is accompanied by degradation and a concomitant decrease in the degree of polymerization which may be explained by the oxidation reaction *per se,* the β-elimination from carbonyls being responsible to the shortening of the chain. BC may be oxidized through different methods: radiation, energy impact or also by the application of oxidizing reagents (108), where the chemical oxidants can be selective or non-selective. Nitrogen oxides, ozone, alkali metal nitrites and nitrates and permanganates are examples of non-selective oxidants, while periodates and nitroxyl radicals are selective (109). Periodates open the pyranose ring leading to the oxidation of C2 and C3 to aldehydes (108,110). Furthermore, chemical modification at C1 and C4 regions usually promotes degradation resulting in a considerable decrease in crystallinity through the reduction of microfibril length and also a loss mechanical properties (107). Alternatively, the 2,2,6,6-Tetramethylpiperidine-1-oxyl (TEMPO) nitroxyl radical has been widely applied to oxidize cellulose since it is able to convert polysaccharides into the corresponding polyuronic acids through the selective oxidation of the primary hydroxyl groups at C6 to carboxyl. In fact, TEMPO is able to promote a selective conversion of alcoholic hydroxyl groups to aldehydes, ketones and, as mentioned, to carboxyl groups (111). In this process (Fig. 2.9), TEMPO is oxidized through a one-electron transfer reaction to the corresponding oxoammonium. This oxoammonium is the active oxidant in the primary alcohol oxidation. Then, the electrooxidation of the hydroxylamine regenerates $TEMPO^{+}$, *in situ*.

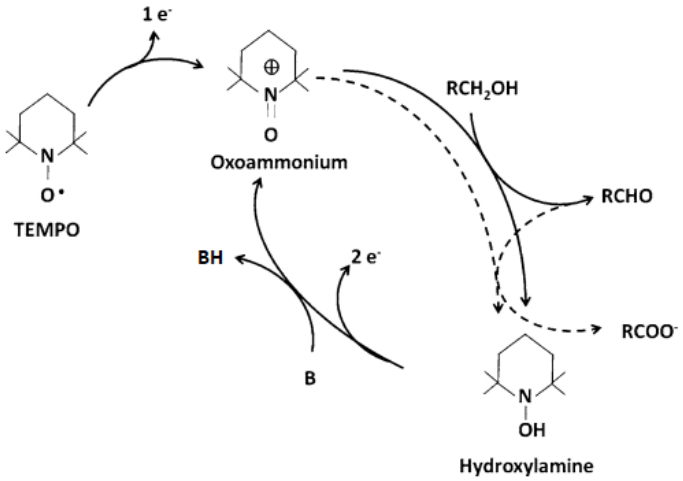

Figure 2.9. Electrochemical oxidation mediated by TEMPO radical [Adapted from (112)].

This electrochemical approach is a suitable alternative to the chemical co-oxidants like NaClO-NaBr and water-acetonitrile-NaClO-$NaClO_2$. The anodic regeneration of the oxidizing species instead of the primary oxidants is considered cleaner (112). Furthermore, TEMPO is also characterized by its stability, non-toxicity and non-mutagenic features (113), high reaction rate and yield, allowing a controlled modification of the polysaccharides (114). However, the selective oxidation of C6 primary hydroxyl only occurs on BC microfibrils surfaces or in cellulose I crystallites without taking place inside the crystallites (115,116) (Fig. 2.10). After oxidation, the carboxylate groups formed on microfibrils surface exhibit negative charges causing repulsive effects between the microfibrils, helping on the individual microfibrils disintegration through mild mechanical treatment in water (117,118).

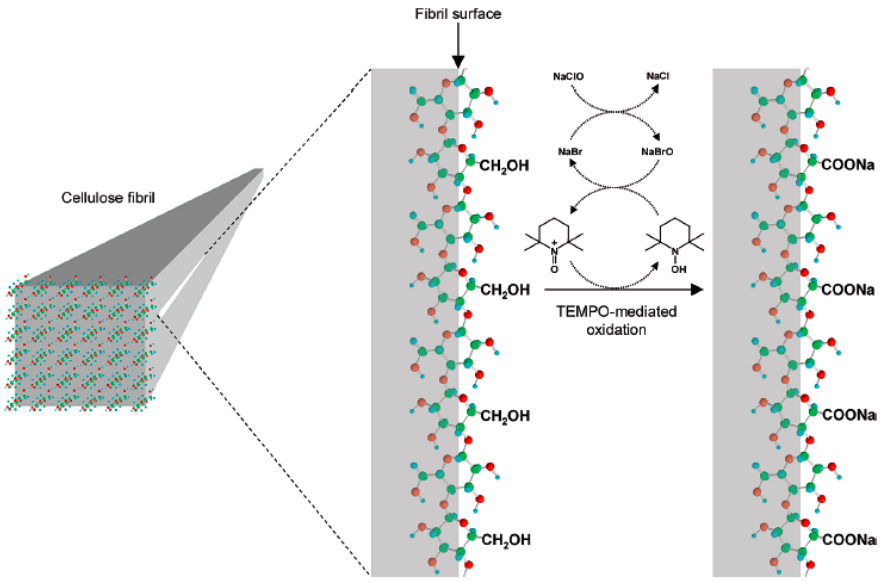

Figure 2.10. Representation of C6 primary hydroxyl oxidation on cellulose microfibril surface mediated by TEMPO [Adapted from (117)].

Additionally, the presence of carboxylate groups on the microfibril surface may affect the surface properties such as topography, composition, roughness and surface free energy (107). Due to all these effects, oxidized BC exhibit new features such as *in vivo* degradability and hemostatic properties (119) which in association with all other BC properties make it an excellent material for biomedical applications.

2.4 – BIOMATERIALS AND BIOCOMPATIBILITY

2.4.1 – Cell-biomaterial interactions

Although considered highly biocompatible, BC may be further improved as a biomaterial. In the last decades, the use of biomaterials in biomedical field, namely as implantable devices or to promote functional tissue regeneration, increased exponentially. According to Williams (2009), a biomaterial is "a substance that has been engineered to take a form which, alone or as part of a complex system, is used to direct, by control of interactions with components of living systems, the course of ant therapeutic or diagnostic procedure" (120). After implantation, biomaterials contact with surrounding cells eliciting a host response that corresponds to the first steps of tissue repair. In fact, the immune response to biomaterials depends of different factors such as the method of implantation, the source of biomaterials

and their physicochemical properties, molecular weight, chemical composition, mechanical properties and degradation rate. Modern implant designs intend to use this immune response to improve implant integration while avoiding chronic inflammation, foreign body reactions and the risk of losing the proposed function (121,122).

Biomaterials can be classified as natural or synthetic. In the former case, they are derived from animals, microbes, or plants and are similar to materials familiar to the body. Also, they are biodegradable and the natural degradation might occur in the body through enzymes. On the other hand, synthetic biomaterials can be divided into four groups: metals, polymers, ceramics and composites and the main advantages and disadvantages of all the groups are present on table 2.3.

Table 2.3. Advantages and disadvantages of synthetic biomaterials [Adapted from (123)].

Biomaterial	Advantages	Disadvantages
Metal	Strong, tough, and ductile	Corrodible, dense, and hard fabrication
Polymers	Resilient and easy fabrication	Fragile, deformable, and degradable
Ceramics	High biocompatibility, inert, and strong in compression	Hard fabrication, brittle, and not resilient
Composites	Strong in compression	Hard fabrication

Metals are essentially used on artificial joints for hips and knees and the most commonly used are stainless steel, pure titanium and, titanium alloys. Polymeric biomaterials are applied in facial prosthesis, tracheal tubes and in medical adhesives and sealants. Polyesters, polytetrafluoroethylenes, and polyurethanes are examples of polymeric biomaterials. On the other hand, due to its poor fracture toughness, the application of ceramics is almost limited to restorative material in dentistry. Finally,

composites are broadly used in prosthetic limbs since their low density/weight and high strength make them suitable for this application (123).

As previous mentioned, after implantation biomaterials will contact with surrounding cells and induce a host response. The human immune system is composed by the innate and adaptive systems that plays an important role in reacting against any foreign materials. Both systems involve several humoral and cellular factors that are crucial to ensure an effective immune response. Figure 2.11 present the cells and proteins that mediate this immune response. The implantation of any biomaterial into the organism may cause a reaction of the immune system called by Foreign Body Reaction/Response (FBR). This reaction is responsible for the formation of a capsule of dense fibrous tissue surrounding the implant, which eventually cause its loss of functionality. In fact, after implantation, host reactions will determine the success of integration and biological performance of the biomaterial (124–127). These reactions involve different steps following the injury associated to the implantation procedure, blood-material interactions, provisional matrix formation, acute and chronic inflammation, granulation tissue development, FBR, and fibrosis/fibrous capsule formation (128).

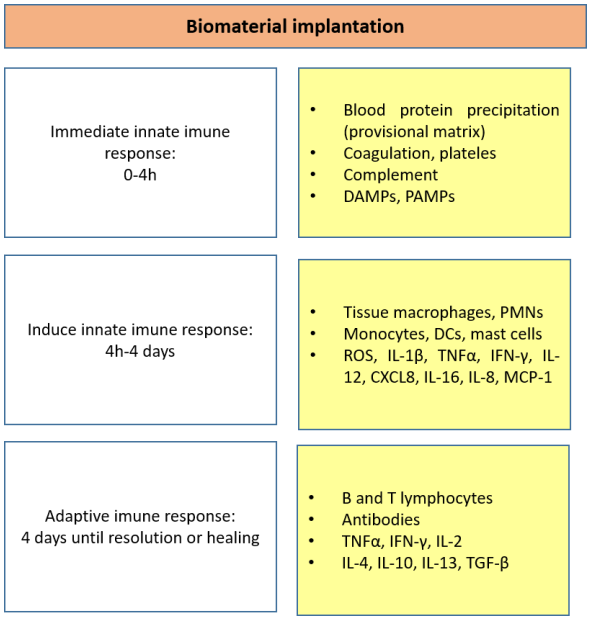

Figure 2.11. Cells and proteins involved in mediating effective immune response [Adapted from (124)].

FBR is a result of a complex interaction between the innate and adaptive immune system which is not yet completely understood. The current understanding of this intricate process encompassed five phases: i) protein adsorption, ii) acute inflammation, iii) chronic inflammations, iv) foreign body giant cell

formation and v) fibrosis or fibrous capsule formation. All the process begins with non-specific protein adsorption on the implant surface, which may lead to complement activation, followed by migration of pro-inflammatory innate immune cells, specifically, neutrophils and macrophages. The protein adsorption is governed by the properties of the biomaterial and the adsorbed proteins may initiate immune-mediated processes that promote the FBR. Soon after implantation, neutrophils appear and they are the primary cell type for the first 2 days after implantation, at which point macrophages that differentiated from infiltrating monocytes become predominant. Neutrophil degranulation is triggered, leading to the secretion of proteolytic enzymes and reactive oxygen species (ROS) intended to killing pathogen infiltration, which may also damage the implant. Meanwhile, the monocytic infiltration induce the secretion of cytokines, such as interleukin-1 (IL-1), IL-8, and chemokines, monocyte chemotactic protein-1 (MCP-1), CXCL13, and macrophage inflammatory protein (MIP). The monocytes can differentiate into macrophages with different phenotypes and polarization states. Macrophages will attempt to internalize the implant, which is not possible when it is too large, yielding the so-called frustrated phagocytosis. The permanent presence of the implant leads to further macrophage differentiation and its fusion into foreign body giant cells (FBGC). The presence of Transforming Growth Factor β (TGf-β), IL-1 and TNF-α seems also to play an important role on the formation of FBGC. TGF-β is also important to induce the transformation of fibroblasts into myofibroblasts, promoting the formation of extracellular matrix and stimulating the contractile state of fibroblasts. In the latter stages of the encapsulation, formation of new blood vessels is induced through the presence of VEFG secreted by myeloid and giant cells. Nevertheless, in the capsule surrounding the implant are also observed other cells such as lymphocytes and B cells (122,124,127–129).

The accurate knowledge about FBR is mandatory and the use of mice with varying degrees of immune perturbations, i.e., genetic knockouts, chemical and/or antibody guided immune cell depletions are very helpful to understand all the process. Regarding this, the most dramatic effect is related to the deletion of macrophages, which eliminates the formation of an FBR completely.

2.4.2 – Biomaterial-associated infections

Another important topic related with the effects of the implantation of biomaterials concerns the biomaterial-associated infections (BAI). BAI are strongly dependent on the presence of a substrate for opportunistic pathogen colonization which culminates into an inflammatory response. As previous described, this inflammatory response is composed by the coagulation cascade, complement system and

the immune cells, which often results in a FBR with granulation tissue formation and fibrotic encapsulation of the implant. The combination between FBR and bacteria creates a dysregulated immune niche more susceptible to bacterial adhesion and infection (130). In fact, depending on the implanted material, the foreign body reaction can induce different phenomena such as: chronic inflammation, granulation tissue development, formation of multinucleated foreign body giant cells, fibrous capsule production and the releasing of reactive oxygen species. Because of that, the host reaction to a foreign material may reduce the effectiveness of the immune system and may induce a refractory period in which bacteria are not properly target, increasing the infection risk (131). In the presence of a foreign body a low number of adhering bacteria could be enough to elicit a BAI. Surface manipulation of implantable biomaterials is one strategy that could be applied in order to control the FBR. Since after implantation, a FBR is generally triggered, surface biomaterial manipulation could modulate macrophage cell response in terms of its function, phenotype and polarization which influences cell shape and elasticity (132). McWhorter et al. investigated the effect of different surface topographies (with 20 to 50 μm grooves) on cell-shape modulation of macrophages and its influence on polarization of M1 (pro-inflammatory) and M2 (pro-healing) phenotypes. The authors found a relation between macrophage elongation itself and the promotion of the M2 phenotype expression. Furthermore, a role of the macrophage cytoskeleton on the macrophage shape-induced polarization was also observed (133).

Beyond the influence of FBR on BAI, the biofilm formation is a consequence of the bacteria adhesion, and it is characterized by a structured group of microorganisms living within a self-produced matrix made up of extracellular polymeric substances (EPS) that can attached on the biomaterials surface (Fig. 2.12). Biofilms can be either mono or multilayered, containing homogenous or heterogeneous populations of bacteria. When a single layered biofilm is present it means that the interactions between cells and the surface are more prominent when compared with interactions between constituent cells. However, a multilayered biofilm is developed when the microorganisms can adhere not only to the surface but also to each other. In all the cases, the biofilm ensures the protection for bacterium from antibiotics, disinfectants, chemical exposure, phagocytosis, pH stress, and dehydration (134–138).

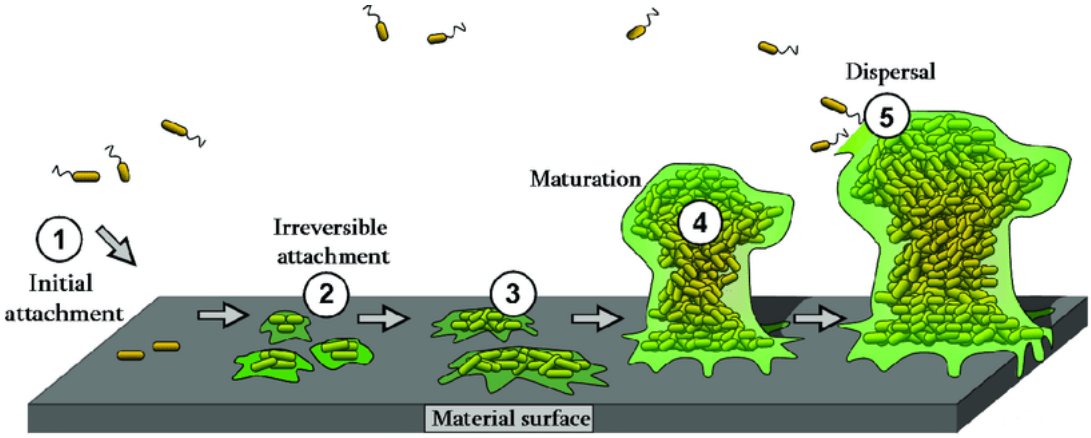

Figure 2.12. Bacterial adhesion to biomaterial surface and the consequent biofilm formation [Adapted from (134)].

In a biofilm environment, the bacteria initiates intercellular communication stimulating the up- and down-regulation of gene expression, which enables the temporal adaption such as phenotypic modification and the ability to survive in low nutrient conditions (135). Biofilm formation is divided into five consecutive stages: i) initial reversible attachment, ii) irreversible attachment, iii) maturation stage I, iv) maturation stage II and v) dispersion. During the first stage, planktonic microbial cells adhere to the biomaterial surface through physical forces (van der Waals forces, steric interactions and electrostatic) and bacterial appendages such as Pilli or flagella. The bacterial adhesion can be modulated by distinct factors such as surface functionality, temperature and pressure. During the second phase, some of the reversibly attached cells become irreversibly immobilized. On this two first stages of biofilm formation, microbial cells firstly loosely associate with the concerned surface, which is then followed by specific and stronger adhesion. On the other hand, on the third stage microbial cells communicate with each other producing autoinducer signals. In this phase, microorganisms secret a matrix of EPS in order to stabilize the biofilm network. In the next stage, microcolonies composed by different microbes increase in size. The close proximity of the cells improves substrate exchange, enhance the distribution of metabolic products and removal of the toxic end products. Therefore, the third and fourth stages are related to cell aggregation and formation of microcolonies followed by the growth and maturation of the adhered cells. Finally, in the last stage, dispersion takes place, whereby the biofilm spreads and colonizes new surfaces. Saccharolytic enzymes produced inside the biofilm will disrupt the EPS, releasing bacteria located on top of the biofilm in order to colonize new surfaces (134,139,140).

Microbial infections on biomedical implants are a big concern in modern medicine, since the biofilm formation is the main responsible to the failure of biomaterial implants. One major problem associated to biofilms is their increased resistance against antimicrobial agents, complicating the treatment of biofilm-related infections (138). All biomedical implants are susceptible to microbial infections and the biofilm infection can induce tissue damage, systemic dissemination of the pathogens and dysfunction of the implant which results in a severe illness and, in some cases, death. Consequently, biomedical implants with a biofilm infection are resistant to immune defense being the treatment with antimicrobial agents ineffective (140). It is pivotal the development of new approaches targeting BAI in order to reduce the negative impact associated to this problematic.

2.4.3 – Topography patterning

When biomaterials/medical devices are implanted, its surface is where interactions between the material and cells - including the microbial community - occurs. Extensive research aiming to mitigate the biofilms formation at the implant-tissue interface has been carried out. Surface engineering arises as a promise alternative to explore and adapt the biomaterial surface properties to meet different requirements. Surface engineering has been widely applied aiming to prevent microbial adhesion and infection and, at the same time, to improve the biocompatibility and functionality of the biomaterials, by controlling the development of FBR. The most significant approaches to create anti-infective biomaterials are related with: i) anti-biofouling surfaces/coatings which are able to prevent bacterial adhesion and subsequent biofilm formation and ii) bactericidal surfaces which release or bear immobilized anti-microbial agents like antibiotics and inorganic metals ions (141,142). These present some side effects and intrinsic limitations, such as bacterial resistance development during antibiotic release, high cytotoxicity in the case of quaternary ammonium salts which induce an immune and inflammatory response and *in vivo* increase of metal ions. The demand for new smart anti-adhesive and anti-biofilm surfaces/coatings is thus necessary. Smart surfaces are characterized by their ability to release active agents “on-demand” in a specific physiological environment or when triggered by external stimuli such as light, temperature, electricity, magnetism, and redox changes. Furthermore, anti-biofilm agents must be able to prevent biofilm formation interfering with its signaling pathways or damaging mature biofilms through its dissolution (142).

Bacterial adhesion to biomedical surfaces is mediated by Van der Waals forces and electrostatic interactions. It can be affected by several factors, including the physical and chemical properties of the

biomaterial surface, topography (area and roughness), free energy, balance of hydrophilicity/hydrophobicity, charge and also by environmental factors such as the bulk medium composition (141–143). The dissociation or protonation of carboxyl, phosphate and amino groups will attribute the bacterial cell surface charge. Under most physiological conditions, it has been assumed that bacteria cell walls are negatively charged, hence their adhesion to negatively charged surfaces is reduced, due to the electrostatic effect (144). Also, the wettability i.e., the influence of hydrophobicity or hydrophilicity, on bacterial adhesion is another important parameter to be addressed. Super hydrophilic to super hydrophobic surfaces are capable to inhibit bacterial adhesion through the formation of trapped liquid/air repellent films on the texturized surfaces acquiring a self-cleaning property (144,145).

The topographical features at micro and nanometer scales offer a promising new methodology to control cell-surface interactions. In fact, bacterial adhesion and biofilm formation is stimulated by the presence of some irregularities on the surface, whereas the smooth surfaces did not encourage the bacterial adhesion. This phenomenon is justified by the fact that a rough surface has a greater surface area where the irregularities provide more favorable sites for bacterial colonization. Researchers attempted mimicking the surface design of natural surfaces which exhibit interesting properties in what concerns cell-surface interactions. Superhydrophobicity, present in several animal skins, plants, and insect wing surfaces among others, is one of those properties, ascribed to the presence of hierarchical or non-hierarchical micro/nano-structured surfaces. Self-cleaning and antibiofouling structured materials are also extensively present in nature, exhibiting surfaces with ability to void of dust, dirt and microorganisms. Shark skin, lotus flower, rice leaves and several insect wings are some examples of surfaces that keep biofouling under control (144,146–148). Biomimetic surfaces, patterned surfaces with micron and sub-micron characteristics have been also investigated against bacterial adhesion. In fact, in the presence of a patterned surface, the bacteria are surrounded by walls, wells, slopes, slants or other geometric curves. The confined surface structures with pillars of defined geometric shapes limit the attachment are able to reduce bacteria adhesion on the biomaterial's surface. Consequently, the interest in fabricating anti-bacterial surfaces with nanoscale topography has been increasing. Photolithography, focused ion beam micromachining, direct writing techniques, or transfer printing are some examples of the several current techniques that can modify surfaces at the micro and nanoscale. Nevertheless, there are some disadvantages related with these techniques, such as the use of toxic chemicals, the need of several steps, sterility is not ensured during the treatment, and the production of hierarchical structures is not always possible. Laser surface texturing (LST; laser texturing, laser structuring or laser patterning) is a potential alternative to these techniques. LST is based on the direct treatment of a surface using a laser

beam and can be performed by the creation of regular or irregular patterns of bumps, dimples, and (linear or non-linear) grooves (Fig. 2.13). It is characterized by the possibility to modify the surface roughness and chemistry in several materials without using toxic substances, enabling the selective design of distinct micro and nano-topographic patterns with high reproducibility. Furthermore, it is a high processing-speed methodology with a low risk of surface contamination due to the absence of direct contact during the process (149).

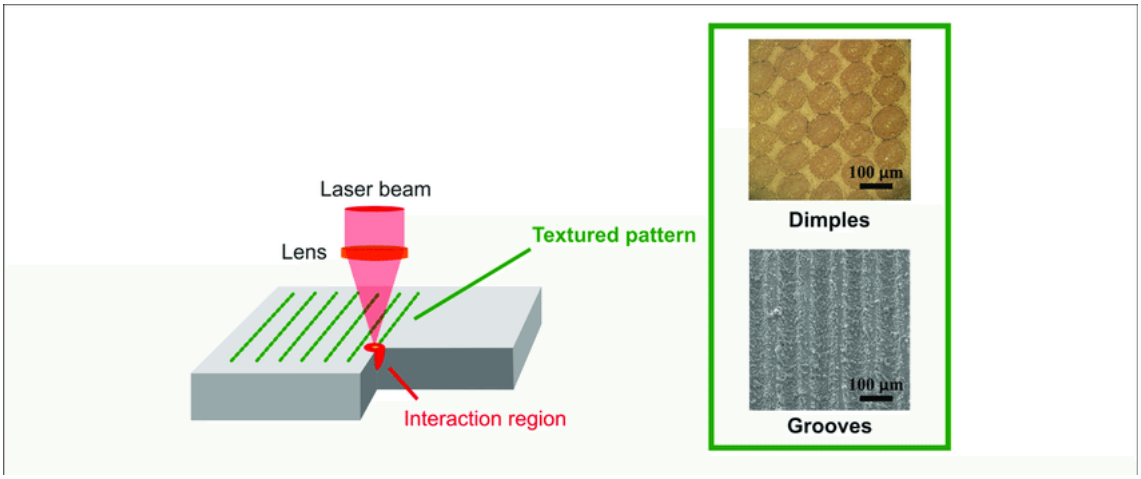

Figure 2.13. Schematic representation of laser surface texturing operation [Adapted from (149)].

The definition of micro and nano-structures on the substrates can be achieved using different lithographic methods. "Soft lithography" is essentially applied to create chemical structures on surfaces that controls the cell-substrate interactions. Soft-lithography is not related with one specific method but rather a group of techniques with the common feature that, during the process, an elastomeric ("soft") material is used to produce the chemical structures (150,151). One of the most relevant limitation of this technique is the requirement of another lithography method, such as photolithography or e-beam lithography, to fabricate the stamp master. Nevertheless, when the master is fabricated, it can be used continuously to produce the stamps. Due to its elasticity, PDMS is usually applied for this purpose. Despite its limitations, soft lithography is less expensive and have been widely applied to transfer micro and nano-antibacterial patterns into polymer substrates through replica molding techniques (152,153). Guided-assembly based-biolithography techniques have been applied to produce distinct topographical features on BC substrates. This way, distinct surface geometries were introduced on BC, such as symmetric arrays of hexagonal pits in the micron range (Fig. 2.14), which influenced the adhesion of cells related with FBR, including fibroblasts and macrophages. Furthermore, a parametric optimization of the pit dimensions and

also of the spatial arrangement on BC substrates was performed, allowing the control of the adhesion and differentiation of the cellular mediators and actuators of fibrosis (154,155).

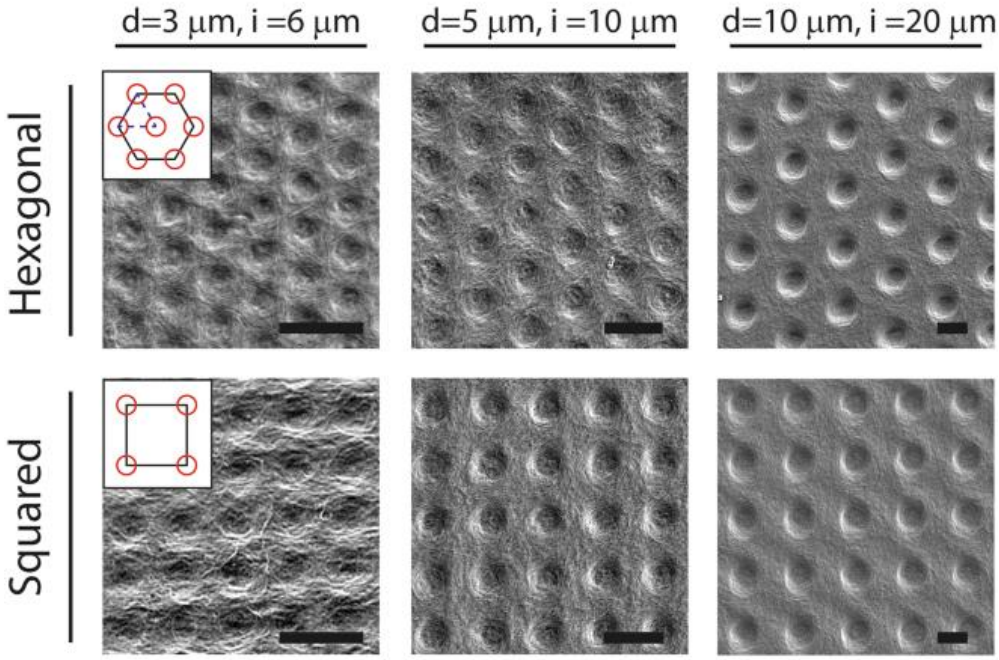

Figure 2.14. Cell morphology on surface structured BC using hexagonal and squared patterns [Adapted from (155)].

Based on these works, Robotti et al. (2020), developed a micro-engineered BC coating for cardiac implantable electronic devices. A set of micro-wells arranged in a hexagonal pattern were created on a BC substrate which was used to coat a cardiac implant. This strategy was proven to reduce by 66% the thickness of the fibrotic tissue around the implant, both the generator and the proximal parts of the leads remaining fully free from fibrotic tissue (156).

Other works have been developed based on BC patterning with laser (157–159). Although BC is considered a promising nanoscaffold for tissue engineering, the absence of large pores for cell ingrowth is a limitation. Thus, laser patterning was used to create regular vertical pore arrays in order to obtain novel porous BC membranes with large pores. The biological properties were also improved through the BC membranes modification with gelatin and hydroxyapatite, making this novel material a suitable alternative in bone tissue engineering fields (157). In the same field, Ahrem et al. (2014) used 3D laser perforation of never-dried BC hydrogels to increase the size and heterogeneity of the pores. Laser perforation slightly performed structural modifications (i.e., fiber or globular aggregates), but did not induce any chemical modifications. Furthermore, the resulting channels supported cell migration into the BC hydrogels, the matrix production and phenotypic stabilization of chondrocytes (158). More recently,

Hu et al. (2019) used low-energy CO_2 laser photolithography to construct a crossed groove/column micropattern on the BC surface, where the tetrapeptide Arginine-Glycine-Aspartic acid-Serine (RGDS) was immobilized, improving the affinity to fibroblasts. After hydrating, the new formulation did not damage the integrity of the micropattern, suggesting its potential to be applied in a highly hydrated environment. Moreover, the crossed groove/column micropattern structure on the BC showed dual affinities to human skin fibroblasts cells and collagen which allowed not only the cell migration but also the manipulation of collagen distribution (159).

To sum up, surface topography may be used to control cell behavior on surfaces, specifically cell adhesion, spreading, proliferation and differentiation. Similarly, surface engineering is an important tool to create anti-biofouling/bactericidal surface topographies on biomaterial implants. Thus, when a biomaterial is conceived for implantation in a permanent way, it is mandatory to find a balance between the repellency ability of the surface against bacteria cell adhesion and surface adhesive properties that are crucial to host tissue integration of implanted biomaterials.

2.5 – References

1. Huang Y, Zhu C, Yang J, Nie Y, Chen C, Sun D. Recent advances in bacterial cellulose. Cellulose. 2014;21(1):1–30.
2. Mondal MIH. Mechanism of structure formation of microbial cellulose during nascent stage. Cellulose. 2013;20(3):1073–88.
3. Foresti ML, Vázquez A, Boury B. Applications of bacterial cellulose as precursor of carbon and composites with metal oxide, metal sulfide and metal nanoparticles: A review of recent advances. Vol. 157, Carbohydrate Polymers. Elsevier Ltd; 2017. p. 447–67.
4. Wang J, Tavakoli J, Tang Y. Bacterial cellulose production, properties and applications with different culture methods – A review. Vol. 219, Carbohydrate Polymers. Elsevier Ltd; 2019. p. 63–76.
5. Uzyol HK, Saçan MT. Bacterial cellulose production by Komagataeibacter hansenii using algae-based glucose. Environ Sci Pollut Res. 2017;24(12):11154–62.
6. Cacicedo ML, Castro MC, Servetas I, Bosnea L, Boura K, Tsafrakidou P, et al. Progress in bacterial

cellulose matrices for biotechnological applications. Vol. 213, Bioresource Technology. Elsevier Ltd; 2016 p. 172–80.

7. Klemm D, Heublein B, Fink HP, Bohn A. Cellulose: Fascinating biopolymer and sustainable raw material. Angew Chemie - Int Ed. 2005;44(22):3358–93.

8. Jozala AF, Pértile RAN, dos Santos CA, de Carvalho Santos-Ebinuma V, Seckler MM, Gama FM, et al. Bacterial cellulose production by Gluconacetobacter xylinus by employing alternative culture media. Appl Microbiol Biotechnol. 2014;99(3):1181–90.

9. Chen G, Wu G, Chen L, Wang W, Hong FF, Jönsson LJ. Performance of nanocellulose-producing bacterial strains in static and agitated cultures with different starting pH. Carbohydr Polym. 2019 Jul 1;215:280–8.

10. Ullah MW, Manan S, Kiprono SJ, Ul-Islam M, Yang G. Synthesis, Structure, and Properties of Bacterial Cellulose. In: Nanocellulose. Weinheim, Germany: Wiley-VCH Verlag GmbH & Co. KGaA; 2019 p. 81–113.

11. Torres FG, Arroyo JJ, Troncoso OP. Bacterial cellulose nanocomposites: An all-nano type of material. Vol. 98, Materials Science and Engineering C. Elsevier Ltd; 2019. p. 1277–93.

12. Portela R, Leal CR, Almeida PL, Sobral RG. Bacterial cellulose: a versatile biopolymer for wound dressing applications. Microb Biotechnol. 2019 ;12(4):586–610.

13. Eslahi N, Mahmoodi A, Mahmoudi N, Zandi N, Simchi A. Processing and Properties of Nanofibrous Bacterial Cellulose-Containing Polymer Composites: A Review of Recent Advances for Biomedical Applications. Vol. 60, Polymer Reviews. Taylor and Francis Inc.; 2020. p. 144–70.

14. Trache D, Hussin MH, Haafiz MKM, Thakur VK. Recent progress in cellulose nanocrystals: sources and production. Nanoscale. 2017;9(5):1763–86.

15. de Olyveira GM, Costa LMM, Riccardi C dos S, Santos ML dos, Daltro PB, Basmaji P, et al. Bacterial cellulose for advanced medical materials. In: Nanobiomaterials in Soft Tissue Engineering. Elsevier; 2016 p. 57–82.

16. Saffarionpour S. Nanocellulose for Stabilization of Pickering Emulsions and Delivery of Nutraceuticals and Its Interfacial Adsorption Mechanism. Food Bioprocess Technol 2020 138. 2020 ;13(8):1292–328.

17. Keshk SMAS, El-Kott AF. Natural bacterial biodegradable medical polymers: bacterial cellulose.

In: Science and Principles of Biodegradable and Bioresorbable Medical Polymers. 2007.

18. da Silva Perez D, Montanari S, Vignon MR. TEMPO-mediated oxidation of cellulose III. Biomacromolecules. 2003;4(5):1417–25.

19. Helenius G, Bäckdahl H, Bodin A, Nannmark U, Gatenholm P, Risberg B. In vivo biocompatibility of bacterial cellulose. J Biomed Mater Res - Part A. 2006;76(2):431–8.

20. Pértile RAN, Moreira S, Gil RM, Correia A, Guãrdao L. Bacterial Cellulose : Long-Term Biocompatibility Studies. J Biomater Sci Polym Ed. 2013;23(10):1339–54.

21. Zhou D, Sun Y, Bao Z, Liu W, Xian M, Nian R, et al. Improved Cell Viability and Biocompatibility of Bacterial Cellulose through in Situ Carboxymethylation. Macromol Biosci. 2019;19(5).

22. Zhang C, Cao J, Zhao S, Luo H, Yang Z, Gama M, et al. Biocompatibility evaluation of bacterial cellulose as a scaffold material for tissue-engineered corneal stroma. Cellulose. 2020;27(5):2775–84.

23. Fu LH, Qi C, Ma MG, Wan P. Multifunctional cellulose-based hydrogels for biomedical applications. Vol. 7, Journal of Materials Chemistry B. Royal Society of Chemistry; 2019. p. 1541–62.

24. Camy S, Montanari S, Rattaz A, Vignon M, Condoret JS. Oxidation of cellulose in pressurized carbon dioxide. J Supercrit Fluids. 2009;51(2):188–96.

25. Liao SB, Xi TF, Lai C, Liao SY, Huang T, Wang SY. TEMPO-mediated oxidation of bacterial cellulose in a bromide-free system. Colloid Polym Sci. 2013;32(6):699–707.

26. Martins D, de Carvalho Ferreira D, Gama M, Dourado F. Dry Bacterial Cellulose and Carboxymethyl Cellulose formulations with interfacial-active performance: processing conditions and redispersion. Cellulose. 2020;27(11):6505–20.

27. Martins D, Estevinho B, Rocha F, Dourado F, Gama M. A dry and fully dispersible bacterial cellulose formulation as a stabilizer for oil-in-water emulsions. Carbohydr Polym. 2020 Feb 15;230:115657.

28. Hestrin S, Schramm M. Synthesis of cellulose by Acetobacter xylinum. II. Preparation of freeze-dried cells capable of polymerizing glucose to cellulose. Biochem J. 1954;58(2):345–52.

29. Campano C, Balea A, Blanco A, Negro C. Enhancement of the fermentation process and properties of bacterial cellulose: a review. Vol. 23, Cellulose. Springer Netherlands; 2016. p. 57–91.

30. de Amorim JDP, de Souza KC, Duarte CR, da Silva Duarte I, de Assis Sales Ribeiro F, Silva GS, et al. Plant and bacterial nanocellulose: production, properties and applications in medicine, food, cosmetics, electronics and engineering. A review. Vol. 18, Environmental Chemistry Letters. Springer; 2020. p. 851–69.

31. Blanco Parte FG, Santoso SP, Chou CC, Verma V, Wang HT, Ismadji S, et al. Current progress on the production, modification, and applications of bacterial cellulose. Vol. 40, Critical Reviews in Biotechnology. Taylor and Francis Ltd; 2020. p. 397–414.

32. Chawla PR, Bajaj IB, Survase SA, Singhal RS. Microbial Cellulose: Fermentative Production and Applications.

33. Czaja W, Romanovicz D, Brown, R malcolm. Structural investigations of microbial cellulose produced in stationary and agitated culture. Cellulose. 2004 Oct 30;11(3/4):403–11.

34. Hu Y, Catchmark JM. Studies on sphere-like bacterial cellulose produced by Acetobacter xylinum under agitated culture. In: American Society of Agricultural and Biological Engineers Annual International Meeting 2010, ASABE 2010. American Society of Agricultural and Biological Engineers; 2010. p. 1771–81.

35. Liu D, Yang F, Xiong F, Gu N. The smart drug delivery system and its clinical potential. Theranostics. 2016;6(9):1306–23.

36. Abeer MM, Mohd Amin MCI, Martin C. A review of bacterial cellulose-based drug delivery systems: Their biochemistry, current approaches and future prospects. J Pharm Pharmacol. 2014;66(8):1047–61.

37. Trovatti E, Silva NHCS, Duarte IF, Rosado CF, Almeida IF, Costa P, et al. Biocellulose membranes as supports for dermal release of lidocaine. Biomacromolecules. 2011;12(11):4162–8.

38. Trovatti E, Freire CSR, Pinto PC, Almeida IF, Costa P, Silvestre AJD, et al. Bacterial cellulose membranes applied in topical and transdermal delivery of lidocaine hydrochloride and ibuprofen: In vitro diffusion studies. Int J Pharm. 2012;435(1):83–7.

39. Silva NHCS, Drumond I, Almeida IF, Costa P, Rosado CF, Neto CP, et al. Topical caffeine delivery using biocellulose membranes: A potential innovative system for cellulite treatment. Cellulose. 2014;21(1):665–74.

40. Silva NHCS, Rodrigues AF, Almeida IF, Costa PC, Rosado C, Neto CP, et al. Bacterial cellulose

membranes as transdermal delivery systems for diclofenac: In vitro dissolution and permeation studies. Carbohydr Polym. 2014;106(1):264–9.

41. Silva NHCS, Mota JP, de Almeida TS, Carvalho JPF, Silvestre AJD, Vilela C, et al. Topical drug delivery systems based on bacterial nanocellulose: Accelerated stability testing. Int J Mol Sci. 2020;21(4).

42. Müller A, Ni Z, Hessler N, Wesarg F, Müller F, Kralisch D, et al. The Biopolymer Bacterial Nanocellulose as Drug Delivery System: Investigation of Drug Loading and Release using the Model Protein Albumin. J Pharm Sci. 2013;102(2):579–92.

43. Moritz S, Wiegand C, Wesarg F, Hessler N, Müller FA, Kralisch D, et al. Active wound dressings based on bacterial nanocellulose as drug delivery system for octenidine. Int J Pharm. 2014;471(1–2):45–55.

44. Li Y, Zhao X, Liu Y, Yang J, Zhang Q, Wang L, et al. Melatonin loaded with bacterial cellulose nanofiber by Pickering-emulsion solvent evaporation for enhanced dissolution and bioavailability. Int J Pharm. 2019;559:393–401.

45. Gao C, Wan Y, Yang C, Dai K, Tang T, Luo H, et al. Preparation and characterization of bacterial cellulose sponge with hierarchical pore structure as tissue engineering scaffold. J Porous Mater. 2011 Apr 20;18(2):139–45.

46. Halib N, Ahmad I, Grassi M, Grassi G. The remarkable three-dimensional network structure of bacterial cellulose for tissue engineering applications. Int J Pharm. 2019;566:631–40.

47. Kirdponpattara S, Khamkeaw A, Sanchavanakit N, Pavasant P, Phisalaphong M. Structural modification and characterization of bacterial cellulose-alginate composite scaffolds for tissue engineering. Carbohydr Polym. 2015 Jul 3;132:146–55.

48. Khan S, Ul-Islam M, Ikram M, Ullah MW, Israr M, Subhan F, et al. Three-dimensionally microporous and highly biocompatible bacterial cellulose-gelatin composite scaffolds for tissue engineering applications. RSC Adv. 2016 Nov 21;6(112):110840–9.

49. Osorio M, Ortiz I, Gañán P, Naranjo T, Zuluaga R, van Kooten TG, et al. Novel surface modification of three-dimensional bacterial nanocellulose with cell-derived adhesion proteins for soft tissue engineering. Mater Sci Eng C. 2019;100:697–705.

50. Klinthoopthamrong N, Chaikiawkeaw D, Phoolcharoen W, Rattanapisit K, Kaewpungsup P,

Pavasant P, et al. Bacterial cellulose membrane conjugated with plant-derived osteopontin: Preparation and its potential for bone tissue regeneration. Int J Biol Macromol. 2020;149:51–9.

51. Amnuaikit T, Chusuit T, Raknam P, Boonme P. Effects of a cellulose mask synthesized by a bacterium on facial skin characteristics and user satisfaction. Med Devices Evid Res. 2011;4(1):77–81.

52. Pacheco G, de Mello CV, Chiari-Andréo BG, Isaac VLB, Ribeiro SJL, Pecoraro É, et al. Bacterial cellulose skin masks—Properties and sensory tests. J Cosmet Dermatol. 2018;17(5):840–7.

53. Perugini P, Bleve M, Redondi R, Cortinovis F, Colpani A. In vivo evaluation of the effectiveness of biocellulose facial masks as active delivery systems to skin. J Cosmet Dermatol. 2020 Mar 1;19(3):725–35.

54. Amorim JDP De, Junior CJG, Costa AFDS, Nascimento H, Vinhas GM, Sarubbo LA. Biomask, a Polymer Blend for Treatment and Healing of Skin Prone to Acne. Chem Eng Trans. 2020 Apr 1;79:205–10.

55. Klemm D, Schumann D, Udhardt U, Marsch S. Bacterial synthesized cellulose - Artificial blood vessels for microsurgery. Vol. 26, Progress in Polymer Science (Oxford). Elsevier Ltd; 2001. p. 1561–603.

56. Schumann DA, Wippermann J, Klemm DO, Kramer F, Koth D, Kosmehl H, et al. Artificial vascular implants from bacterial cellulose: Preliminary results of small arterial substitutes. Cellulose. 2009 Dec 11;16(5):877–85.

57. Andrade FK, Costa R, Domingues L, Soares R, Gama M. Improving bacterial cellulose for blood vessel replacement: Functionalization with a chimeric protein containing a cellulose-binding module and an adhesion peptide. Acta Biomater. 2010;6(10):4034–41.

58. Tang J, Bao L, Li X, Chen L, Hong FF. Potential of PVA-doped bacterial nano-cellulose tubular composites for artificial blood vessels. J Mater Chem B. 2015 Sep 17;3(43):8537–47.

59. Leitão AF, Faria MA, Faustino AMR, Moreira R, Mela P, Loureiro L, et al. A Novel Small-Caliber Bacterial Cellulose Vascular Prosthesis: Production, Characterization, and Preliminary in Vivo Testing. Macromol Biosci. 2016 Jan 1;16(1):139–50.

60. Li X, Tang J, Bao L, Chen L, Hong FF. Performance improvements of the BNC tubes from unique double-silicone-tube bioreactors by introducing chitosan and heparin for application as small-

diameter artificial blood vessels. Carbohydr Polym. 2017 Dec 15;178:394–405.

61. Dhivya S, Padma V, Santhini E. Wound dressings - a review. BioMedicine. 2015;5(4):24–8.

62. Gonzalez AC de O, Costa TF, Andrade Z de A, Medrado ARAP. Wound healing - A literature review. An Bras Dermatol. 2016;91(5):614–20.

63. Gurtner GC, Werner S, Barrandon Y, Longaker MT. Wound repair and regeneration. Nature. 2008;453(7193):314–21.

64. Chawla PR, Bajaj IB, Survase S a., Singhal RS. Microbial cellulose: Fermentative production and applications. Food Technol Biotechnol. 2009;47(2):107–24.

65. Kwak MH, Kim JE, Go J, Koh EK, Song SH, Son HJ, et al. Bacterial cellulose membrane produced by Acetobacter sp. A10 for burn wound dressing applications. Carbohydr Polym. 2015;122:387–98.

66. Pandey M, Mohamad N, Low WL, Martin C, Mohd Amin MCI. Microwaved bacterial cellulose-based hydrogel microparticles for the healing of partial thickness burn wounds. Drug Deliv Transl Res. 2017;7(1):89–99.

67. Fürsatz M, Skog M, Sivlér P, Palm E, Aronsson C, Skallberg A, et al. Functionalization of bacterial cellulose wound dressings with the antimicrobial peptide ε-poly-L-Lysine. Biomed Mater. 2018;13(2):025014.

68. Loh EYX, Mohamad N, Fauzi MB, Ng MH, Ng SF, Mohd Amin MCI. Development of a bacterial cellulose-based hydrogel cell carrier containing keratinocytes and fibroblasts for full-thickness wound healing. Sci Rep. 2018 Dec 1;8(1):1–12.

69. Ciecholewska-Juśko D, Żywicka A, Junka A, Drozd R, Sobolewski P, Migdał P, et al. Superabsorbent crosslinked bacterial cellulose biomaterials for chronic wound dressings. 2020;1–40.

70. Greaves NS, Iqbal SA, Baguneid M, Bayat A. The role of skin substitutes in the management of chronic cutaneous wounds. Wound Repair Regen. 2013;21(2):194–210.

71. Augustine R, Kalarikkal N, Thomas S. Advancement of wound care from grafts to bioengineered smart skin substitutes. Prog Biomater. 2014;3(2–4):103–13.

72. Shores JT, Gabriel A, Gupta S. Skin Substitutes and Alternatives. Adv Skin Wound Care.

2007;20(9):493–508.

73. Sun BK, Siprashvili Z, Khavari PA. Advances in skin grafting and treatment of cutaneous wounds. Science (80). 2014;346(6212):941–5.

74. Boateng J, Matthews K, Stevens H, Gillian E. Wound Healing Dressings and Drug Delivery Systems: A Review. J Pharm Sci. 2008;97(2):2892–923.

75. Gorgieva, Trček. Bacterial Cellulose: Production, Modification and Perspectives in Biomedical Applications. Nanomaterials. 2019;9(10):1352.

76. Stassen JM, Arnout J, Deckmyn H. The hemostatic system. Curr Med Chem. 2004;11(17):2245–60.

77. Gale AJ. Current Understanding of Hemostasis. Toxicol Pathol. 2011;39(1):273–80.

78. Monagle P, Massicotte P. Developmental haemostasis: Secondary haemostasis. Semin Fetal Neonatal Med. 2011;16(6):294–300.

79. Palta S, Saroa R, Palta A. Overview of the coagulation system. Indian J Anaesth. 2014;58(5):515–23.

80. Samudrala S. Topical Hemostatic Agents in Surgery: A Surgeon's Perspective. AORN J. 2008;88(3):2–11.

81. Kraft P, De Meyer SF, Kleinschnitz C. Next-generation antithrombotics in ischemic stroke: Preclinical perspective on bleeding-free antithrombosis. J Cereb Blood Flow Metab. 2012;32(10):1831–40.

82. Vogler EA, Siedlecki CA. Contact activation of blood-plasma coagulation. Biomaterials. 2009;30(10):1857–69.

83. Yang X, Liu W, Li N, Wang M, Liang B, Ullah I, et al. Design and development of polysaccharide hemostatic materials and their hemostatic mechanism. Vol. 5, Biomaterials Science. Royal Society of Chemistry; 2017. p. 2357–68.

84. Hickman DSA, Pawlowski CL, Sekhon UDS, Marks J, Gupta A Sen. Biomaterials and Advanced Technologies for Hemostatic Management of Bleeding. Vol. 30, Advanced Materials. Wiley-VCH Verlag; 2018.

85. Samudrala S. Topical Hemostatic Agents in Surgery: A Surgeon's Perspective. AORN J.

2008;88(3):S2-11.

86. Palm MD, Altman JS. Topical hemostatic agents: A review. Vol. 34, Dermatologic Surgery. 2008. p. 431–45.

87. Bracey A, Shander A, Aronson S, Boucher BA, Calcaterra D, Chu MWA, et al. The Use of Topical Hemostatic Agents in Cardiothoracic Surgery. Vol. 104, Annals of Thoracic Surgery. Elsevier USA; 2017. p. 353–60.

88. Ito TE, Martin AL, Henderson EF, Gaskins JT, Vaughn VM, Biscette SM, et al. Systematic Review of Topical Hemostatic Agent Use in Minimally Invasive Gynecologic Surgery. JSLS J Soc Laparoendosc Surg. 2018 Oct 1;22(4).

89. Tompeck AJ, Gajdhar AUR, Dowling M, Johnson SB, Barie PS, Winchell RJ, et al. A comprehensive review of topical hemostatic agents: The good, the bad, and the novel. Vol. 88, Journal of Trauma and Acute Care Surgery. Lippincott Williams and Wilkins; 2020. p E1–21.

90. Behrens AM, Sikorski MJ, Li T, Wu ZJ, Griffith BP, Kofinas P. Blood-aggregating hydrogel particles for use as a hemostatic agent. Acta Biomater. 2014;10(2):701–8.

91. Sirlak M, Eryilmaz S, Yazicioglu L, Kiziltepe U, Eyileten Z, Durdu MS, et al. Comparative study of microfibrillar collagen hemostat (Colgel) and oxidized cellulose (Surgicel) in high transfusion-risk cardiac surgery. J Thorac Cardiovasc Surg. 2003 Sep 1;126(3):666–70.

92. Achneck HE, Sileshi B, Jamiolkowski RM, Albala DM, Shapiro ML, Lawson JH. A comprehensive review of topical hemostatic agents: Efficacy and recommendations for use. Vol. 251, Annals of Surgery. 2010 p. 217–28.

93. Kaur R, Siegel D, Glick J. Achieving hemostasis in dermatology-Part II: Topical hemostatic agents. Indian Dermatol Online J. 2013;4(3):172.

94. Yang X, Liu W, Li N, Wang M, Liang B, Ullah I, et al. Design and development of polysaccharide hemostatic materials and their hemostatic mechanism. Vol. 5, Biomaterials Science. Royal Society of Chemistry; 2017 p. 2357–68.

95. Ryšavá J, Dyr JE, Homola J, Dostálek J, Křížová P, Mášová L, et al. Surface interactions of oxidized cellulose with fibrin(ogen) and blood platelets. In: Sensors and Actuators, B: Chemical. Elsevier; 2003. p. 243–9.

96. Demirekin ZB, Sezer UA, Karatopuk DU, Sezer S. Development of Metal Ion Binded Oxidized

Regenerated Cellulose Powder as Hemostatic Agent: A Comparative Study with in Vivo Performance. Ind Eng Chem Res. 2015 May 13;54(18):4906–14.

97. Hickman DSA, Pawlowski CL, Sekhon UDS, Marks J, Gupta A Sen. Biomaterials and Advanced Technologies for Hemostatic Management of Bleeding. Vol. 30, Advanced Materials. Wiley-VCH Verlag; 2018.

98. Royds J, Kieran S, Timon C. Oxidized cellulose (Surgicel) based reaction post thyroidectomy mimicking an abscess: A case report. Int J Surg Case Rep. 2012 Jan 1;3(7):338–9.

99. Wang H, Chen P. Surgicel® (oxidized regenerated cellulose) granuloma mimicking local recurrent gastrointestinal stromal tumor: A case report. Oncol Lett. 2013 Oct;5(5):1497–500.

100. Ibrahim MF, Aps C, Young CP. A foreign body reaction to Surgicel mimicking an abscess following cardiac surgery. Eur J Cardiothorac Surg. 2002.22(3):489–90;

101. Lin B, Yang H, Cui M, Li Y, Yu J. Surgicel™ application in intracranial hemorrhage surgery contributed to giant-cell granuloma in a patient with hypertension: case report and review of the literature. World J Surg Oncol. 2014;12(1):101.

102. Brodbelt AR, Miles JB, Foy PM, Broome JC. Intraspinal oxidised cellulose (Surgicel) causing delayed paraplegia after thoracotomy–a report of three cases. Ann R Coll Surg Engl. 2002;84(2):97.

103. Banerjee T, Goldschmidt K. "Surgiceloma" manifested as cauda equina syndrome. South Med J. 1998;91(5):481–3.

104. Vosmanska V, Kolarova K, Rimpelova S, Svorcik V. Surface modification of oxidized cellulose haemostat by argon plasma treatment. Cellulose. 2014 Jun 15;21(4):2445–56.

105. Sukul M, Ventura RD, Bae SH, Choi HJ, Lee SY, Lee BT. Plant-derived oxidized nanofibrillar cellulose-chitosan composite as an absorbable hemostat. Mater Lett. 2017 Jun 15;197:150–5.

106. Cheng F, Wu Y, Li H, Yan T, Wei X, Wu G, et al. Biodegradable N, O-carboxymethyl chitosan/oxidized regenerated cellulose composite gauze as a barrier for preventing postoperative adhesion. Carbohydr Polym. 2019;207:180–90.

107. Lai C, Sheng L, Liao S, Xi T, Zhang Z. Surface characterization of TEMPO-oxidized bacterial cellulose. Surf Interface Anal. 2013;45(11):1673–9.

108. Potthast A, Kostic M, Schiehser S, Kosma P, Rosenau T. Studies on oxidative modifications of cellulose in the periodate system: Molecular weight distribution and carbonyl group profiles. Holzforschung. 2007;61(6):662–7.

109. Quintana E, Roncero MB, Vidal T, Valls C. Cellulose oxidation by Laccase-TEMPO treatments. Carbohydr Polym. 2017;157:1488–95.

110. Calvini P, Gorassini A, Luciano G, Franceschi E. FTIR and WAXS analysis of periodate oxycellulose: Evidence for a cluster mechanism of oxidation. Vib Spectrosc. 2006;40(2):177–83.

111. Isogai A, Saito T, Fukuzumi H. TEMPO-oxidized cellulose nanofibers. Vol. 3, Nanoscale. The Royal Society of Chemistry; 2011. p. 71–85.

112. Parpot P, Servat K, Bettencourt AP, Huser H, Kokoh KB. TEMPO mediated oxidation of carbohydrates using electrochemical methods. Cellulose. 2010;17(4):815–24.

113. Carlsson DO, Lindh J, Nyholm L, Stromme M, Mihranyan A, Strømme M, et al. Cooxidant-free TEMPO-mediated oxidation of highly crystalline nanocellulose in water. RSC Adv. 2014;4(94):52289–98.

114. Bragd PL, van Bekkum H, Besemer AC. TEMPO-Mediated Oxidation of Polysaccharides: Survey of Methods and Applications. Top Catal. 2004;27(1–4):49–66.

115. Saito T, Nishiyama Y, Putaux JL, Vignon M, Isogai A. Homogeneous suspensions of individualized microfibrils from TEMPO-catalyzed oxidation of native cellulose. Biomacromolecules. 2006;7(6):1687–91.

116. Saito T, Kimura S, Nishiyama Y, Isogai A. Cellulose nanofibers prepared by TEMPO-mediated oxidation of native cellulose. Biomacromolecules. 2007;8(8):2485–91.

117. Okita Y, Saito T, Isogai A. Entire surface oxidation of various cellulose microfibrils by TEMPO-mediated oxidation. Biomacromolecules. 2010 Jul 14;11(6):1696–700.

118. Wu CN, Cheng KC. Strong, thermal-stable, flexible, and transparent films by self-assembled TEMPO-oxidized bacterial cellulose nanofibers. Cellulose. 2017 Jan 1;24(1):269–83.

119. Zhang S, Li J, Chen S, Zhang X, Ma J, He J. Oxidized cellulose-based hemostatic materials. Vol. 230, Carbohydrate Polymers. Elsevier Ltd; 2020. p. 115585.

120. Williams DF. On the nature of biomaterials. Biomaterials. 2009;30(30):5897–909.

121. Sarkar K, Xue Y, Sant S. Host response to synthetic versus natural biomaterials. In: The Immune Response to Implanted Materials and Devices: The Impact of the Immune System on the Success of an Implant. Springer International Publishing; 2016. p. 81–105.

122. Franz S, Rammelt S, Scharnweber D, Simon JC. Immune responses to implants - A review of the implications for the design of immunomodulatory biomaterials. Vol. 32, Biomaterials. 2011. p. 6692–709.

123. Aramwit P. Introduction to biomaterials for wound healing. In: Wound Healing Biomaterials. Elsevier Inc.; 2016. p. 3–38.

124. Vishwakarma A, Bhise NS, Evangelista MB, Rouwkema J, Dokmeci MR, Ghaemmaghami AM, et al. Engineering Immunomodulatory Biomaterials To Tune the Inflammatory Response. Vol. 34, Trends in Biotechnology. Elsevier Ltd; 2016. p. 470–82.

125. Klopfleisch R, Jung F. The pathology of the foreign body reaction against biomaterials. Vol. 105, Journal of Biomedical Materials Research - Part A. John Wiley and Sons Inc.; 2017. p. 927–40.

126. Jewell CM, Collier JH. Biomaterial interactions with the immune system. Vol. 7, Biomaterials Science. Royal Society of Chemistry; 2019. p. 713–4.

127. Veiseh O, Vegas AJ. Domesticating the foreign body response: Recent advances and applications. Vol. 144, Advanced Drug Delivery Reviews. Elsevier B.V.; 2019. p. 148–61.

128. Anderson JM, Rodriguez A, Chang DT. Foreign body reaction to biomaterials. Vol. 20, Seminars in Immunology. 2008. p. 86–100.

129. Chung L, Maestas DR, Housseau F, Elisseeff JH. Key players in the immune response to biomaterial scaffolds for regenerative medicine. Vol. 114, Advanced Drug Delivery Reviews. Elsevier B.V.; 2017. p. 184–92.

130. Zaat S, Broekhuizen C, Riool M. Host tissue as a niche for biomaterial-associated infection. Vol. 5, Future Microbiology. 2010. p. 1149–51.

131. Daghighi S, Sjollema J, van der Mei HC, Busscher HJ, Rochford ETJ. Infection resistance of degradable versus non-degradable biomaterials: An assessment of the potential mechanisms. Biomaterials. 2013;34(33):8013–7.

132. Sridharan R, Cameron AR, Kelly DJ, Kearney CJ, O'Brien FJ. Biomaterial based modulation of macrophage polarization: a review and suggested design principles. Mater Today. 2015 Jul

1;18(6):313–25.

133. McWhorter FY, Wang T, Nguyen P, Chung T, Liu WF. Modulation of macrophage phenotype by cell shape. Proc Natl Acad Sci. 2013; 110(43):17253–8.

134. Moriarty TF, Grainger DW, Richards RG. Challenges in linking preclinical anti-microbial research strategies with clinical outcomes for device-associated infections. Eur Cells Mater. 2014;28:112–28.

135. Alam F, Kumar S, Varadarajan KM. Quantification of Adhesion Force of Bacteria on the Surface of Biomaterials: Techniques and Assays. ACS Biomater Sci Eng. 2019 May 13;5(5):2093–110.

136. Santhosh Kumar S, Hiremath SS, Ramachandran B, Muthuvijayan V. Effect of Surface Finish on Wettability and Bacterial Adhesion of Micromachined Biomaterials. Biotribology. 2019 Jun 1;18:100095.

137. Arciola CR, Campoccia D, Montanaro L. Implant infections: Adhesion, biofilm formation and immune evasion. Vol. 16, Nature Reviews Microbiology. Nature Publishing Group; 2018. p. 397–409.

138. Satpathy S, Sen SK, Pattanaik S, Raut S. Review on bacterial biofilm: An universal cause of contamination. Vol. 7, Biocatalysis and Agricultural Biotechnology. Elsevier Ltd; 2016. p. 56–66.

139. Gupta P, Sarkar S, Das B, Bhattacharjee S, Tribedi P. Biofilm, pathogenesis and prevention—a journey to break the wall: a review. Vol. 198, Archives of Microbiology. Springer Verlag; 2016. p. 1–15.

140. Veerachamy S, Yarlagadda T, Manivasagam G, Yarlagadda PK. Bacterial adherence and biofilm formation on medical implants: A review. Vol. 228, Proceedings of the Institution of Mechanical Engineers, Part H: Journal of Engineering in Medicine. SAGE Publications Ltd; 2014. p. 1083–99.

141. Junter GA, Thébault P, Lebrun L. Polysaccharide-based antibiofilm surfaces. Vol. 30, Acta Biomaterialia. Elsevier Ltd; 2016. p. 13–25.

142. Li X, Wu B, Chen H, Nan K, Jin Y, Sun L, et al. Recent developments in smart antibacterial surfaces to inhibit biofilm formation and bacterial infections. Vol. 6, Journal of Materials Chemistry B. Royal Society of Chemistry; 2018. p. 4274–92.

143. Jaggessar A, Shahali H, Mathew A, Yarlagadda PKDV. Bio-mimicking nano and micro-structured

surface fabrication for antibacterial properties in medical implants. Vol. 15, Journal of Nanobiotechnology. BioMed Central Ltd.; 2017. p. 1–20.

144. Zhang X, Wang L, Levänen E. Superhydrophobic surfaces for the reduction of bacterial adhesion. Vol. 3, RSC Advances. Royal Society of Chemistry; 2013. p. 12003–20.

145. Dou XQ, Zhang D, Feng C, Jiang L. Bioinspired Hierarchical Surface Structures with Tunable Wettability for Regulating Bacteria Adhesion. ACS Nano. 2015; 9(11):10664–72.

146. Hasan J, Chatterjee K. Recent advances in engineering topography mediated antibacterial surfaces. Vol. 7, Nanoscale. Royal Society of Chemistry; 2015. p. 15568–75.

147. Wu S, Zhang B, Liu Y, Suo X, Li H. Influence of surface topography on bacterial adhesion: A review (Review). Biointerphases. 2018;13(6):060801.

148. Adlhart C, Verran J, Azevedo NF, Olmez H, Keinänen-Toivola MM, Gouveia I, et al. Surface modifications for antimicrobial effects in the healthcare setting: a critical overview. Vol. 99, Journal of Hospital Infection. W.B. Saunders Ltd; 2018. p. 239–49.

149. Riveiro A, Maçon ALB, del Val J, Comesaña R, Pou J. Laser surface texturing of polymers for biomedical applications. Vol. 5, Frontiers in Physics. Frontiers Media S.A.; 2018. p. 16.

150. Flemming RG, Murphy CJ, Abrams GA, Goodman SL, Nealey PF. Effects of synthetic micro- and nano-structured surfaces on cell behavior. Biomaterials. 1999 Mar;20(6):573–88.

151. Falconnet D, Csucs G, Michelle Grandin H, Textor M. Surface engineering approaches to micropattern surfaces for cell-based assays. Vol. 27, Biomaterials. Elsevier; 2006. p. 3044–63.

152. Lakshminarayanan S. Micro/Nano Patterning on Polymers Using Soft Lithography Technique. In: Micro/Nanolithography - A Heuristic Aspect on the Enduring Technology. InTech; 2018.

153. Sahin O, Ashokkumar M, Ajayan PM. Micro- and nanopatterning of biomaterial surfaces. In: Fundamental Biomaterials: Metals. Elsevier; 2018. p. 67–78.

154. Bottan S, Robotti F, Jayathissa P, Hegglin A, Bahamonde N, Heredia-Guerrero JA, et al. Surface-structured bacterial cellulose with guided assembly-based biolithography (GAB). ACS Nano. 2015;9(1):206–19.

155. Robotti F, Bottan S, Fraschetti F, Mallone A, Pellegrini G, Lindenblatt N, et al. A micron-scale surface topography design reducing cell adhesion to implanted materials. Sci Rep. 2018;8(1):1–

13.

156. Robotti F, Sterner I, Bottan S, Monné Rodríguez JM, Pellegrini G, Schmidt T, et al. Microengineered biosynthesized cellulose as anti-fibrotic in vivo protection for cardiac implantable electronic devices. Biomaterials. 2020 Jan 1;229:119583.

157. Jing W, Chunxi Y, Yizao W, Honglin L, Fang H, Kerong D, et al. Laser patterning of bacterial cellulose hydrogel and its modification with gelatin and hydroxyapatite for bone tissue engineering. Soft Mater. 2013;11(2):173–80.

158. Ahrem H, Pretzel D, Endres M, Conrad D, Courseau J, Müller H, et al. Laser-structured bacterial nanocellulose hydrogels support ingrowth and differentiation of chondrocytes and show potential as cartilage implants. Acta Biomater. 2014 (3):1341–53.

159. Hu Y, Liu H, Zhou X, Pan H, Wu X, Abidi N, et al. Surface engineering of spongy bacterial cellulose via constructing crossed groove/column micropattern by low-energy CO 2 laser photolithography toward scar-free wound healing. Mater Sci Eng C. 2019;99:333–43.

Chapter 3

The influence of different fermentation conditions on bacterial cellulose properties

The influence of fermentation conditions on BC properties was evaluated. Different parameters were tested: distinct bacterial strains, different times of culture and the influence of static versus agitated fermentation. Two bacterial strains were evaluated (ATCC 53582 and ATCC700718) and two distinct culture media were used (HS and MOL). On static conditions, three times of culture were tested (6,15 and 30 days) while in agitated culture, BC was only cultivated for 8 days. The samples obtained were characterized using different techniques, such as: XRD, ATR-FTIR and the degree of polymerization was also determined. The obtained results revealed only slight differences (with no statistical relevance) between static and agitated conditions in what concerns to BC properties. A slight decrease on degree of polymerization and BC's crystallinity on agitated culture seems to occur, when compared to static fermentation. Although, the chemical structure of BC was preserved since in both fermentation methods and all the time-points, the crystallinity and the fraction of Iα was high for all the samples.

3.1 - INTRODUCTION

Bacterial cellulose is a biopolymer widely present in nature and produced by different organisms, ranging from plant to algae, fungi and bacteria (1). Even though plant and bacterial cellulose are chemically identical, substantial differences have been found between them in what concerns macromolecular properties and also in purity since, contrarily to plant cellulose, BC is secreted without hemicelluloses and lignin (2).

The synthesis of BC is an intricate process involving several enzymes and complexes of catalytic and regulatory proteins. The process includes the formation of the cellulose precursor Uridine diphosphate glucose (UDP glucose) followed by glucose polymerization into the (1,4) glucan chain. Then, the secreted glucan chains aggregate and assemble, creating cellulose ribbons at nanoscale size, which in turns produced a network structure with high porosity. After that, a 3D structure is generated through crosslinking with other elementary fibrils and development pf microfibrils (3).

Overall, BC may be produced using two different fermentation methods, e.g., static or agitated. Static culture is the most common technique due to its simplicity as it involves low, or no shear power being extensively applied to produce BC pellicles. The culture can be performed for several days or weeks after inoculation. The production of BC occurs at the air-liquid interface. Nevertheless, the commercial application of BC produced this way is still limited due to its low productivity and increased incubation time-scale (1,4). On the other hand, the BC produced through agitated culture exhibit several different forms such as fibrous suspensions, pellets, spheres or even irregular masses, due to the agitation and availability of oxygen and nutrients in adequate amounts in the bulk phase. Moreover, features like size, shape and amount of BC are associated to the rotating speed, oxygen supply, agitator configuration, the duration of the culture and the shear force in culture medium (5,6). The main drawback of agitated culture is the possibility of converting some cells into non-cellulose producing mutants decreasing the productivity (6). Beyond this, strains and culture conditions have a considerable effect on the microstructure and physicochemical properties of the produced BC, namely on properties such as crystallinity and fraction of the Iα allomorph (7).

In this work, we intended to study the influence of culture medium, the time of culture and the used strain on the BC's properties.

3.2 – MATERIALS AND METHODS

3.2.1 – Fermentation conditions

3.2.1.1 – Bacterial strains

Komagataeibacter xylinus (ATCC 700718 and ATCC 53582), from the American Type Culture Collection were used to produce BC under static and agitated conditions. The strains were kept in Hestrin-Schramm culture medium (HS medium) (8), in solid state with 2% (m/v) agar (Acros Organics). For agitated fermentation only ATCC 700718 strain was used.

3.2.1.2 – Inoculum preparation

The inoculum preparation procedure was the same for both ATCC 700178 and ATCC 53582, according the previous work developed by the group (9). In short, *Komagataeibacter xylinus* cells were grown in 1 L conical flasks with 100 mL of HS medium, comprising (in % m/v): 2.0 glucose (Fisher Chemical), 0.5 peptone (OXOID), 0.5 yeast extract (OXOID), 0.27 disodium phosphate di-hydrated ($Na_2HPO_4.2H_2O$) (Panreac) and 0.115 citric acid (Panreac). The initial pH was set at 5.5 using 18% (v/v) HCl (Fisher-Chemical). Before inoculation, the cultivation medium was autoclaved at 121°C, 1 bar for 20 min. The medium was incubated for 48 h at 30°C under static conditions. The inoculum preparation was the same for both static and agitated fermentation.

3.2.1.3 – Static fermentation

In the static fermentation both ATCC 700178 and ATCC 53582 strains were used, and different culture media were evaluated. In the case of ATCC 700178, two distinct culture media were tested: HS medium supplemented with absolute ethanol (referred to as ATCC 700178_HS) and a culture media prepared using molasses (referred to as ATCC 700178_MOL). On the other hand, in the case of ATCC 53582 only HS medium was used without ethanol supply (ATCC 53582_HS), since according to previous studies ethanol does not increase the production of BC by this strain.

For both strains, after inoculum preparation, the formed cellulose pellicle was shaken to release the bacteria entrapped within the cellulose matrix into the residual medium and culture in fresh culture medium. Furthermore, only for ATCC 700178 and prior to culture, the cells were transferred to sterile conical flasks with new culture medium, making up 10% (v/v) of the final volume of fermentation

containing a culture media, prepared using (in % m/v): 4.0 molasses (a gift from RAR - Refinarias de Açúcar Reunidas, S.A; Portugal), 0.7 Corn Steep Liquor (a gift from COPAM Companhia Portuguesa de Amidos, S.A; Portugal), 0.15 citric acid (Panreac), and 0.26 disodium phosphate di-hydrated (Panreac).

In order to simplify the distinguish between HS and MOL medium, on table 3.1 are present the main components of both culture media:

Table 3.1.The main components of HS and MOL medium.

Culture media	Components
HS	• 2.0 of glucose (% m/v); • 0.5 of peptone (m/v); • 0.5 of yeast extract (% m/v); • 0.27 of disodium phosphate di-hydrated (% m/v); • 0.115 of citric acid (% m/v).
MOL	• 4.0 of molasses (% m/v); • 0.7 of Corn Steep Liquor (% m/v); • 0.15 of citric acid (% m/v) • 0.26 of ammonium sulphate (%m/v).

ATCC 53582_HS cells were incubated with a ratio of 1% (v/v) of inoculum to 99% (v/v) of fresh HS medium while both ATCC 700178_HS and ATCC 700178_MOL cells were incubated with a ratio of 0.5% (v/v) of inoculum to 1.5% (v/v) of absolute ethanol and to 98% (v/v) of fresh HS medium supplemented with absolute ethanol for ATCC 700178_HS and fresh culture media prepared using molasses for ATCC 700178_MOL.

In all tested conditions cells were incubated at 30°C for 6, 15 and 30 days under static conditions.

3.2.1.4 – Agitated fermentation

Cells were grown in 1L conical flasks, as described on the "Inoculum preparation" section. Agitated fermentation was performed in an Eppendorf DASGIP® Parallel Bioreactor System for Microbial

Applications (Switzerland) with 2L vessels, with a working volume of 1L. Since for this fermentation method only ATCC 700178_HS was used, the experiments were performed by mixing 0.5% (v/v) of the inoculum with 1.5% (v/v) of absolute ethanol and 98% (v/v) of HS medium for a final volume of 1 L, using a stirring speed of 150 rpm. The temperature was kept at 30 ºC and the air flow rate was controlled at 1.5 vvm. Initial pH was 5.5 and the initial dissolved oxygen was 30 % of saturation. The experiments were performed for 8 days in quadruplicate.

In order to summarize the tested parameters, in the follow diagram the tested conditions are present:

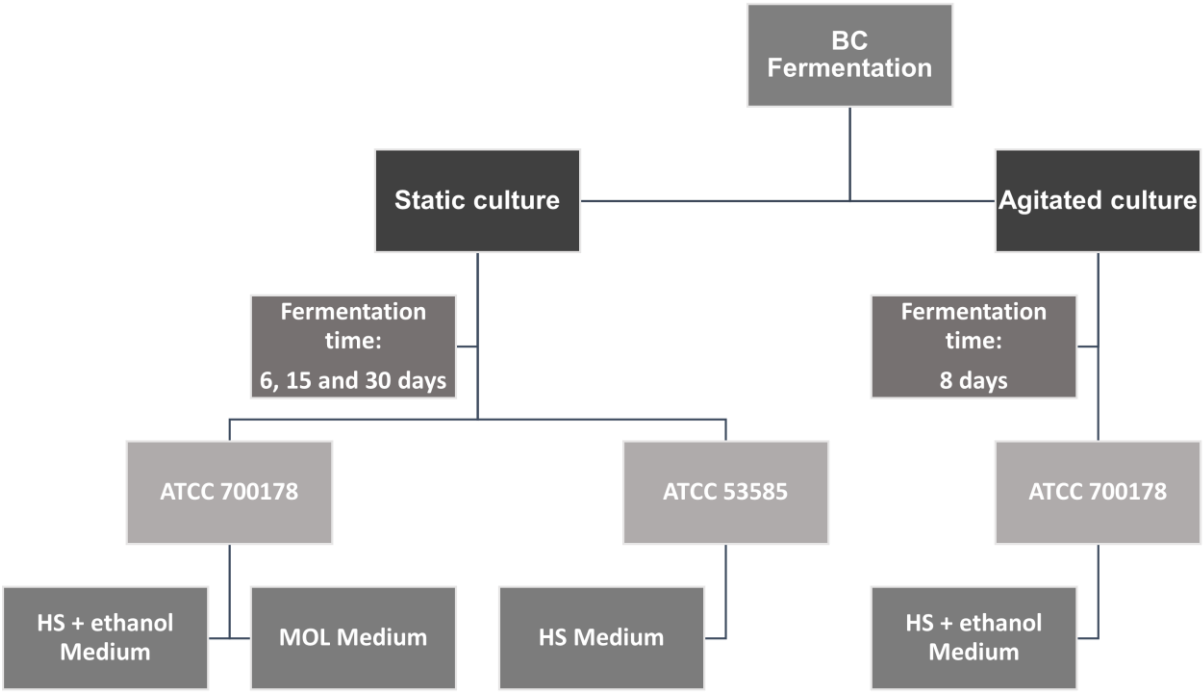

Figure 3.1. Diagram of all tested conditions on BC production.

3.2.2 – BC purification

After incubation, the culture medium was discharged and BC was collected, crushed and washed thoroughly to remove the remaining medium components and eliminate bacterial cells. First of all, BC was treated with 0.1M sodium hydroxide solution (NaOH) during 72h, with changes of the washing solution every 24h. After that, NaOH was rejected, and BC was washed three times (30 minutes each) with 2% (v/v) Divosan Hypochlorite and then with distilled water. Subsequently, BC was treated with 4% (v/v) acetic acid to decrease the pH and then with distilled water until the pH of the supernatant became

neutral. The purified BC was autoclaved at 121°C, 1 bar, for 20 min and stored at 4°C until used. Prior to use, BC was frozen at -80°C and freeze-dried at -100°C (Scanvac Coolsafe) during 5 days. This procedure was applied for both static and agitated conditions.

3.2.3 – BC characterization

3.2.3.1 – SEM

The lyophilized BC samples were placed onto the sample stage and sputter-coated with an Au 5nm film. Observations were performed using a Scanning Electron Microscope, SU8010, Hitachi, Japan, at an accelerating voltage of 5.0 kV. For each sample, the nanofibers diameters were measured by analyzing two different SEM micrograph with Fiji ImageJ, performing an average of 100 readings per sample.

3.2.3.2 – TEM

The lyophilized BC samples obtained by static fermentation. For ATCC 700178 the high-resolution morphologies were performed using a Field Emission Transmission Electron Microscope (FETEM, Talos F200X, FEI Company, Hillsboro, USA). To obtain individual BC fibers for FETEM characterization, 0.2-0.3 mg BC was dispersed in 2 ml ethanol, followed by ultrasound dispersion for 4 hours.

For ATCC 53582 the high-resolution morphologies were performed using a Field Emission Transmission Electron Microscope JEOL JEM 2100. To obtain individual BC fibers for FETEM characterization, a suspension of 0.02 % of BC fibers was dispersed in Mili-Q water followed by homogenization vortex and ultrasound dispersion for 2 hours and 3-5 drops of sample on a TEM grid placed on filter paper.

3.2.3.3 – XRD

The crystallinity was assessed using a PANalytical X'Pert Pro MPD diffractometer equipped with X'Celerator detector and secondary monochromator. All BC samples were analyzed at room temperature using a CuKα radiation and Bragg-Bentano geometry, 0.017°/step and 100 s/step.

The crystallinity index (CrI) (Equation 1) was calculated using the Segal, Creely, Martin & Conrad (1959) (10) equation, i.e., it was calculated as a function of the maximum intensity of the diffraction peak

from the crystalline region (I_{200}), at an angle of $2\theta \sim 22.5°$, and the minimum intensity from the amorphous region (I_{am}), at an angle of $2\theta \sim 18°$.

$$CrI\ (\%) = \frac{(I_{200} - I_{am})}{I_{200}} \quad (1)$$

The apparent crystallite size (CS) in the crystallographic planes (1–10), (110) and (200) were calculated assuming that the crystals exhibited uniform size and shape and according to Scherrer's equation (Equation 2):

$$CS = \frac{K\lambda}{FWHM \cos\theta} \quad (2)$$

where K is a dimensionless factor dependent on the method used to calculate the amplitude (K = 0.9), λ is the wavelength of the incident X-ray (λ = 0.15 nm), *FWHM* is the width of the diffraction peak at half-maximal height (in radians) and θ is the angle of the diffraction peak of the crystalline phase (Bragg's angle). The diffractograms were analyzed by Rietveld refinement with Powder Cell software.

3.2.3.4 – ATR-FTIR

All BC samples were analyzed using an ALPHA II- Bruker spectrometer (Ettlingen, Germany) with a diamond-composite attenuated total reflectance (ATR) cell. Data were collected using OPUS software, which is integrated in the FTIR equipment. The measurements were recorded with a wavenumber range from 4000 cm^{-1} to 400 cm^{-1}, with a resolution of 4 cm^{-1} and 64 scans per sample. The ATR clamp and platform were cleaned with a cotton swab dampened with isopropyl alcohol and then allowed to dry between the analysis of each sample. All assays were done in duplicate for each sample.

3.2.3.5 – Determination of % Iα mass fraction

Through FTIR spectra, hydrogen-bonding vibrational bands are present in the 700-800 cm^{-1} range (11). Allomorphs Iα and Iβ have their bands around 750 cm^{-1} and 710 cm^{-1}, respectively, and they have been used to estimate the ratio of these two allomorphs. The Gaussian function was fitted under the peaks around 750 cm^{-1} and 710 cm^{-1}. The mass fraction of the Iα allomorph was calculated using the following equation (12) (Equation 3):

$$\% I\alpha = 2.55 \times \frac{A_{I\alpha}}{(A_{I\alpha} - A_{I\beta})} - 0.32 \quad (3)$$

where $A_{I\alpha}$ and $A_{I\beta}$ are ascribed to the integrated intensities of the contributions from celluloses Iβ and Iα at 710 cm^{-1} and 750 cm^{-1}, respectively. The Iα mass fractions in the celluloses was determined by the Gaussian deconvolution of the peaks, subtracted from a local linear background, and their integration using OriginPro software.

3.2.3.6 – Degree of polymerization

All BC samples were cut into small pieces and mixed with 5 mL of distilled water under agitation for 30 min. Then, 5 mL of cupri-ethylenediamine (CED, Sigma-Aldrich) saturated with copper (II) hydroxide was added; the mixture was agitated for 60 min and then centrifuged for 5 min at 7000 rcf. Finally, the intrinsic viscosities of the BC samples were obtained using an Ubbelohde capillary-tube viscometer from Rheotek, placed in a water bath at 25°C. The viscosity values were obtained according to the standard ES ISO 5351:2012 (Pulps—Determination of limiting viscosity number in cupri-ethylenediamine (CED) solution). Thus, the viscosity ratio η_{ratio} (dimensionless unit) was calculated using the following equation (Equation 4):

$$\eta_{ratio} = \frac{\eta}{\eta_0} = h \times t \quad (4)$$

where h is the viscometer constant that was determined to be 0.132 s^{-1}, and t is the efflux time (in seconds) of the test solution. The viscosity-averaged degree of polymerization (DP_v) was calculated using the Mark–Houwink–Sakurada equation (13):

$$[\eta] = K \times DPv^{\alpha} \quad (5)$$

where, for BC samples, K = 0.0002 and α = 1.9705 (14).

Finally, the molecular mass of BC was calculated from the relationship:

$$DP_v = \frac{M}{162} \quad (6)$$

where *M* is the molecular mass of the BC and *162* (g/mol) equals the molecular mass of an anhydroglucose unit (15). All the samples were analyzed in triplicate.

3.3 – Results and discussion

The results presented on SEM and TEM sections (3.3.1 and 3.3.2, respectively) were obtained only for static fermentation and only for 6 days of culture. Furthermore, in the case of ATCC 700178 only one media was used: ATCC 700178_MOL. Besides the high costs ascribed to agitated conditions, on this type of fermentation, the produced BC stayed attached on the blades of the bioreactor which causes some losses on the obtained material. Thus, and aiming to reduce the costs associated to this process, both techniques were applied for both strains but only for static fermentation. Despite using only one type of fermentation, these results were very important since it gave some insights about the influence of the strain on some BC properties. In Fig. 3.2 are illustrated the BC appearance obtained for both static and agitated fermentations.

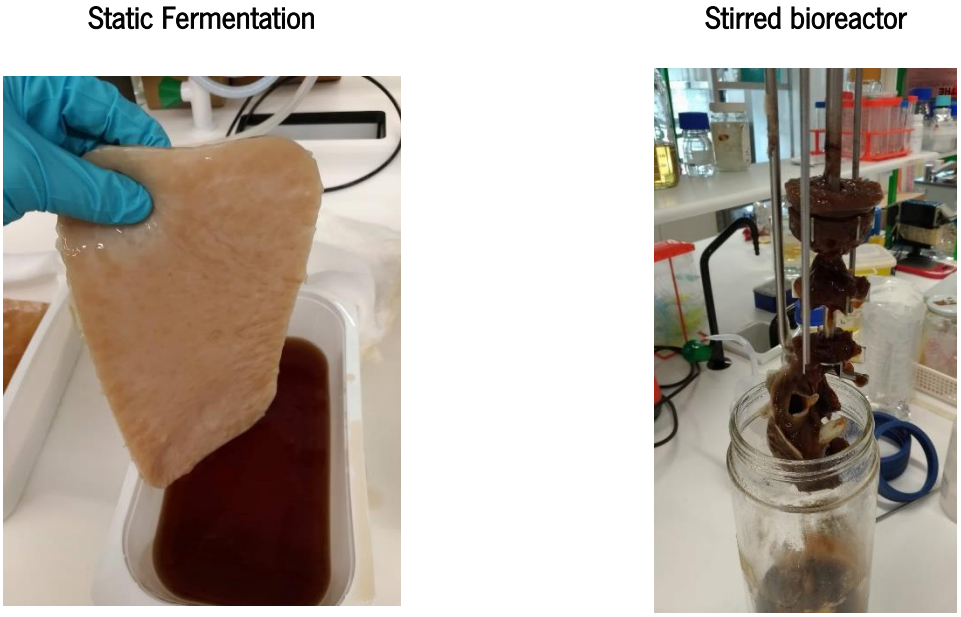

Figure 3.2. The appearance of obtained BC after static and agitated fermentation.

3.3.1 – SEM

In order to understand the influence of producing BC using ATCC 53582 and ATCC 700178 strains on its morphology, it was performed a SEM analysis and the results are presented on Fig. 3.3.

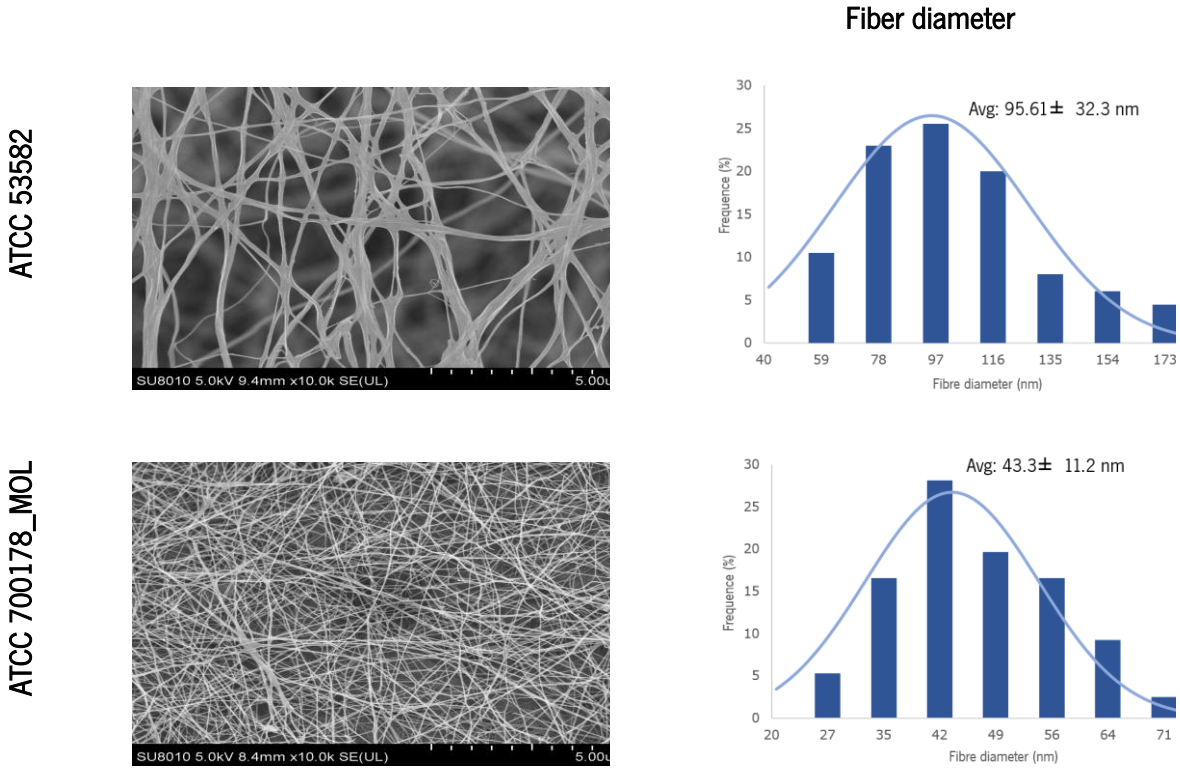

Figure 3.3. SEM images and mean fiber diameter of BC produced by different strains under static conditions. Scale bar: 5 µm.

According to Fig. 3.3, for both strains, the complex structure of BC composed by a 3D randomly network with interconnected fibers was presented in both strains. Furthermore, the calculated mean fiber diameter of the BC samples was around 96 nm for ATCC 58532 (16,17) and around 43 nm for ATCC 700178_MOL. The higher values obtained for ATCC 53582 might be explained by the assembling of several fibers, as shown on the figure 3.3. On the other hand, the values obtained for ATCC 700178_MOL are in the range of the mean values obtained by Chen et al. (2017) (18).

3.3.2 – TEM

TEM analysis was also applied on BC samples produced by both strains under static conditions, and the obtained results are presented on Fig. 3.4.

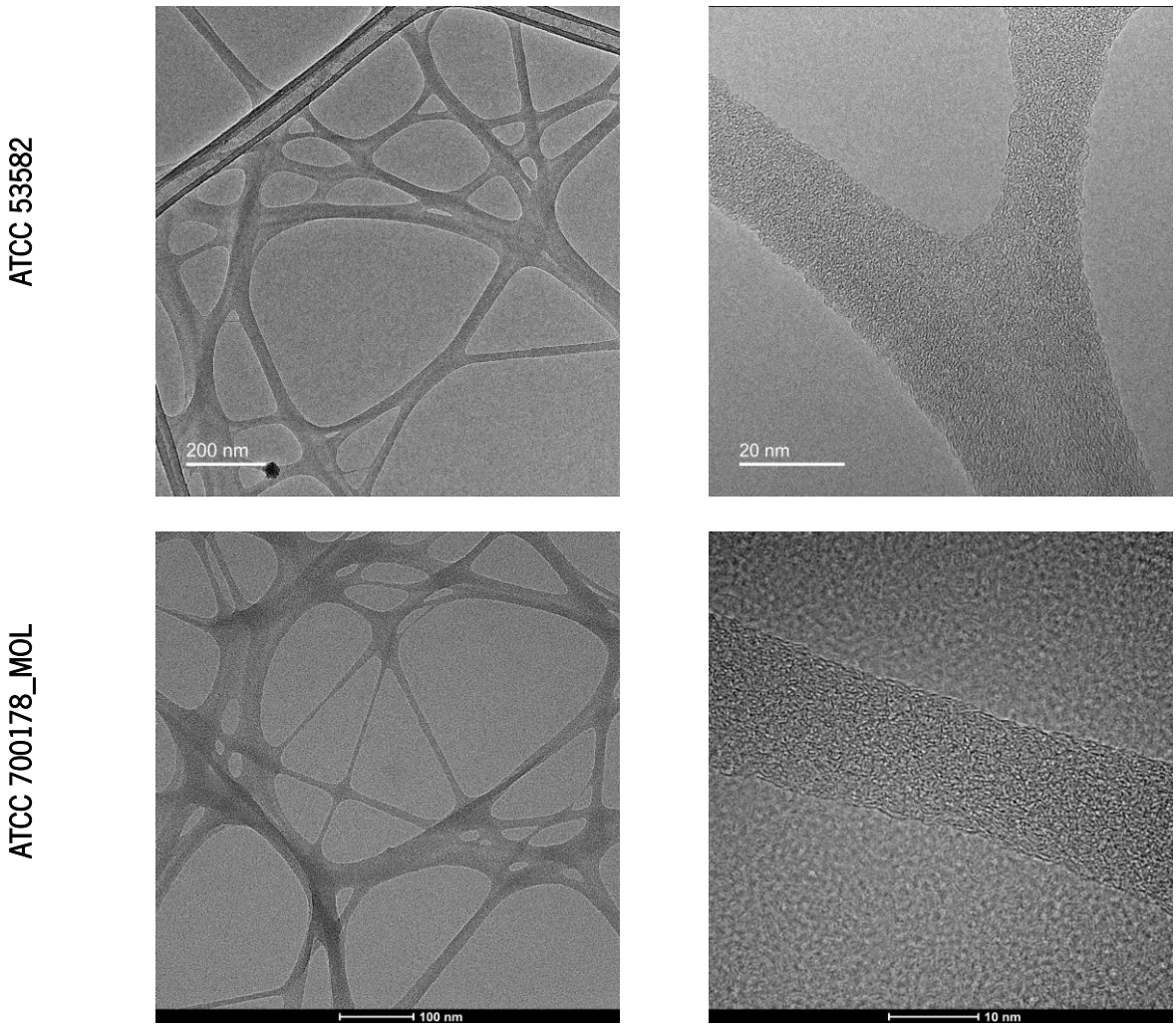

Figure 3.4. TEM images of BC produced by different strains under static conditions.

Similarly, to SEM results, also the TEM images revealed the intricate structure of BC. Moreover, it confirmed the similarity of the fibers obtained by both strains. On the particular case of ATCC 53582, the produced fibers had values between 10-20 nm confirming some bundling on these fibers which makes hard to distinguished them by SEM technique. Considering this, TEM analyses expose the fact that the thicker BC fibers, indeed comprise bundled fibers. Thus, while fibril aggregation may vary with the type of strain, the elementary BC fibrils are very similar in diameter, among strains.

3.3.3 – XRD

Cellulose has different allomorphs, but only cellulose I is found in nature. This is found in two crystalline forms, Iα and Iβ that coexist in the same sample. Cellulose Iα has a triclinic unit cell, while Iβ has a monoclinic and the ratio of Iα and Iβ varies depending on the source of the cellulose. Cellulose Iα is essentially available in algae or produced by some bacterial species, while cellulose Iβ is essentially available on cell walls of higher plants (19). Cellulose is not purely crystalline since it is possible to find some amorphous regions. The relative amount of crystalline and amorphous regions can be assessed by the crystallinity index (CrI) (20). X-ray diffraction is widely used to determine the crystallinity of cellulose, however, the diffraction patterns of both allomorphs overlap which makes particularly hard to differentiate them by this technique (20).

The crystallinity index was obtained using the Segal equation (21), by measuring the peak intensities of the (200) peak (I_{002}) and the height of the minimum (I_{am}) between the (200) and the (110) peaks. The crystallite size was also calculated based on the crystal planes (1-10) (110) and (200) of BC samples. The obtained x-ray diffractograms are present on Fig. 3.5 and the calculated results on table 3.2 and 3.3.

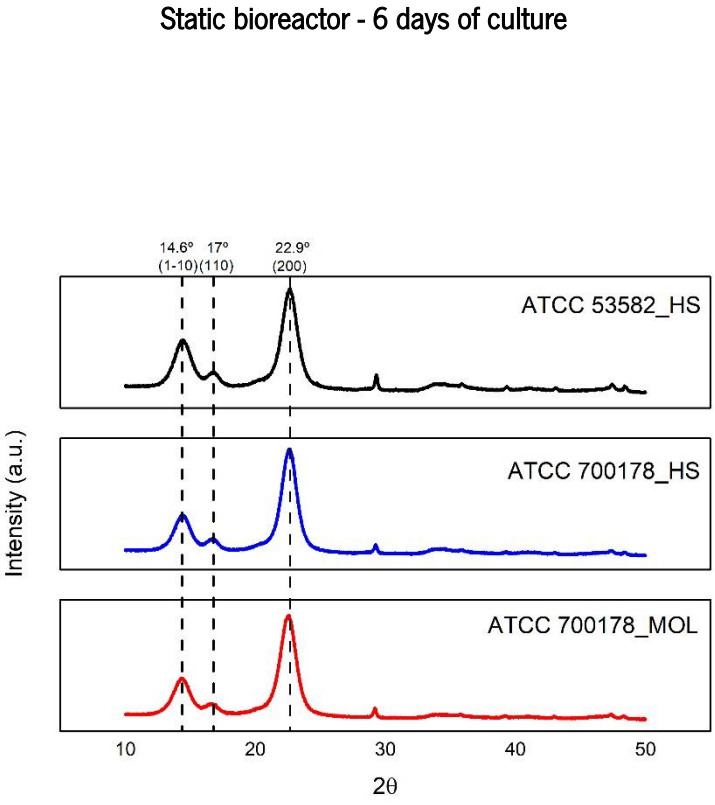

Static bioreactor - 15 days of culture

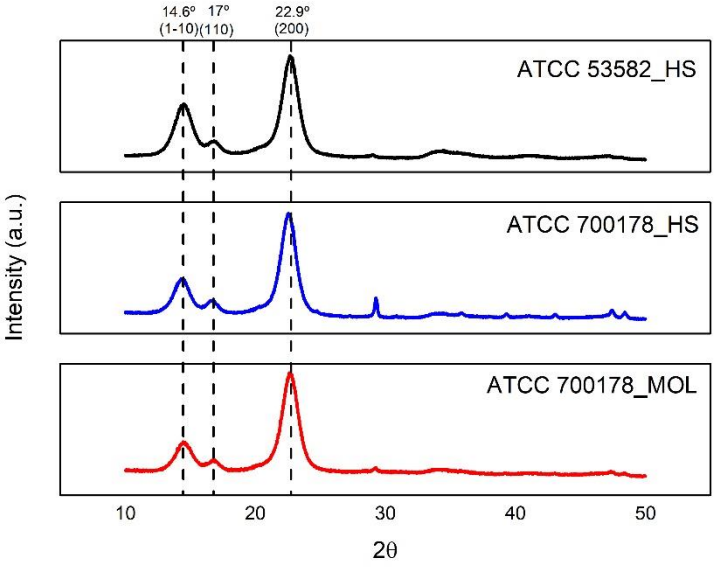

Static bioreactor - 30 days of culture

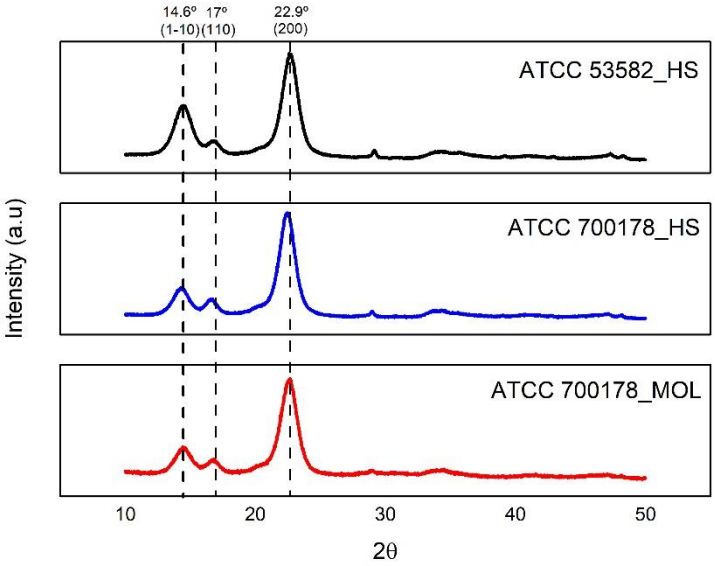

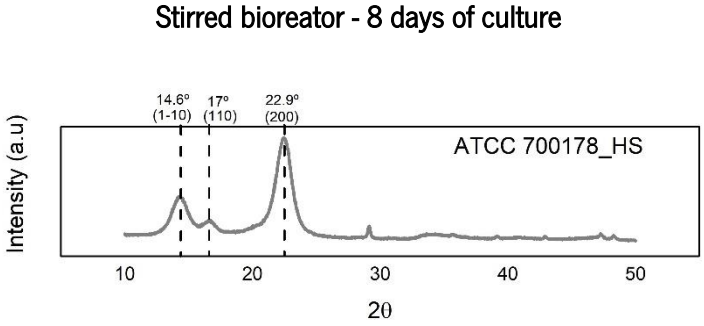

Figure 3.5. XRD diffraction patterns for all tested conditions.

As it is possible to observe on Fig. 3.5, the obtained diffractograms were very similar for all the time-points, for both static and agitated culture and for both strains. Indeed, for all the samples, BC exhibited the usual diffraction peaks at 14.6°, 17° and 22.9° corresponding to the primary diffraction of the crystal planes (1-10), (110) and (200), respectively (20,22–25). The higher intensity of the peak around 14.6° comparing to the peak around 17° may suggest the predominant cellulose Iα allomorph while the highest intensity and well separated peak at 22.9° is related with the higher perfection of the crystal lattice in the (200) plane, as compared to the other peaks. As previous mentioned, the three main peak positions at 14.6°, 17° and 22.9° of the two allomorph types are very close to each other, which makes hard to distinguish the two allomorphs based only on the XRD peak positions. Thus, the presence of the two allomorphs was analyzed by FTIR-ATR data (results shown in the next section).

Table 3.2. d-spacings, crystallite sizes (D(hkl)) and crystallinity (CrI) of bacterial cellulose in static conditions determined by XRD diffractograms.

Sample	d-spacings (Å)			$D_{(hkl)}$ (nm)			CrI (%)
	(1-10)	(110)	(200)	(1-10)	(110)	(200)	
6 days							
ATCC 53582_HS	6.14	5.28	3.92	4.68	5.78	4.99	89.88

ATCC 700718_HS	6.15	5.30	3.93	4.89	5.85	5.13	91.64
ATCC 700718_MOL	6.18	5.30	3.94	4.76	4.47	4.89	91.62
15 days							
ATCC 53582_HS	6.11	5.26	3.91	4.67	5.26	4.79	89.32
ATCC 700718_HS	6.17	5.30	3.94	4.77	5.54	5.06	91.01
ATCC 700718_MOL	6.10	5.27	3.91	4.79	5.67	4.81	89.47
30 days							
ATCC 53582_HS	6.13	5.27	3.92	4.63	5.71	4.91	90.66
ATCC 700718_HS	6.18	5.33	3.95	5.10	6.33	5.03	90.05
ATCC 700718_MOL	6.04	5.24	3.89	5.55	7.60	5.19	90.04

Table 3.3. d-spacings, crystallite sizes (D(hkl)) and crystallinity (CrI) of bacterial cellulose in agitated conditions determined by XRD diffractograms.

Sample	d-spacings (Å)			$D_{(hkl)}$ (nm)			CrI (%)
	(1-10)	(110)	(200)	(1-10)	(110)	(200)	

ATCC 700718_HS	5.14	4.96	4.99	6.16	5.11	3.94	88.11

Table 3.2 and 3.3 exhibit information related with the d-spacings and crystallite sizes $D_{(hkl)}$ at different crystallographic planes and the percentage of crystallinity (CrI) of BC for all tested situations. The obtained results revealed that all the BC samples, in all tested conditions, displayed high values of CrI, around 90%, despite the slight decrease (~88%) on samples treated under agitated conditions when compared with samples treated under static conditions. The high values of crystallinity are in the range reported in the literature (1,22,26,27). On the other hand, the obtained values for the crystallite size were very similar for all the tested conditions, with values between 4 and 6 nm being consistent with the literature (28,29).

3.3.4 – ATR-FTIR

The ATR-FTIR spectra of the obtained BC samples are present in Fig. 3.6.

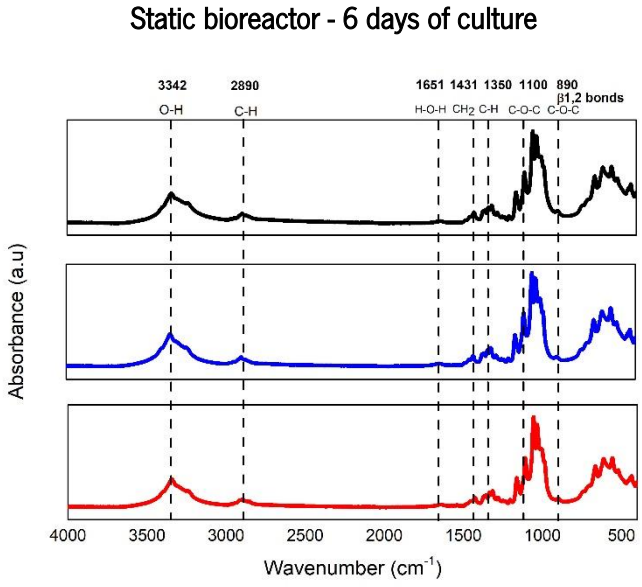

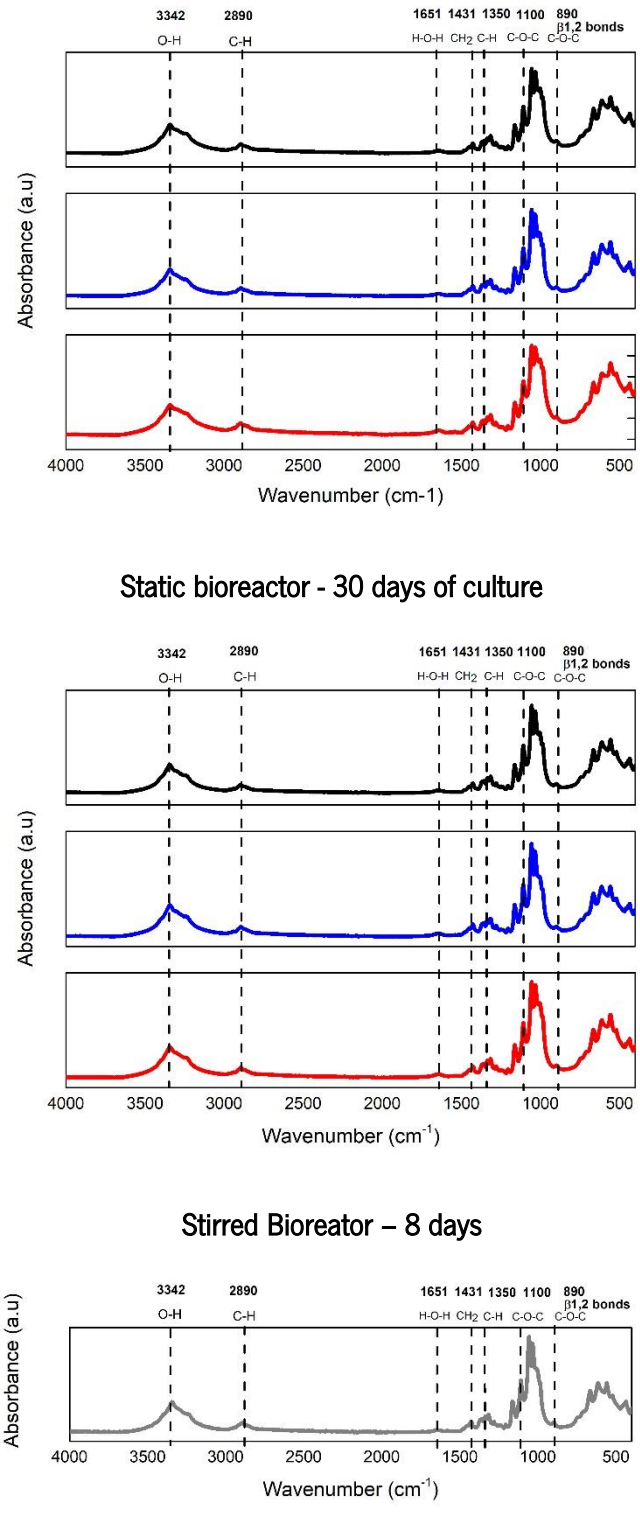

Figure 3.6. ATR-FTIR spectra for all tested conditions. (–) ATCC 53582_HS; (–) ATCC 700178_HS; (–) ATCC 700178_MOL and (–) ATCC 700178_HS under agitated conditions.

All the samples exhibited the typical bands ascribed to the chemical structure of BC: (O–H symmetrical stretching around 3350 cm^{-1}; C–H stretching around 2900 cm^{-1}; C–O–C stretching around 1162 cm^{-1}; C–O stretching at 1030 cm^{-1}; vibration of amorphous cellulose (stretching of the glucose ring) around 899 cm^{-1} (30–33). Moreover, there were no other significant differences between the spectra since in all of them, all peaks appeared in the same position and at comparable intensities.

3.3.5 – Determination of % Iα mass fraction

Figure 3.7 show the typical bands ascribed to both allomorphs, Iα and Iβ, at 750 cm^{-1} and 710 cm^{-1} respectively, demonstrating the ability of the bacteria to produce both allomorphs simultaneously. According to Imai et al.(1998) the absorbance bands at 3240 cm^{-1} and 3270 cm^{-1} are ascribed to Iα, and Iβ, respectively (34). The Iα mass fractions in the celluloses was determined by the Gaussian deconvolution of the peaks and the obtained results are presented in the following figure.

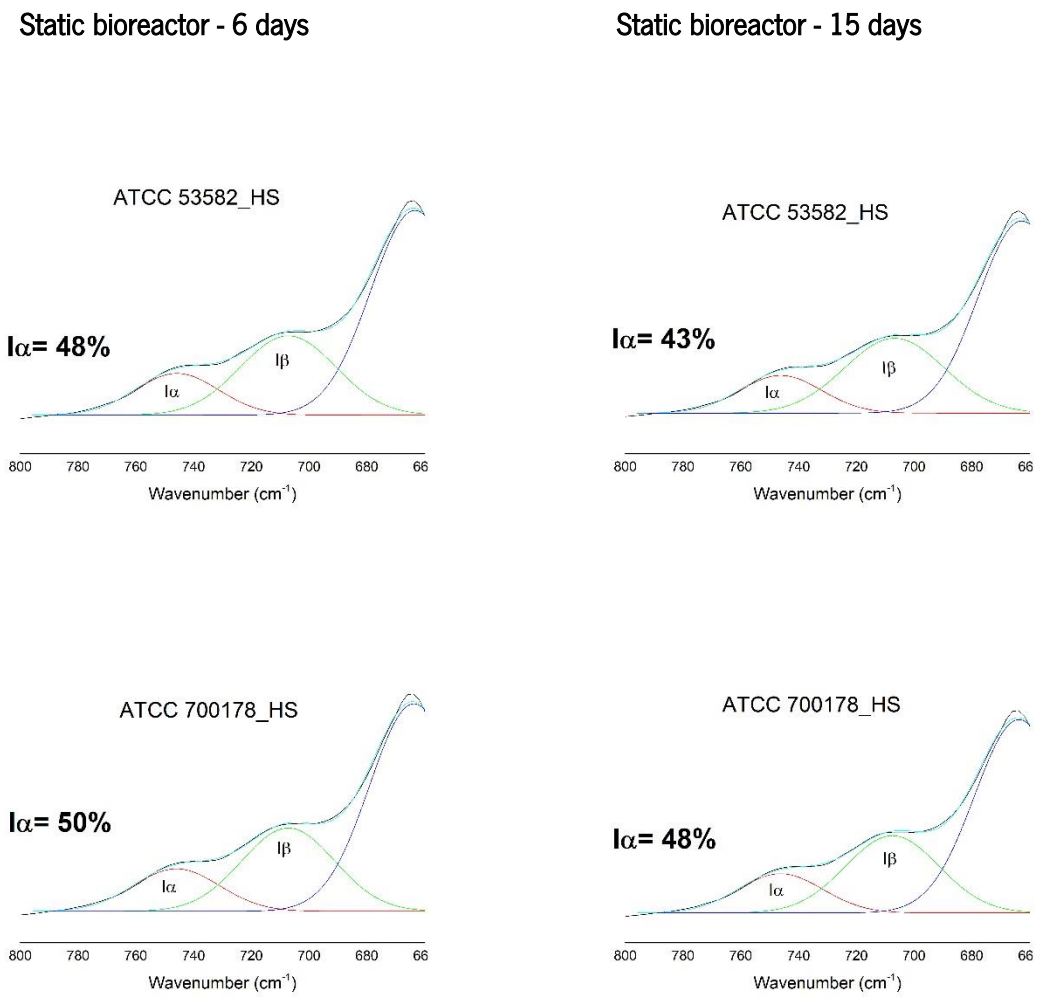

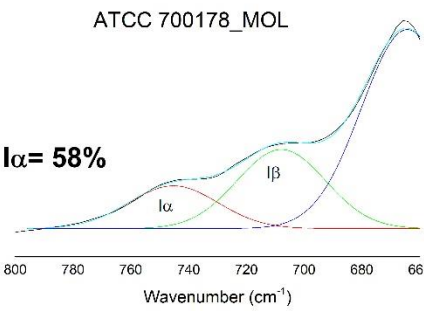

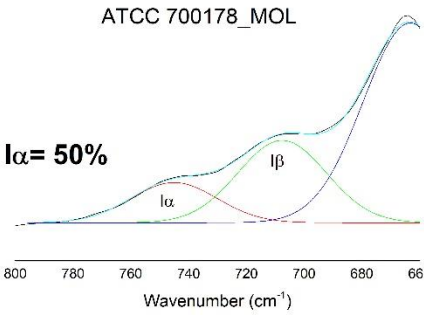

Static bioreactor - 30 days

Stirred bioreactor – 8 days

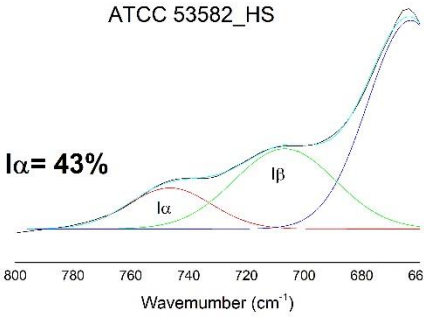

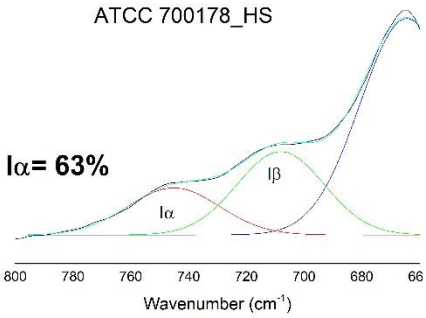

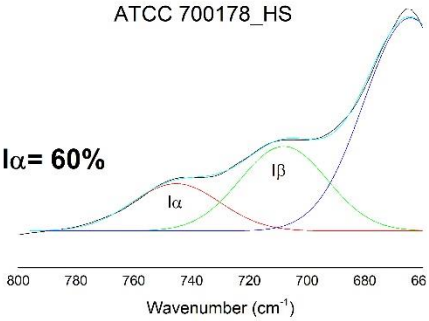

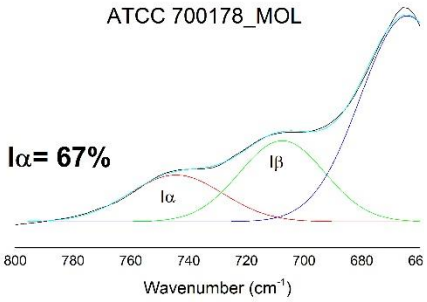

Figure 3.7. The deconvoluted absorption peaks attributed to the Iα (750 cm^{-1}) and Iβ (719 cm^{-1}) crystalline forms of cellulose obtained by ATR-FTIR.

Figure 3.7 show that the Iα values vary between 43 and 67%. These values were in agreement with the literature (35–38). Moreover, the mass fraction of Iα slight increased all over the time for all the samples that were tested in static conditions, since for 6 days of culture the values were between 43% and 48%, while for 30 days these values varied from 50% to 67%. The strain ATCC 700178 seems to have a slightly higher amount of Iα allomorph, both in static (50-67%) and agitated (63%) conditions. However, the differences observed are not dramatic. The results suggest that fermentation method does not affect significantly the mass fraction of Iα, although slight differences were observed for both strains and also for the culture medium.

3.3.6 – Degree of polymerization

The degree of polymerization characterizes the number of repeating units present in a polymer. According Isogai et al. (1998) the degree of polymerization of cellulose may have some variations related to its source (39). The influence of fermentation conditions - culture medium, time of culture and the strain – on the degree of polymerization was evaluated and the obtained results are summarized on table 3.4.

Table 3.4. Degree of polymerization (DP) of bacterial cellulose for all tested conditions.

	ATCC 53582_HS	ATCC 700178_HS	ATCC 700178_MOL
	DP		
6 days	3070 ± 116	3010 ± 131	2866 ± 97
15 days	3004 ± 55	2976 ± 86	2565 ± 8
30 days	2942 ± 48	2852 ± 47	2436 ± 42
Stirred bioreactor			
8 days		2659 ± 75	

According to table 3.4, the degree of polymerization exhibited high values (2500-3000), which is expectable for BC samples (40–42). The value observed decreased over the cultivation time for all strains. Moreover, and despite the different fermentation times (6 versus 8 days), it seems possible to conclude that under agitated conditions the degree of polymerization tend to be smaller, comparing to static culture. The value obtained for 8 days of agitated culture the DP was 2659, while for the same strain in static culture a value of 2866 was obtained after 6 days. A similar reduction of DP in agitated samples was also observed by Xiang et al. (2017) (41) and might be explained by the shear stress present under stirred conditions (43).

3.4 – CONCLUSIONS

This work aimed to study the influence of using different fermentations conditions, as well different strains, culture media and times of culture, on the BC properties. In general, the obtained results revealed only slight differences (with no statistical relevance) between static and agitated conditions in what concerns to BC properties. In fact, agitated culture seems to induce a slight decrease on degree of polymerization and on BC's crystallinity. Beside this, the obtained ATR-FTIR results confirmed that the chemical structure of BC was preserved since in both culture methods and all the time-points, the mass fraction of Iα was higher for all the samples.

3.5 – REFERENCES

1. Wang J, Tavakoli J, Tang Y. Bacterial cellulose production, properties and applications with different culture methods – A review. Vol. 219, Carbohydrate Polymers. Elsevier Ltd; 2019. p. 63–76.

2. Kim H, Son J, Lee J, Yoo HY, Lee T, Jang M, et al. Improved production of bacterial cellulose through investigation of effects of inhibitory compounds from lignocellulosic hydrolysates. GCB Bioenergy. 2021;13(3):436–44.

3. Pandit A, Kumar R. A Review on Production, Characterization and Application of Bacterial Cellulose and Its Biocomposites. J Polym Environ. 2021.

4. Blanco Parte FG, Santoso SP, Chou CC, Verma V, Wang HT, Ismadji S, et al. Current progress on the production, modification, and applications of bacterial cellulose. Vol. 40, Critical Reviews in Biotechnology. Taylor and Francis Ltd; 2020 p. 397–414.

5. Wang J, Tavakoli J, Tang Y. Bacterial cellulose production, properties and applications with different culture methods – A review. Vol. 219, Carbohydrate Polymers. 2019 p. 63–76.

6. Andriani D, Apriyana AY, Karina M. The optimization of bacterial cellulose production and its applications: a review. Cellulose. 2020;27(12):6747–66.

7. Gao H, Sun Q, Han Z, Li J, Liao B, Hu L, et al. Comparison of bacterial nanocellulose produced by different strains under static and agitated culture conditions. Vol. 227, Carbohydrate Polymers. 2020.

8. Hestrin S, Schramm M. Synthesis of cellulose by Acetobacter xylinum. II. Preparation of freeze-dried cells capable of polymerizing glucose to cellulose. Biochem J. 1954;58(2):345–52.

9. Rodrigues AC, Fontão AI, Coelho A, Leal M, Soares da Silva FAG, Wan Y, et al. Response surface statistical optimization of bacterial nanocellulose fermentation in static culture using a low-cost medium. N Biotechnol. 2019;49:19–27.

10. L S, CM C, JJ C, AE M. An Empirical Method for Estimating the Degree of Crystallinity of Native Cellulose Using the X-Ray Diffractometer. Text Res J Publ Text Res Institute, Inc Text Found. 1959;29(10):786–94.

11. Szymańska-Chargot M, Cybulska J, Zdunek A. Sensing the structural differences in cellulose from apple and bacterial cell wall materials by Raman and FT-IR Spectroscopy. Vol. 11, Sensors. 2011 p. 5543–60.

12. Yamamoto H, Horii F, Hirai A. In situ crystallization of bacterial cellulose II. Influences of different polymeric additives on the formation of celluloses Iα and Iβ at the early stage of incubation. Cellulose. 1996;3(1):229–42.

13. Evans R, Wallis AFA. Cellulose molecular weights determined by viscometry. J Appl Polym Sci. 1989;37(8):2331–40.

14. Tsouko E, Kourmentza C, Ladakis D, Kopsahelis N, Mandala I, Papanikolaou S, et al. Bacterial cellulose production from industrial waste and by-product streams. Int J Mol Sci. 2015;16(7):14832–49.

15. Ryu DDY, Lee SB, Tassinari T, Macy C. Effect of compression milling on cellulose structure and on enzymatic hydrolysis kinetics. Biotechnol Bioeng. 1982;24(5):1047–67.

16. Numata Y, Kono H, Mori A, Kishimoto R, Tajima K. Structural and rheological characterization of bacterial cellulose gels obtained from Gluconacetobacter genus. Vol. 92, Food Hydrocolloids. 2019. p. 233–9.

17. Jacek P, Kubiak K, Ryngajłło M, Rytczak P, Paluch P, Bielecki S. Modification of bacterial nanocellulose properties through mutation of motility related genes in Komagataeibacter hansenii ATCC 53582. N Biotechnol. 2019;52:60–8.

18. Chen S-Q, Mikkelsen D, Lopez-Sanchez P, Wang D, Martinez-Sanz M, Gilbert EP, et al. Characterisation of bacterial cellulose from diverse Komagataeibacter strains and their application to construct plant cell wall analogues. Cellul 2017 243.;24(3):1211–26.

19. Srivastava D, Kuklin MS, Ahopelto J, Karttunen AJ. Electronic band structures of pristine and chemically modified cellulose allomorphs. Carbohydrate Polymers. 2020

20. Santmartí A, Lee K-Y. Crystallinity and Thermal Stability of Nanocellulose. In: Nanocellulose and Sustainability. 2018. p. 67–86.

21. Segal L, Creely JJ, Martin AE, Conrad CM. An Empirical Method for Estimating the Degree of Crystallinity of Native Cellulose Using the X-Ray Diffractometer. Text Res J. 1959;29(10):786–94.

22. Vasconcelos NF, Feitosa JPA, da Gama FMP, Morais JPS, Andrade FK, de Souza Filho M de SM, et al. Bacterial cellulose nanocrystals produced under different hydrolysis conditions: Properties and morphological features. Vol. 155, Carbohydrate Polymers. 2017 p. 425–31.

23. Tang S, Chi K, Xu H, Yong Q, Yang J, Catchmark JM. A covalently cross-linked hyaluronic acid/bacterial cellulose composite hydrogel for potential biological applications. Vol. 252, Carbohydrate Polymers. 2021

24. Arserim-Uçar DK, Korel F, Liu LS, Yam KL. Characterization of bacterial cellulose nanocrystals: Effect of acid treatments and neutralization. Vol. 336, Food Chemistry. 2021

25. Vasconcelos NF, Andrade FK, Vieira L de AP, Vieira RS, Vaz JM, Chevallier P, et al. Oxidized bacterial cellulose membrane as support for enzyme immobilization: properties and morphological features. Cellulose. 2020;27(6):3055–83.

26. Kashcheyeva EI, Gladysheva EK, Skiba EA, Budaeva V V. A study of properties and enzymatic hydrolysis of bacterial cellulose. Cellulose. 2019;26(4):2255–65.

27. Meza-Contreras JC, Manriquez-Gonzalez R, Gutiérrez-Ortega JA, Gonzalez-Garcia Y. XRD and solid state 13C-NMR evaluation of the crystallinity enhancement of 13C-labeled bacterial cellulose biosynthesized by Komagataeibacter xylinus under different stimuli: A comparative strategy of analyses. Vol. 461, Carbohydrate Research. 2018 p. 51–9.

28. Illa MP, Sharma CS, Khandelwal M. Tuning the physiochemical properties of bacterial cellulose: effect of drying conditions. J Mater Sci. 2019;54(18):12024–35.

29. Rozenberga L, Skute M, Belkova L, Sable I, Vikele L, Semjonovs P, et al. Characterisation of films and nanopaper obtained from cellulose synthesised by acetic acid bacteria. Carbohydr Polym. 2016;144:33–40.

30. Andrade FK, Morais JPS, Muniz CR, Nascimento JHO, Vieira RS, Gama FMP, et al. Stable microfluidized bacterial cellulose suspension. Cellulose. 2019;26(10):5851–64.

31. Ghozali M, Meliana Y, Chalid M. Synthesis and characterization of bacterial cellulose by Acetobacter xylinum using liquid tapioca waste. In: Materials Today: Proceedings. Elsevier Ltd; 2021. p. 2131–4.

32. Auta R, Adamus G, Kwiecien M, Radecka I, Hooley P. African Journal of Biotechnology Production

and characterization of bacterial cellulose before and after enzymatic hydrolysis. 2017;16(10):470–82.

33. Kotcharat P, Chuysinuan P, Thanyacharoen T, Techasakul S, Ummartyotin S. Development of bacterial cellulose and polycaprolactone (PCL) based composite for medical material. Sustain Chem Pharm. 2021;20:100404.

34. Imai T, Sugiyama J. Nanodomains of Iα and Iβ cellulose in algal microfibrils. Macromolecules. 1998;31(18):6275–9.

35. Supian NNI, Zakaria J, Amin KNM, Mohamad S, Mohamad SFS. Effect of fermentation period on bacterial cellulose production from oil palm frond (OPF) juice. IOP Conf Ser Mater Sci Eng. 2021;1092(1):012048.

36. Mikkelsen D, Flanagan BM, Dykes GA, Gidley MJ. Influence of different carbon sources on bacterial cellulose production by Gluconacetobacter xylinus strain ATCC 53524. J Appl Microbiol. 2009;107(2):576–83.

37. Czaja W, Romanovicz D, Brown, R malcolm. Structural investigations of microbial cellulose produced in stationary and agitated culture. Cellulose. 2004;11(3/4):403–11.

38. Carlsson DO, Lindh J, Strømme M, Mihranyan A. Susceptibility of Iα- and Iβ-dominated cellulose to TEMPO-mediated oxidation. Biomacromolecules. 2015;16(5):1643–9.

39. Isogai A, Atalla RH. Dissolution of cellulose in aqueous NaOH solutions. Cellulose. 1998;5(4):309–19.

40. Molina-Ramírez C, Enciso C, Torres-Taborda M, Zuluaga R, Gañán P, Rojas OJ, et al. Effects of alternative energy sources on bacterial cellulose characteristics produced by Komagataeibacter medellinensis. Int J Biol Macromol. 2018;117:735–41.

41. Xiang Z, Liu Q, Chen Y, Lu F. Effects of physical and chemical structures of bacterial cellulose on its enhancement to paper physical properties. Cellulose. 2017;24(8):3513–23.

42. Chen SQ, Cao X, Li Z, Zhu J, Li L. Effect of lyophilization on the bacterial cellulose produced by different Komagataeibacter strains to adsorb epicatechin. Carbohydr Polym. 2020;246:116632.

43. Hur DH, Rhee HS, Lee JH, Shim WY, Kim TY, Lee SY, et al. Enhanced production of cellulose in Komagataeibacter xylinus by preventing insertion of IS element into cellulose synthesis gene.

Biochem Eng J. 2020;156:107527.

Chapter 4

Hemostatic oxidized bacterial cellulose membranes

Surgicel® (regenerated oxidized cellulose) is a bio-absorbable hemostatic material widely applied to prevent surgery-derived adhesions. Some critical issues have been reported associated with this biomaterial, which we aimed to overcome by producing bacterial cellulose membranes with hemostatic activity, through electrochemical oxidation using TEMPO radical. Samples were characterized by FTIR, NMR, SEM, XRD and their degree of polymerization. The oxidation degree was evaluated by titration of the carboxyl groups and the hemostatic behavior by whole-blood-clotting assays. *In vitro* and *in vivo* biodegradability of oxidized BC membranes were evaluated and compared with that of Surgicel®. The oxidation degree increased from 4% to 7% and up to 15%, corresponding to an applied charge of 400, 700 and 1200 Coulombs, respectively. The oxidized BC preserved the crystallinity and the 3D nano-fibrillar network, and demonstrated hemostatic activity, although not as effective as that of Surgicel®. *In vivo* assays demonstrated that the oxidized membranes did not induce an inflammatory response, revealing a good biocompatibility. However, non-degraded oxidized BC was still detected at the implantation site after 56 days.

4.1 - INTRODUCTION

Hemostasis involves a complex interaction between four key elements: the vascular endothelium, platelets, the coagulation pathway and fibrinolysis. When the natural physiologic hemostasis is not enough to control a hemorrhagic episode, it is essential to use hemostatic materials. Different hemostatic approaches may be applied according to the type of injury, and they can be constituted of materials based on polyethylene glycol (1,2), regenerated oxidized cellulose (Surgicel®) (3) or proteins like thrombin, collagen (Colgel®) and fibrin (TachoSil®) (4,5). Surgicel®, made by Ethicon Inc. of Johnson & Johnson, is a bio-absorbable material widely applied for intraoperative hemostasis and adhesion prevention in surgery. Surgicel® seems to act as a mesh for platelets adhesion and aggregation, helping on the formation of an artificial clot, while its negative charge is likely to activate the secondary hemostasis as well. It is advisable to remove Surgicel® when the hemostasis is controlled. However, the most common procedure is to leave the hemostatic *in situ* to reabsorb spontaneously, usually without any secondary effects. If left *in situ*, the complete degradation should occur between 4 and 8 weeks (6,7). Nevertheless, some issues were reported associated with the use of Surgicel®. The presence of a recurrent gastrointestinal stromal tumor four months after surgical resection was ascribed to the intra-abdominal foreign-body granuloma caused by the presence of Surgicel® residues in an 83-year-old male patient (7). Another case reported the formation of a foreign body reaction, contributing to the development of an intracranial giant-cell granuloma. In this case, the patient was diagnosed with intracranial hemorrhage which was ascribed to the use of Surgicel® (8,9). It is thus essential to develop new hemostatic dressings able to overcome these drawbacks.

Bacterial cellulose (BC) represents an alternative source of cellulose with great potential for some specific applications, giving its very special technical properties (10,11). BC has good mechanical properties (Young's modulus around 15-35 GPa and tensile strength of 200-300 MPa), high crystallinity, high degree of polymerization and high water content - up to 200 times its dry weight (10,12,13). In addition, BC is a biocompatible material that exhibits high purity since it does not have hemicelluloses, pectin and lignin, as its vegetable counterpart. *Komagataeibacter xylinus* (14) is the most efficient producer and depending on the cultivation method and the bioreactor used, BC may be produced in different shapes such as membranes, hollow tubes, pellets or thin fibrous materials. When cultivated in static culture, a nanofibrillar pellicle is obtained, where one side displays a denser surface, while the other one exhibits a gelatinous layer (15,16). Some BC-based materials are commercially available for biomedical application, e.g. as wound dressings, such as CelMat®, EpiProtect® and Nanoskin®. The

excellent biocompatibility of BC has been demonstrated in several works. For instance, Helenius et al. assessed the *in vivo* biocompatibility through subcutaneous implantation in rats for 1, 4 and 12 weeks. The chronic inflammation, foreign body responses, cell ingrowth and angiogenesis were evaluated through histology, immunohistochemistry and electron microscopy. The obtained results showed that there were no macroscopic and microscopic evidences of inflammation around the implants. Also, there were no signs of fibrotic capsule or giant cells and BC was well integrated into the host tissue and did not induce any chronic inflammatory reactions (17). Pértile et al. also showed the good biocompatibility of BC in a long-term biocompatibility study. The BC samples were implanted in mice and it was showed that a mild and benign inflammatory reaction occurred which decreased along time and did not induce a foreign body reaction. Furthermore, there were no signs of chronic inflammatory reaction or encapsulation, while formation of new blood vessels around and inside the implants were observed (18). More recently, Zhang et al. evaluated the *in vitro* biocompatibility of a BC scaffold for corneal stroma replacement, through the cultured of rabbit corneal epithelial and stromal cells on the BC scaffold, during a 3-month follow-up. The obtained results showed that BC supported cell adhesion, proliferation and differentiation. On the other hand, *in vivo* tests further confirmed the good biocompatibility and stability of BC in rabbit cornea, making BC an attractive option for tissue engineering of corneal stroma (19). Beyond biocompatibility, in biomedical field, another desirable requirement for many applications is biodegradability. The modification of BC in order to increase and improve its biodegradability has been attempted. Thus, an improvement on biodegradation may be achieved through oxidation, making BC resorbable by the organism (20,21).

The chemical modification of BC can be achieved through the carboxylic functionalization on C2, C3 and C6 of the glucose residue. In this process, the hydroxyl group at C2, C3 and C6 is first oxidized into an aldehyde, which in turn is further oxidized into a carboxylic group (22). Oxidation is commonly accompanied by degradation and a concomitant decrease in the degree of polymerization, which can be a consequence of the oxidation reaction *per se* or can be triggered by subsequent pH changes. The 2,2,6,6-Tetramethylpiperidine-1-oxyl (TEMPO) has been widely applied to oxidized cellulose. In the last few years, TEMPO has been chosen as the primary method to convert polysaccharides into the corresponding polyuronic acids through the selective oxidation of the primary hydroxyl groups at C6 to carboxyl groups (23,24). During the process, TEMPO is oxidized through a one-electron transfer reaction to the corresponding oxoammonium (active oxidant in the primary alcohol oxidation). Furthermore, at the anode occurs the electrooxidation of the hydroxylamine regenerating the $TEMPO^{+}$ *in situ*. This approach is cleaner than the alternative chemical method, that use co-oxidants like NaClO-NaBr, water-acetonitrile-

NaClO-$NaClO_2$ (25). Moreover, contrarily to the enzymatic or metal catalyzed oxidation, TEMPO-oxidation method is very efficient on the conversion of high molecular weight polysaccharides (26). Furthermore, TEMPO is also characterized by its stability, non-toxicity and non-mutagenic features (27), high reaction rate and yield, allowing a controlled modification of the polysaccharides (26). Thus, the oxidation of cellulose by TEMPO radical may be used to facilitate the mechanical disintegration of cellulose fibers into nano fibrils, reducing energy and mechanical action. Besides, unreacted TEMPO may be recovered from reaction medium after the removal of $NaHCO_3$ and Na_2CO_3 (carbonate buffer) through neutralization using a cation exchange resin. On electrochemical oxidation carbonate buffer is used as electrolyte, the increase of ionic strength providing a decrease of internal resistance of the electrochemical cell (28).

We aimed at oxidizing BC through electrochemical methods in order to increase its biodegradability, while conferring hemostatic properties. Since BC fibers are ultrathin, we hypothesize that surface oxidation may lead to a substantial improvement of the biodegradability of the BC fibers. While the hemostatic behavior was achieved after oxidation, the *in vivo* degradability was not satisfactory, despite the good biocompatibility of the oxidized BC membranes.

4.2 – Materials and Methods

4.2.1 – BC membranes purification

Commercial BC membranes (purchased from HTK CO., LTD, Vietnam) with an initial thickness of 12-15 mm were washed once with distilled water and then with 5% (w/v) of sodium dodecyl sulphate (SDS; Sigma-Aldrich), to remove endotoxins for 5 days (solution renewed everyday), followed by extensive washing with distilled water; all washings were done at room temperature. Afterwards, membranes were sliced to a final thickness of 3.3 mm and then sterilized by autoclaving at 121°C, for 20 minutes, prior to storage in distilled water and at 4°C. For all the characterization tests, BC membranes were then frozen at -80°C and freeze-dried at -100°C (Scanvac Coolsafe) during 5 days.

4.2.2 – Electrochemical setup

Cyclic voltammetry (CV) and constant potential electrolysis were the applied electrochemical techniques. The electrolysis was carried out in aqueous solution using TEMPO radical (Sigma-Aldrich)

and 0.2 M carbonate buffer ($NaHCO_3$ and Na_2CO_3) (pH=10). CV was performed at a constant scan rate of 50 mV s^{-1} to assess the oxidation-reduction process.

The voltammetric study was performed in a thermostated three electrode and two-compartment glass cell separated by an ion exchange membrane (Nafion 417). Toray carbon paper was used as working electrode. A tap was introduced into the Luggin bridge in order to establish the contact between the reference and the electrolyte solutions without any contamination of the later by the ions of the reference electrode solution. A saturated calomel electrode (SCE) and a platinum foil (99.95%) were used as reference and counter electrodes, respectively. Before each experiment, the solutions were deaerated with ultra-pure argon (U Quality from Air Liquide) and the nitrogen stream was maintained over the solution during the measurements. The electrochemical instrumentation consists of a potentiostat/galvanostat from Amel Instruments coupled to a microcomputer through an AD/DA converter. The Labview Software (National Instruments) and a PCI-MIO-16E-4 I/O module were used for generating and applying the potential program as well as acquiring data, such as current intensities (28).

4.2.3 – Oxidation degree

The oxidation degree of BC was evaluated by titration with sodium hydroxide (NaOH). A potassium hydrogen phthalate ($C_8H_5KO_4$) solution was used to determine the concentration of NaOH (0.012 M) by titration, using phenolphthalein as indicator. Freeze-dried oxidized BC membranes (~100 mg, the exact mass was recorded) were cut into small pieces and dispersed in 30 mL into distilled water, and the pH was adjusted to 2.40 with HCl (1 M). The samples were placed at 4°C during 5 days under agitation, and the pH was adjusted again before starting the titration.

The oxidation degree was calculated by the following equation:

$$Oxidation\ degree\ (OD)(\%) = \frac{C \times V \times M}{m} \times 100 \quad (7)$$

where C is the concentration of NaOH (mol/L), V the volume of NaOH (L) used in the titration, rectified considering the value used in a blank titration (without BC), M the molecular weight of the BC monomer (162g/mol) and m the dry mass of BC (g) (29). The titration was terminated only when protonation equilibrium was achieved and no changes on pH was observed.

4.2.4 – Degree of polymerization

Both oxidized and non-oxidized freeze-dried BC membranes (50 mg) were cut into small pieces and mixed with 5 mL of distilled water under agitation during 30 minutes. Then, 5 mL of cupri-ethylenediamine (CED, Sigma-Aldrich) saturated with copper (II) hydroxide was added and the mixture was agitated for 60 minutes and, afterwards, centrifuged for 5 minutes at 7000 rcf. Finally, the intrinsic viscosities of the BC samples were obtained using a Ubbelohde capillary-tube viscometer from Rheotek placed in a water bath at 25°C. The viscosity values were obtained according to the standard ES ISO 5351:2012 Pulps – Determination of limiting viscosity number in cupri-ethylenediamine (CED) solution. Thus, the viscosity ratio η_{ratio} was calculated using the following equation:

$$\eta_{ratio} = \frac{\eta}{\eta_0} = h \times t \quad (4)$$

where, h is the viscometer constant that it was determined as to be 0.132 s^{-1} and t is the efflux time (in seconds) of the test solution. The viscosity averaged degree of polymerization (DP_v) was calculated using Mark-Houwink-Sakurada equation (30):

$$[\eta] = K \times DPv^{\alpha} \quad (5)$$

where, for BC samples, K=0.0002 and α=1.9705 (31).

Finally, the molecular mass of BC was calculated from the relationship:

$$DP_v = \frac{M}{162} \quad (6)$$

where M is the molecular mass of the BC and *162* (g/mol) equals the molecular mass of an anhydroglucose unit (32). All the samples were analyzed in triplicate.

4.2.5 – NMR

The BC membranes were analysed by NMR using a Spectrometer Bruker Avance III 400 wide-bore (400 MHz, 1H Larmor frequency). A 4 mm double-resonance MAS probe was employed at 100.6 MHz (13C) Larmor frequency. Oxidized and non-oxidized BC samples were spun in ZrO_2 rotors using a spinning rate of 12 kHz. ^{13}C-CP/MAS NMR spectra were recorded using a ramp step (varying from 100% to 50% in

amplitude using 100 points), with a recycle delay of 5 s, a contact time of 2.0 ms and 1H 90° excitation pulse of 3.10 μs. All chemical shifts are quoted in parts per million from tetramethylsilane (TMS).

4.2.6 – ATR-FTIR

Freeze-dried oxidized and non-oxidized BC membranes were analyzed using an ALPHA II- Bruker spectrometer (Ettlingen, Germany) with a diamond-composite attenuated total reflectance (ATR) cell. Data was collected using OPUS software which is integrated on the FTIR equipment. The measurements were recorded with a wavenumber range from 4000 to 400 cm^{-1}, with a resolution of 4 cm^{-1} and 64 scans per sample. The ATR clamp and platform were cleaned with a cotton swab dampened with isopropyl alcohol and allowed to dry between analysis of each coupon. All assays were done in duplicate for each sample.

4.2.7 – SEM

Freeze-dried oxidized and non-oxidized BC membranes morphology was assessed by SEM (FEI Quanta 650 FEG; acceleration voltage from 3-10 kV). Both oxidized and non-oxidized BC membranes were added to aluminum pin stubs with electrically conductive carbon adhesive tape (PELCO Tabs™), with the excess removed using compressed air. Samples were coated with 2,5 nm of Au for improved conductivity. The analysis was conducted at (3-10 kV) with intensity point. For the quantitative analysis of the length of the fibers, at the least five different fibers were selected using the software ImageJ.

4.2.8 – XRD

The crystalline structure was assessed using a PANalytical X'Pert Pro MPD diffractometer equipped with X'Celerator detector and secondary monochromator. Freeze-dried oxidized and non-oxidized BC membranes were analyzed at room temperature using a CuKα radiation and Bragg-Bentano geometry, 0.017°/step and 100 s/step.

The crystallinity index (CrI) (Equation 1) was calculated using Segal, Creely, Martin & Conrad (1959) (33) equation, i.e., it was calculated as a function of the maximum intensity of the diffraction peak from the crystalline region (I_{200}), at an angle of $2\theta \sim 22.5°$, and the minimum intensity from the amorphous region (I_{am}), at an angle of $2\theta \sim 18°$

$$CrI\ (\%) = \frac{(I_{200} - I_{am})}{I_{200}} \quad (1)$$

The apparent crystallite size (CS) in the crystallographic planes (1-10), (110) and (200) were calculated assuming that the crystals exhibit uniform size and shape and using Scherrer's equation:

$$CS = \frac{K\lambda}{FWHM \cos\theta} \quad (2)$$

where *K* is a dimensionless factor dependent upon the method used to calculate the amplitude (K = 0.9), λ is the wavelength of the incident X-ray (λ = 0.15 nm), *FWHM* is the width of the diffraction peak at half-maximal height (in radians), and θ is the angle of the diffraction peak of the crystalline phase (Bragg's angle). The diffractograms were analyzed by Rietveld refinement with Powder Cell software.

4.2.9 – *In vitro* degradation of oxidized BC membranes

The degradation of oxidized and non-oxidized BC membranes was tested *in vitro* using ultra-pure water at 37°C. The freeze-dried BC membranes were cut into pieces weighting between 8 to 12 milligrams (the exact mass was recorded). Then, they were immersed in 2 mL of ultra-pure water in centrifuge tubes. After incubation during 3, 7, 14 and 63 days the samples were taken out, dried in a woven at 50°C overnight, and weighed. The original mass of each sample was designated as m_i while the mass after degradation was designated as m_f. Thus, the mass loss rate was calculated using the following equation (29):

$$Mass\ loss = \frac{m_i - m_f}{m_i} \times 100 \quad (8)$$

4.2.10 – Biological assays and hemostatic behaviour of BC membranes

4.2.10.1 – Preparation of blood samples

Whole blood was collected from healthy bovine animals from on Izicar – Fábrica do Produtos Porcinos, Lda (Vila Nova de Famalicão, Portugal) using citrated (3.2%) 3 mL vacuum blood-collection tubes (Vacuette, Portugal) and transported on ice.

4.2.10.2 – Whole blood clotting samples

Three mL of whole blood were placed in each well of a 24-well plate. Then, 300 µL of 0.1 M $CaCl_2$ (Riedel-de Haën) were added to induce clotting and the mixture was incubated for 0, 5, 10, 15 and 25 minutes at room temperature, with i) oxidized; ii) non-oxidized BC membranes; iii) Surgicel® (reference material); iv) glass microspheres (Ø0.40-0.60mm, Startorius) (positive control) and v) bare polystyrene (empty well, negative control). A volume of 100 µL of activated whole blood were collected for each time point and 2.5 mL of distilled water were added to each well followed by incubation for 5 minutes, to lyse the red blood cells which were not trapped in the thrombus, and release hemoglobin. Afterwards, the concentration of the released hemoglobin was measured by transferring 200 µL of the supernatant to a 96-well plate and analyzed in a spectrophotometer at λ=540 nm. In this method, a faster clot formation leads to a faster reduction of the detected absorbance value. All the samples were analyzed in triplicate (34).

4.2.11 – *In vivo* biocompatibility tests of BC membranes

All the procedures were carried out in strict accordance with the recommendations for care and use of laboratory animals of the EU directive (2010/63/EU) and National (Decreto-Lei 113/2013) legislation for animal experimentation and welfare. The experimental procedures were carried out with the approval of the Portuguese competent authority, Direção Geral de Alimentação e Veterinária (DGAV, Lisboa, Portugal) with animal ethic approval number 0421/000/000/2017.

Eighteen Wistar female rats (Charles River Laboratories, Les Oncins, France) weighing approximately 250 g were used in this study. All animals were kept in ventilation, humidity and temperature-controlled rooms with a 12/12-hour light/dark cycle. The animals were housed on cages (3 animals/cage) with corn kernels and received food pellets and water ad libitum. All animals were implanted subcutaneously with 3 untreated BC disks with 13 mm in diameter on the left side and 3 oxidized BC disks with 13 mm in diameter in the right side on the animal's back. Animals were randomly assigned and blindly divided into 3 groups. The first group (n=6) in which the implants were removed after 3 days. A second group (n=6) in which the implants were removed after 14 days. The third group (n=6) in which the implants were removed after 56 days.

4.2.11.1 – Surgical procedures

Rats were anaesthetized with ketamine (80 mg/kg) and dexmedetomidine (0.2 mg/kg) by intraperitoneal injection, and then prepared for surgery as follows: the back of the animal, form the neck trough the tail, was shaved, antisepticised with chlorhexidine, and dried. Bodies were covered with sterile sheets except for the incision line. Three skin incisions (length, 2–3 cm) were made on the midline of the back of the animal. On each side three subcutaneous pockets (with approximately 30 mm) were carefully created using mosquito forceps. The implants were introduced into the pockets without fixation, located 20 mm from the line of incision without touching one another. The soft tissues and the skin were reapproximated with monofilament absorbable synthetic sutures (glyconate USP 5/0). Implant site location was performed by placing a subcutaneous stitch with non-absorbable suture. An ophthalmologic gel was applied to prevent drying of the eyes. Additionally, buprenorphine (0.05 mg/kg) was administered at the end of the surgical procedure immediately before the wound closure was completed. Postoperative pain control was also carried out with buprenorphine (0.05 mg/kg subcutaneous, twice daily) for 2 days.

The animals were sacrificed under general anesthesia with a lethal dose of pentobarbital (80 mg/kg), delivered by intracardiac injection. Implants were then carefully removed in conjunction with all surrounding tissues and fixed with 4% neutral buffered formalin. After that, both oxidized and non-oxidized BC membranes were fixed in 10% neutral buffered formalin, dehydrated and embedded in paraffin. Cross sections (5 μm) were cut and stained with Hematoxylin and Eosin (H&E) for cellular infiltration and inflammatory response (35), as described below.

4.2.11.2 – Histological evaluations

The implants and the surrounding tissue were collected at 3, 14- and 56-days post implantation. Samples were fixed in 10% formalin, paraffin embedded, cut in 5 μm and stained with H&E for histological evaluation. For each sample, the biological response parameters were evaluated at the implant–tissue interface with three high power fields (×400) by two pathologists and recorded in an appropriate formulary. All the biological response parameters were evaluated according to the ISO standard 10993-6 which included the extent of fibrosis/ fibrous capsule (layer in micrometers) and inflammation; degeneration, as determined by changes in tissue morphology; the number and distribution from the material–tissue interface of the inflammatory cell types, namely polymorphonuclear neutrophilic leucocytes (PMN), lymphocytes, plasma cells, macrophages and multinucleated cells; the presence, extent and type of necrosis; other tissue alterations such as vascularization and fatty infiltration. Based

on the scoring system for the parameters, a total value was obtained for each animal in each group (35). The collected data were submitted to statistical analyses. The data were analyzed with one-way analysis of variance followed by the Tukey multiple comparisons test was used to evaluate the statistical differences between the groups using GraphPad Prism 5.0 software. Differences were considered statistically significant at $P < 0.05$.

4.3 – Results and discussion

BC with three different oxidation degrees i.e., 4%, 7% and 15%, corresponding to the generation of 400, 700 and 1200 Coulombs (samples BC 400C, BC 700C and BC 1200C, respectively), were obtained and analyzed by FTIR, SEM, XRD and for *in vitro* degradation. However, the more oxidized membranes were very fragile, making their handling quite difficult after preparation. Hence, BC 1200C samples were excluded from degree of polymerization measurements, NMR analysis and hemostatic assays. Finally, and in order to reduce the number of animals, the *in vivo* biocompatibility tests were performed using only the BC 700C membranes.

4.3.1 – CV

Before each electrolysis, a CV study of the BC oxidation using TEMPO mediator and carbonate buffer electrolyte was performed. Taking into account the preliminary voltammetric study carried out, the applied potential values were set between 0.7 and 0.8 V vs. SCE. Three electrolysis were carried out on the carbon Toray electrode in the presence of BC and TEMPO. The voltammetric study was performed also with TEMPO, in the absence of the BC membrane, as well as at the beginning and at end of the BC electrolysis (Fig. 4.1). In addition, CV was also used to evaluate the electroreactivity of TEMPO and its chemical stability.

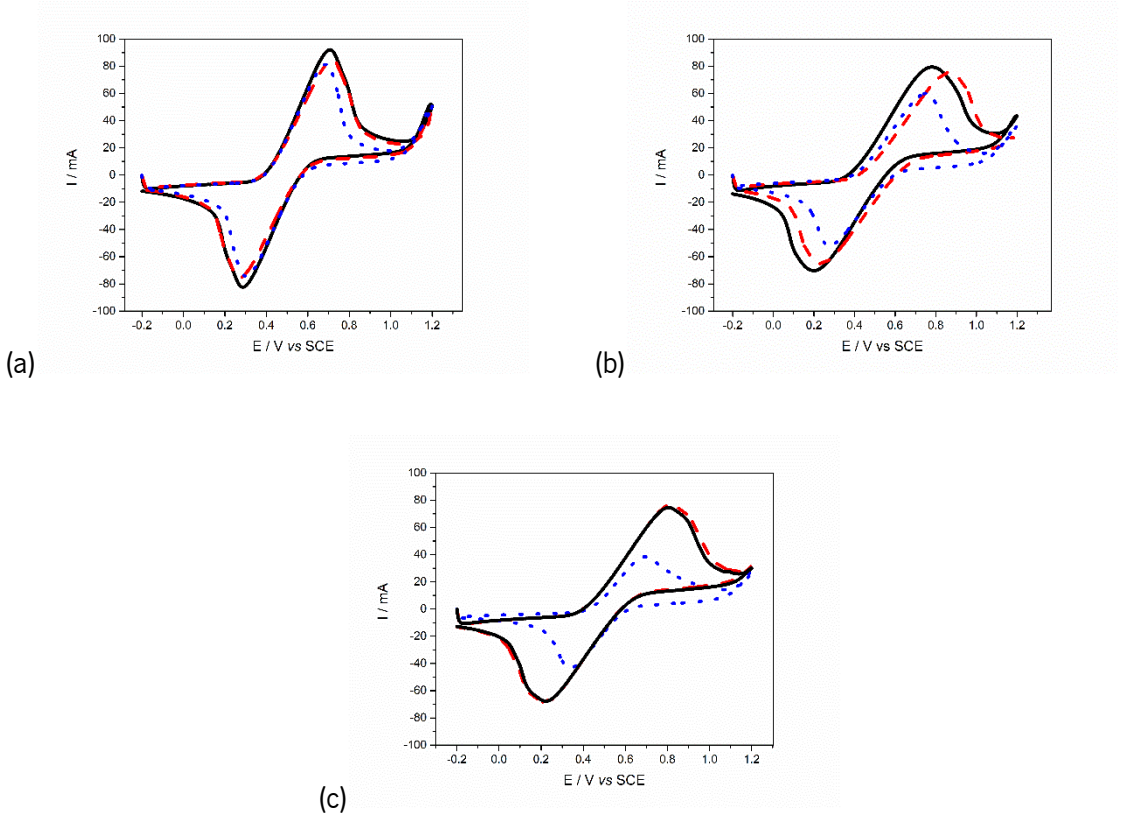

Figure 4.1. Cyclic voltammograms of Toray Carbon electrode in presence of TEMPO (____) and of TEMPO with BC membrane at the beginning (____) and at the end of the electrolysis (____). The voltammograms corresponding to (a) BC 400C, (b) BC 700C and (c) BC 1200C membranes were acquired at room temperature and at scan rate of 50 mV s^{-1}.

The successively obtained voltammograms remained unchanged, showing the stability of the electrocatalytic materials. Furthermore, they were similar to those obtained by other authors (36–38) and all of them exhibiting a characteristic profile and good reversibility, featuring the anodic peak ascribed to the reversible oxidation of TEMPO corresponding to the active oxidant, the ion oxoammonium ($TEMPO^+$), which was reduced into its hydroxylamine form during the cathodic sweep (28). The current intensities remained almost unchanged after the introduction of BC, accompanied by a slight shift in the oxidation potential towards more anodic values. On the other hand, at the end of electrolysis, a decrease on the current intensity was observed in the anodic peak, revealing the oxidation of BC membranes. This decrease in the current intensity also was directly related to an increase in the oxidation degree of the BC membranes.

4.3.2 – Oxidation degree

The oxidation degree of BC membranes was determined by titration. The values obtained using Equation 1 are shown on table 4.1.

Table 4.1. Oxidation degree (in %) corresponding to different applied charges and the duration of electrolysis.

Sample	% Oxidation degree	Duration of electrolysis (h)
BC 400C	3.68 ±1.03	2.39 ± 0.52
BC 700C	6.45 ± 1.13	6.07 ± 1.25
BC 1200C	14.92 ± 0.31	14.5 ± 4.94

The results showed that the duration of the electrolysis was proportional to the applied charged and that roughly, the oxidation degree increased directly with the applied charge, with the values increasing from 4 to 15% of oxidation depending on the conditions used. These relatively small oxidation degrees were expected, since the reaction occurs only at the surface of the fibers, and the mediator is not able to penetrate the crystalline domains of cellulose. Moreover, the obtained values were similar to those obtained by Sezer et al. (39) where for 6h of reaction, the oxidation degree was around 7, and for 12h was approximately 9.

4.3.3 – Degree of polymerization

The obtained results show that the degree of polymerization decrease with an increase on the oxidation degree, as follow: 1959 ± 63 for non-oxidized BC > 1841 ± 36 for BC 400C > 1401 ± 65 for BC 700C. These results are in accordance with other works (31,40–43). Considering that the inner part of the crystallites is not expected to undergo depolymerization, this must occur to significant extent at the surface level as to lead to the observed average reduction in DP, which justifies the increasing fragility of the membranes as the oxidation increases.

4.3.4 – NMR

NMR was used to confirm the specific oxidation of C6 of the BC membranes. The obtained spectra are presented on Fig. 4.2.

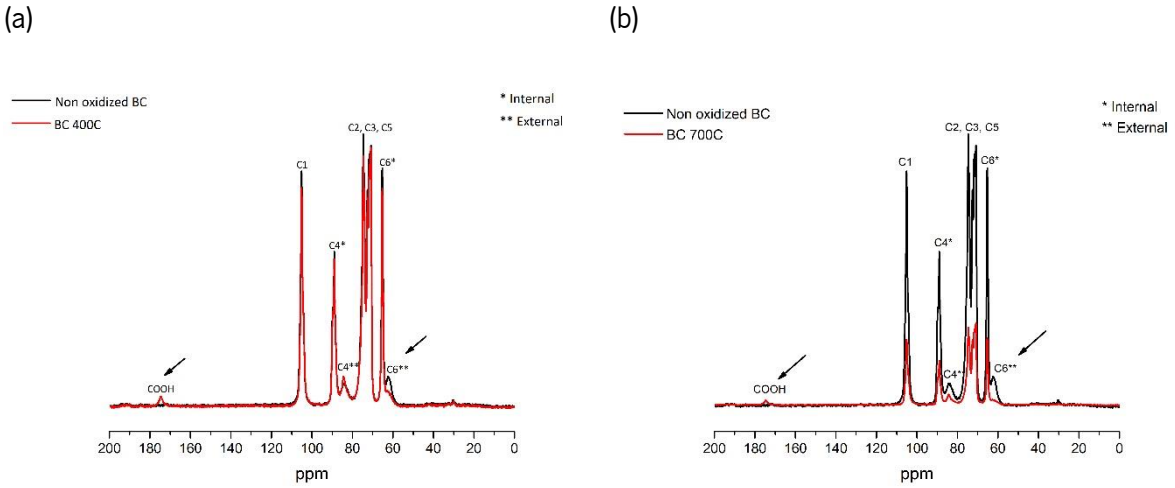

Figure 4.2. NMR spectra of (a) 400C and (b) 700C membranes compared with non-oxidized BC membranes.

The signal at 104.5, 84.5 and 61.7 ppm were assigned to C1, C4 and C6, respectively. However, the peaks between 75.3-70 ppm, corresponding to C2, C3 and C5, were not easily assessed since the resolution was not good enough (29,44,45). The peak at 61.7 ppm, related to C6 primary hydroxyl groups, presented a lower intensity in the oxidized membranes. On the other hand, the peak at 64.9 ppm corresponding to the C6 primary hydroxyl groups inside the crystalline fibrils and the C2/C3 peaks remained unchanged, as expected, since the hydroxyl groups located in the inner structure of the crystallites hardly suffer oxidation (46). Finally, the peak around 174.6 ppm, that corresponds to the carboxylate groups produced during the electrolysis, further confirm the oxidation of hydroxyl groups (21). As expected, the intensity of this peak was found to be directly related with the oxidation degree.

4.3.5 – ATR-FTIR

ATR-FTIR spectra of the non-oxidized BC and different degrees of oxidized BC are shown in Fig. 4.3. The usual bands ascribed to the chemical structure of BC were observed: (O–H symmetrical stretching around 3350 cm^{-1}; C–H stretching around 2900 cm^{-1}; C–O–C stretching around 1162 cm^{-1}; C–O stretching at 1030 cm^{-1}; vibration of amorphous cellulose (stretching of the glucose ring) around 899

cm^{-1}. Regarding the oxidized BC, the most relevant modifications were the appearance of a C=O stretching band at around 1628 cm^{-1} that confirmed the formation of carboxylic groups (–COOH) (23,47). This peak also confirmed that the hydroxyl groups at the C6 position in the BC had been successfully converted into carboxyl groups.

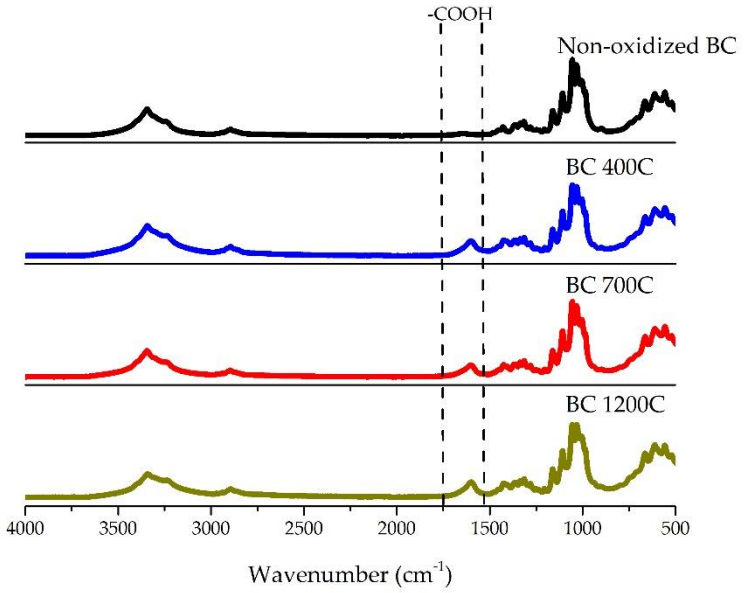

Figure 4.3. FTIR spectra of oxidized and non-oxidized BC membranes.

There were no other relevant differences between the spectra of the BC and oxidized BC membranes; thus, as it was observed from the NMR analysis, it may be concluded that highly selective oxidation was achieved.

4.3.6 – SEM

The influence of oxidation on BC membranes morphology was assessed by SEM. The obtained images are present on Fig. 4.4. The width of the fibers was also measured, and the values are presented on table 4.2.

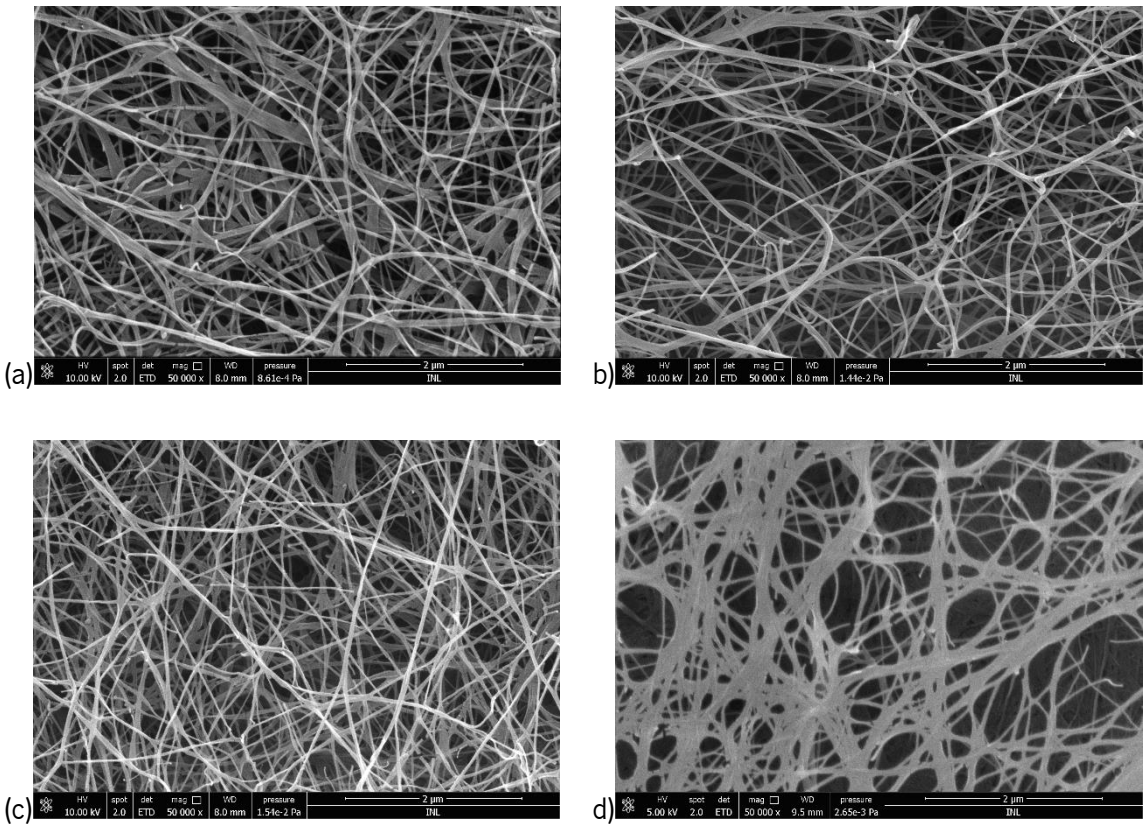

Figure 4.4. SEM images of (a) non-oxidized and (b) 400C, (c) 700C and (d) 1200C BC membranes. (Magnification: 50000 x).

Table 4.2. Width of the oxidized and non-oxidized BC fibers.

Sample	Width of the fibers (nm)
Non-oxidized BC	44.3 ± 2.14
BC 400C	39.13 ± 2.04
BC 700C	38.75 ± 1.15
BC 1200C	29.56 ± 1.83

SEM images revealed that oxidation did not affect the morphology of the fibers. The BC exhibited the usual compact 3D network structure of the nanofibrils, which remained almost similar after oxidation, showing that the electrochemical oxidation did not considerably affect their structure (48). According to

table 4.2, the average width of the fibers was approximately 44 nm for pristine BC while for oxidized samples the values varied between 29 nm and 39 nm depending on the oxidation degree. Thus, the obtained values for both oxidized and non-oxidized samples were in accordance to the literature (49–51). On the other hand, it is possible to observe that oxidation induced a slight decrease on the width of the fibers, although not so effective when compared to the work developed by Jun et al. (52) in which the average width of the fibers decreased from 100 nm to 30-50 nm after oxidation. Taking these results into account, we would expect a more expressive decrease on the width of the fibers, which was not observed.

4.3.7 – XRD

Crystalline native cellulose exhibits high crystallinity, being a combination of two crystalline structures: triclinic (I_α) and monoclinic (I_β), present in distinct proportions, depending on the source. The first one is the major polymorph for most algae and bacteria while the second one is dominant for higher plant cell wall cellulose and in tunicates (53). XRD analyses were performed to understand the effect of oxidation on material crystallinity. Figure 4.5 shows the obtained diffractograms for the pristine and oxidized BC samples with different oxidation degrees.

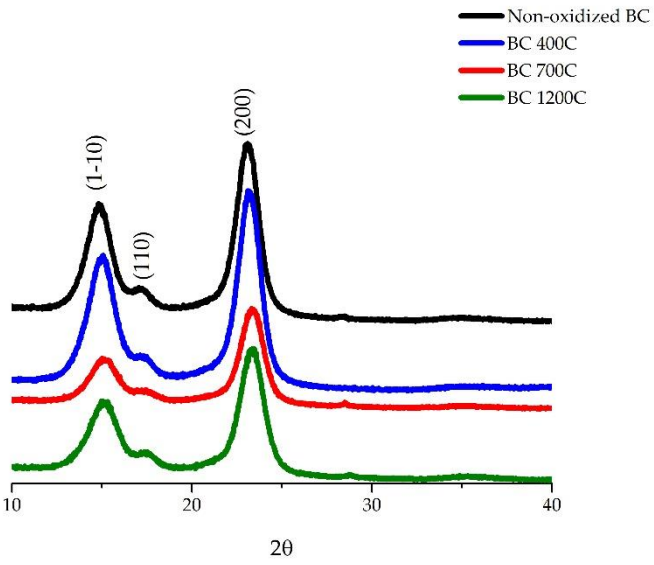

Figure 4.5. XRD patterns of oxidized and non-oxidized BC membranes.

Pristine BC exhibited the diffraction peaks at 14.5°, 16.5° and 22.5° corresponding to the primary diffraction of the crystal planes (1-10), (110) and (200) which is ascribed to cellulose I (54,55).

On the other hand, the obtained crystallinity indexes were very high for all samples (table 4.3) and similar to those obtained by other authors (56,57).

Table 4.3. Crystallite size and crystallinity index of pristine and oxidized BC.

Sample	Crystallite size (nm)	Crystallinity index (%)
Non-oxidized BC	7.2	91.6
BC 400C	6.9	89.4
BC 700C	6.8	89.8
BC 1200C	6.5	87.8

Table 4.3 also shows a slight decrease in the crystallinity index and in the crystallite size, related to an increase on oxidation degree (58,59), which may be explained by a destructuring effect of the cellulose intermolecular hydrogen bonds at the nanocrystallite surface (21). Nevertheless, the diffraction peaks obtained for all the oxidized samples were very similar to pristine BC membranes suggesting that the oxidation process had a small effect on the crystal structure of the cellulose microfibrils (60).

4.3.8 – *In vitro* degradation of oxidized BC membranes

The degradation of BC was assessed by gravimetry, after incubation of the samples in ultra-pure water for 3, 7, 14 and 63 days. The obtained results are presented in Fig. 4.6.

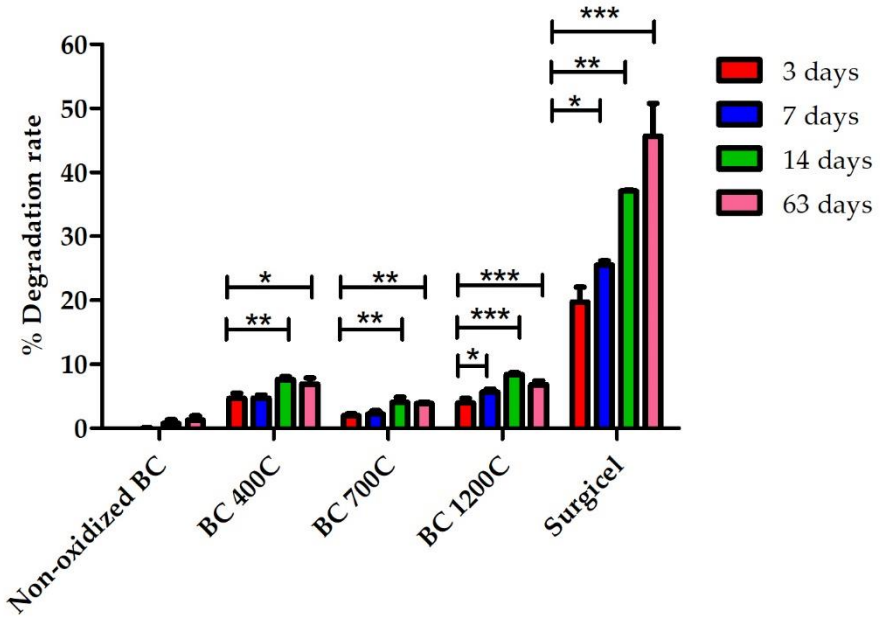

Figure 4.6. *In vitro* degradation of oxidized and non-oxidized BC membranes. Significant differences are indicated as follow: * P<0.05, **P<0.01 and *** P<0.001.

As expected, non-oxidized BC did not suffer degradation even after 63 days of incubation (the variation of the dry weight observed is not statistically significant). For all the oxidized samples and Surgicel® the degradation rate increased over time revealing statistically significant differences (P<0.05) from 3 days to the remaining time-points. However, unexpectedly, BC 700C degraded to a slightly lower extent as compared to BC 400C, which in turn degraded to a similar extent as the BC 1200C membranes, approximately up 5% to 9%. In spite of these small differences, the degradation of the three membranes can be considered similar, the comparison of the data corresponding to days 14 and 63 suggesting that the fraction of degradable oxidized cellulose was lower than 10%. On the other hand, Surgicel® degradation increased over time but complete degradation did not occur even after 63 days of incubation. In the human body, Surgicel® is expected to be fully degraded in a period between 7 and 14 days (61) however, in ultra-pure water, *in vitro* degradation was only of 46% after 63 days. The use of simulated body fluid (SBF) could provide a more realistic degradation rate (62,63), but we chose using ultra-pure water in the *in vitro* assays (degradation was qualitatively monitored also in vivo, as described below), since the degradation was monitored by gravimetry, and the residues from SBF could interfere in the results. The obtained results confirm that the oxidation improved the degradability of BC membranes. Since the BC 1200C membrane was already quite fragile for the envisaged applications, we did not try to further increase the oxidation. We attributed the difficulty in achieving more extensive oxidation and

biodegradability to the fact that the reaction occurs mainly on the surface of the fibers. This surface layer, oxidized to some extent, becomes degradable, but the inner layers are still non-biodegradable.

4.3.9 – Biological assays and hemostatic behavior of BC membranes

The whole-blood-clotting assay was applied to assess the pro-coagulative properties of oxidized BC. In this technique, fresh blood is placed in direct contact with BC samples, and at different time-points, deionized water is added in order to promote the release of hemoglobin from those erythrocytes which are not immobilized in the forming blood clot. This way, lower absorbance values are directly related with higher blood clotting ability. The kinetics of whole blood clotting is presented on Fig. 4.7.

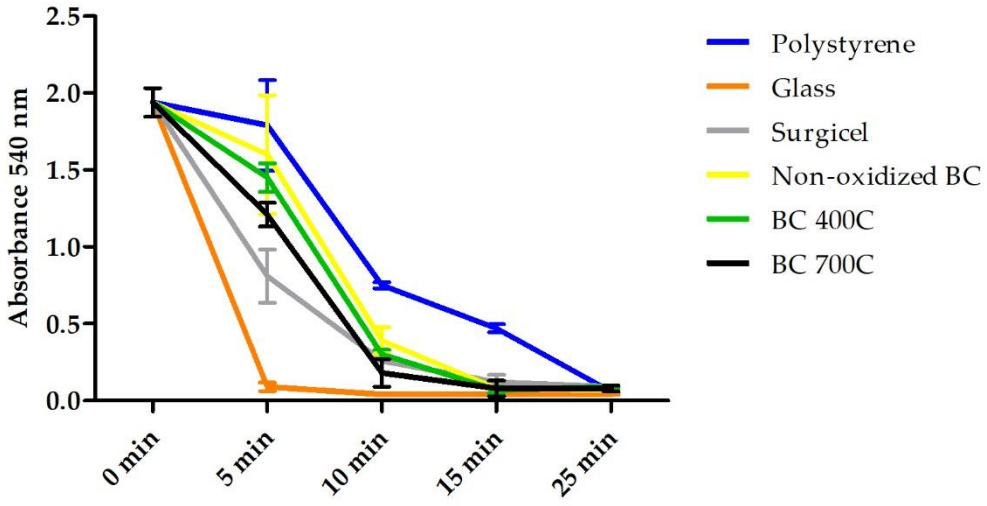

Figure 4.7. Whole blood clotting time using of oxidized and non-oxidized BC membranes.

Figure 4.7 displays the decrease of the absorbance values over the time, showing that in every case blood coagulation occurred within 25 min. The following relative behavior of the samples, from the highest to the lowest coagulation power can be observed: glass microspheres > Surgicel® > oxidized BC 700C > oxidized BC 400C > non oxidized BC > polystyrene. In accordance to Andrade et al.(64), the obtained results revealed that BC is slightly hemostatic, as compared to polystyrene. After oxidation, BC acquired improved hemostatic features, the results obtained for BC 700C being closer to those of Surgicel®.

The hemostatic action of oxidized BC can be assigned to the negative charge provided by the carboxyl groups, which is known to start the blood coagulation cascade by changing the conformation of the coagulation factor FXII upon adsorption. Indeed, the contact pathway can be started by negatively

charged surfaces through the activation of the coagulation factors FXII, FXI, high-molecular-weight-kininogen (HMWK) and pre-kallikrein. It has been demonstrated that the adsorption of coagulation factor FXII might be more intense on negatively charged surfaces, governing its activation via positively charged amino acids on its heavy chain (65–68).

4.3.10 – *In vivo* biocompatibility of BC membranes

The biocompatibility of BC membranes was assessed through the ability to induce irritation, inflammation or necrosis of the surrounding tissues, in vivo. The samples were subcutaneously implanted in the rat, and the tissue response was evaluated.

In general, the implants preserved their location, size and shape until explantation (Fig. 4.8). They could be easily identified and removed, since full degradation in vivo was not observed in any of the cases. After 3, 14 and 56 days of implantation, there were no macroscopic evidences of inflammation, such as redness, edema, or exudates around the implanted BC samples (17,18,,35,69). All the animals survived during the study period and no infection or surgery-related complications occurred in both groups.

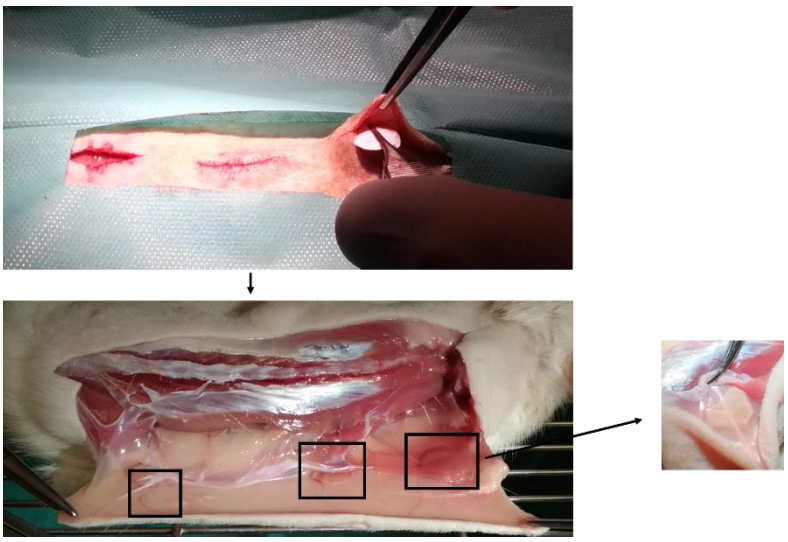

Figure 4.8. Photographs of the implantation and explantation process.

Histological assessment of the membranes was performed on days 3, 14 and 56 post-surgery. Histological images of the BC membranes and surrounding tissues are presented on Fig. 4.9, and the histological inflammation scores in table 4.4.

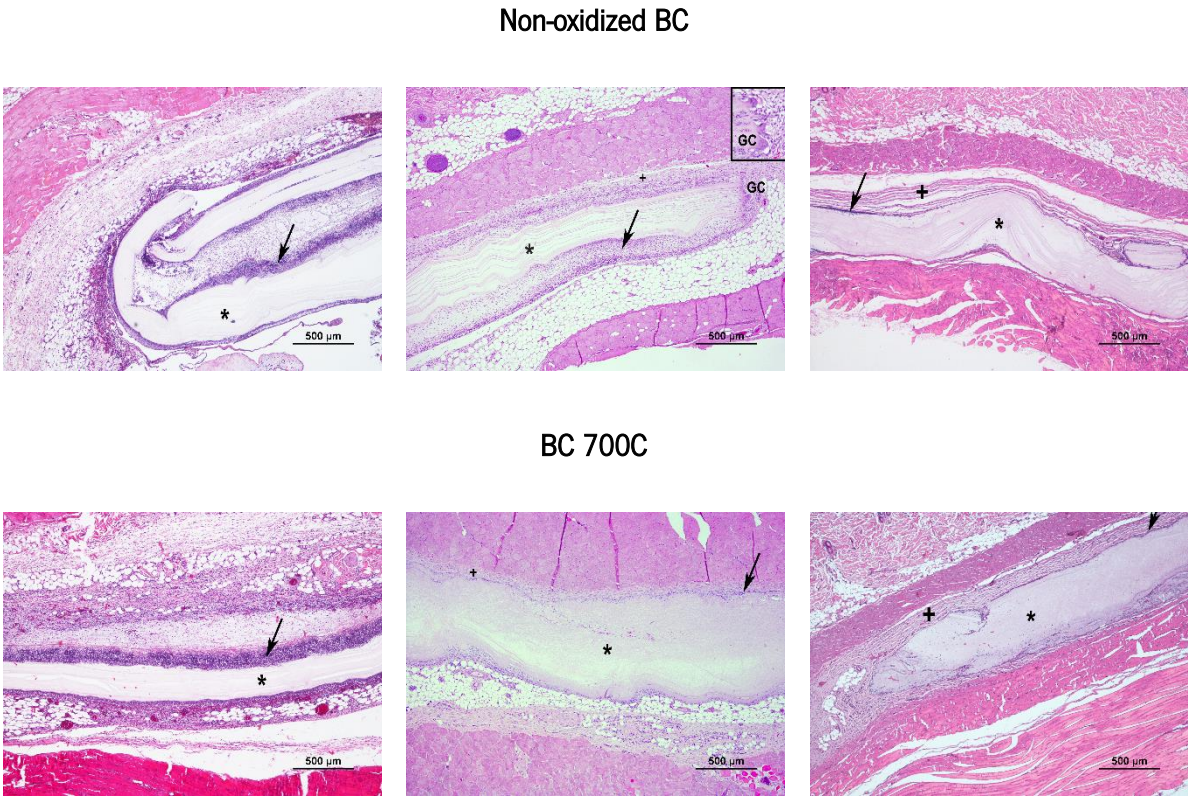

Figure 4.9. Histomorphology of oxidized and non-oxidized BC membranes implanted subcutaneously in rat model (+ → fibrosis; **black arrow** → PMN; * → BC and **GC** → Giant cells).

Table 4.4. Histological assessment scores of oxidized and non-oxidized BC membranes according to ISO standard 10993-6 (annex E).

	PMN	Lymphocytes	Plasma cells	Macrophages	Giant cells	Necrosis	Neo	Fatty infiltration
3 days								
Non-oxidized BC	4	2	1	2	0	2	2	0	0
BC 700C	2	2	0	1	0	0	0	0	0

14 days									
Non-oxidized BC	3	2	1	2	1	0	1	1	0
BC 700C	2	2	0	2	1	0	0	3	0
56 days									
Non-oxidized BC	1	2	0	2	1	0	0	3	0
BC 700C	1	2	0	2	0	0	0	4	0

0= Same as when implanted; 1= Minimal; 2= Mild; 3= Moderate; 4 = Severe

According to Fig. 4.9 and table 4.4, 3 days post implantation, there was a predominance of neutrophils, lymphocytes, polymorphonuclear cells (PMN) and macrophages infiltrated at the implant-tissue interface in both experimental groups. However, the tissue reaction was more evident on non-oxidized samples comparing to oxidized ones revealing that the acute response was more expressive in the former case. This was also confirmed by the presence of necrosis only in this experimental group. At days 14 and 56, the inflammatory reaction was still more expressive in the non-oxidized samples, with mononuclear cells being the predominant ones. As expected, fibrosis only occurred after 14 days of implantation, being more expressive after 56 days around the oxidized BC membranes, which induced a higher fibroplasia. For all the time-points, the presence of giant cells was minimal, suggesting that the possible foreign body reaction (FBR) would be also minimal. This was confirmed macroscopically since BC membranes were well integrated with the rat connective tissue (35). Even after 56 days of implantation, the oxidized membranes where still in place. Although the *in vitro* results showed that these samples were degrade to limited extension in 63 days, more extensive degradation was expected to occur *in vivo*. This cannot be quantified, but a significant fractions of material remained at the end of the trials.

Although the *in vivo* biocompatibility of BC has been characterized by several authors (17,18,35,69–73), no studies have been performed to assessed the behavior of oxidized BC *in vivo*. Interestingly, the oxidized BC seemed to attract fewer inflammatory cells than the pristine material, which is generally considered highly biocompatible, although it gives rise to a thicker fibrosis comparing to non-oxidized samples.

4.4 – CONCLUSIONS

Bacterial cellulose membranes were oxidized using electrochemical methods, acquiring hemostatic features and became partially degradable. The obtained results using FTIR and NMR techniques allowed us to conclude that the oxidation reaction occurred mainly at the surface layer of the cellulose fibers. Furthermore, both morphology and crystallinity of the oxidized membranes were preserved, although a slight reduction in crystallinity occurred after oxidation. This decrease in crystallinity was only around 4%, even for the samples with higher oxidation degree, e.g., the pristine BC had approximately 92%, while the oxidized sample had around 88%. The *in vitro* degradability of oxidized membranes and their hemostatic potential were evaluated using Surgicel® as a control. The obtained results demonstrated that the oxidized BC exhibited higher hemostatic activity than the pristine material, although not as effective as that of Surgicel®. The *in vivo* biodegradability and biocompatibility of oxidized membranes were assessed through subcutaneous implantation of the membranes in the rat, and the results showed a highly biocompatible behavior, triggering only a mild inflammation process. We hypothesize that a pre-treatment able to reduce BC crystallinity followed by oxidation may yield a more oxidized, more biodegradable material that exhibits improved hemostatic features. This will be the goal of further work aimed at developing BC oxidized membranes dressing to prevent hemorrhagic episodes.

4.5 – REFERENCES

1. Bu Y, Zhang L, Sun G, Sun F, Liu J, Yang F, et al. Tetra-PEG Based Hydrogel Sealants for In Vivo Visceral Hemostasis. Adv Mater. 2019;31(28):1901580.
2. Yang X, Liu W, Shi Y, Xi G, Wang M, Liang B, et al. Peptide-immobilized starch/PEG sponge with rapid shape recovery and dual-function for both uncontrolled and noncompressible hemorrhage. Acta Biomater. 2019;99:220–35.
3. Sirlak M, Eryilmaz S, Yazicioglu L, Kiziltepe U, Eyileten Z, Durdu MS, et al. Comparative study of microfibrillar collagen hemostat (Colgel) and oxidized cellulose (Surgicel) in high transfusion-risk cardiac surgery. J Thorac Cardiovasc Surg. 2003;126(3):666–70.
4. Gabay M, Boucher BA. An essential primer for understanding the role of topical hemostats, surgical sealants, and adhesives for maintaining hemostasis. Pharmacotherapy.

2013;33(9):935–55.

5. Agarwal MM, Mandal AK, Agarwal S, Lal A, Prakash M, Mavuduru R, et al. Surgicel granuloma: Unusual cause of "recurrent" mass lesion after laparoscopic nephron-sparing surgery for renal cell carcinoma. Urology. 2010;76(2):334–5.

6. Alpaslan C, Alpaslan GH, Oygur T. Tissue reaction to three subcutaneously implanted local hemostatic agents. Br J Oral Maxillofac Surg. 1997;35(2):129–32.

7. Wang H, Chen P. Surgicel® (oxidized regenerated cellulose) granuloma mimicking local recurrent gastrointestinal stromal tumor: A case report. Oncol Lett. 2013;5(5):1497–500.

8. Ibrahim MF, Aps C, Young CP. A foreign body reaction to Surgicel mimicking an abscess following cardiac surgery. Eur J Cardiothorac Surg. 2002;22(3):489–90.

9. Lin B, Yang H, Cui M, Li Y, Yu J. Surgicel™ application in intracranial hemorrhage surgery contributed to giant-cell granuloma in a patient with hypertension: case report and review of the literature. World J Surg Oncol. 2014;12(1):101.

10. Portela R, Leal CR, Almeida PL, Sobral RG. Bacterial cellulose: a versatile biopolymer for wound dressing applications. Vol. 12, Microbial Biotechnology. John Wiley and Sons Ltd; 2019. p. 586–610.

11. Pang M, Huang Y, Meng F, Zhuang Y, Liu H, Du M, et al. Application of bacterial cellulose in skin and bone tissue engineering. Vol. 122, European Polymer Journal. Elsevier Ltd; 2020. p. 109365.

12. Gorgieva S, Trček J. Bacterial cellulose: Production, modification and perspectives in biomedical applications. Vol. 9, Nanomaterials. 2019

13. Eslahi N, Mahmoodi A, Mahmoudi N, Zandi N, Simchi A. Processing and Properties of Nanofibrous Bacterial Cellulose-Containing Polymer Composites: A Review of Recent Advances for Biomedical Applications. Vol. 60, Polymer Reviews. Taylor and Francis Inc.; 2020. p. 144–70.

14. Volova TG, Prudnikova S V., Sukovatyi AG, Shishatskaya EI. Production and properties of bacterial cellulose by the strain Komagataeibacter xylinus B-12068. Appl Microbiol Biotechnol. 2018;102(17):7417–28.

15. Uzyol HK, Saçan MT. Bacterial cellulose production by Komagataeibacter hansenii using algae-based glucose. Environ Sci Pollut Res. 2017;24(12):11154–62.

16. Klemm D, Heublein B, Fink HP, Bohn A. Cellulose: Fascinating biopolymer and sustainable raw material. Angew Chemie - Int Ed. 2005;44(22):3358–93.

17. Helenius G, Bäckdahl H, Bodin A, Nannmark U, Gatenholm P, Risberg B. In vivo biocompatibility of bacterial cellulose. J Biomed Mater Res - Part A. 2006;76(2):431–8.

18. Pértile RAN, Moreira S, Gil Da Costa RM, Correia A, Guardão L, Gartner F, et al. Bacterial cellulose: Long-term biocompatibility studies. J Biomater Sci Polym Ed. 2012;23(10):1339–54.

19. Zhang C, Cao J, Zhao S, Luo H, Yang Z, Gama M, et al. Biocompatibility evaluation of bacterial cellulose as a scaffold material for tissue-engineered corneal stroma. Cellulose. 2020;27(5):2775–84.

20. Camy S, Montanari S, Rattaz A, Vignon M, Condoret JS. Oxidation of cellulose in pressurized carbon dioxide. J Supercrit Fluids. 2009;51(2):188–96.

21. Liao SB, Xi TF, Lai C, Liao SY, Huang T, Wang SY. TEMPO-mediated oxidation of bacterial cellulose in a bromide-free system. Colloid Polym Sci. 2013;32(6):699–707.

22. Davis NJ, Flitsch SL. Selective oxidation of monosaccharide derivatives to uronic acids. Tetrahedron Lett. 1993;34(7):1181–4.

23. Pahlevan M, Toivakka M, Alam P. Mechanical properties of TEMPO-oxidised bacterial cellulose-amino acid biomaterials. Eur Polym J. 2018;101:29–36.

24. Lai C, Sheng L, Liao S, Xi T, Zhang Z. Surface characterization of TEMPO-oxidized bacterial cellulose. Surf Interface Anal. 2013;45(11):1673–9.

25. Isogai A, Kato Y. Preparation of polyuronic acid from cellulose by TEMPO-mediated oxidation. Cellulose. 1998;5(3):153–64.

26. Bragd PL, van Bekkum H, Besemer AC. TEMPO-Mediated Oxidation of Polysaccharides: Survey of Methods and Applications. Top Catal. 2004;27(1–4):49–66.

27. Carlsson DO, Lindh J, Nyholm L, Stromme M, Mihranyan A, Strømme M, et al. Cooxidant-free TEMPO-mediated oxidation of highly crystalline nanocellulose in water. RSC Adv. 2014;4(94):52289–98.

28. Parpot P, Servat K, Bettencourt AP, Huser H, Kokoh KB. TEMPO mediated oxidation of carbohydrates using electrochemical methods. Cellulose. 2010;17(4):815–24.

29. Cui Q, Zheng Y, Lin Q, Song W, Qiao K, Liu S. Selective oxidation of bacterial cellulose by NO2-HNO 3. RSC Adv. 2014;4(4):1630–9.

30. Evans R, Wallis AFA. Cellulose molecular weights determined by viscometry. J Appl Polym Sci. 1989;37(8):2331–40.

31. Tsouko E, Kourmentza C, Ladakis D, Kopsahelis N, Mandala I, Papanikolaou S, et al. Bacterial cellulose production from industrial waste and by-product streams. Int J Mol Sci. 2015;16(7):14832–49.

32. Ryu DDY, Lee SB, Tassinari T, Macy C. Effect of compression milling on cellulose structure and on enzymatic hydrolysis kinetics. Biotechnol Bioeng. 1982;24(5):1047–67.

33. Segal L, Creely JJ, Martin AE, Conrad CM. An Empirical Method for Estimating the Degree of Crystallinity of Native Cellulose Using the X-Ray Diffractometer. Text Res J. 1959;29(10):786–94.

34. Leitão AF, Silva JP, Dourado F, Gama M. Hemocompatibility study of a bacterial cellulose/poly(Vinyl Alcohol) nanocomposite. Colloids Surfaces B Biointerfaces. 2013;6(111):493–502.

35. Andrade FK, Alexandre N, Amorim I, Gartner F, Maurício AC, Luís AL, et al. Studies on the biocompatibility of bacterial cellulose. J Bioact Compat Polym. 2013;28(1):97–112.

36. Zhang Y, Zhou Z, Wen F, Yuan K, Tan J, Zhang Z, et al. Tubular structured bacterial cellulose-based nitrite sensor: preparation and environmental application. J Solid State Electrochem. 2017;21(12):3649–57.

37. Zaid MHM, Abdullah J, Yusof NA, Wasoh H, Sulaiman Y, Noh MFM, et al. Reduced Graphene Oxide/TEMPO-Nanocellulose Nanohybrid-Based Electrochemical Biosensor for the Determination of Mycobacterium tuberculosis. J Sensors. 2020;2020.

38. Gomes NO, Carrilho E, Machado SAS, Sgobbi LF. Bacterial cellulose-based electrochemical sensing platform: A smart material for miniaturized biosensors. Electrochim Acta. 2020 Jul 20;349:136341.

39. Aydemir Sezer U, Sahin İ, Aru B, Olmez H, Yanıkkaya Demirel G, Sezer S. Cytotoxicity, bactericidal and hemostatic evaluation of oxidized cellulose microparticles: Structure and oxidation degree approach. Carbohydr Polym. 2019;219:87–94.

40. Saito T, Isogai A. TEMPO-mediated oxidation of native cellulose. The effect of oxidation conditions

on chemical and crystal structures of the water-insoluble fractions. Biomacromolecules. 2004;5(5):1983–9.

41. Hiraoki R, Ono Y, Saito T, Isogai A. Molecular mass and molecular-mass distribution of TEMPO-oxidized celluloses and TEMPO-oxidized cellulose nanofibrils. Biomacromolecules. 2015;16(2):675–81.

42. Fukuzumi H, Saito T, Isogai A. Influence of TEMPO-oxidized cellulose nanofibril length on film properties. In: Carbohydrate Polymers. Elsevier; 2013. p. 172–7.

43. Motta Neves R, Silveira Lopes K, Zimmermann MGV, Poletto M, Zattera AJ. Cellulose Nanowhiskers Extracted from Tempo-Oxidized Curaua Fibers. J Nat Fibers. 2020;17(9):1355–65.

44. Sang X, Qin C, Tong Z, Kong S, Jia Z, Wan G, et al. Mechanism and kinetics studies of carboxyl group formation on the surface of cellulose fiber in a TEMPO-mediated system. Cellulose. 2017;24(6):2415–25.

45. Tang R, Yu Z, Renneckar S, Zhang Y. Coupling chitosan and TEMPO-oxidized nanofibrilliated cellulose by electrostatic attraction and chemical reaction. Carbohydr Polym. 2018;202:84–90.

46. Lai C, Zhang S, Chen X, Sheng L. Nanocomposite films based on TEMPO-mediated oxidized bacterial cellulose and chitosan. Cellulose. 2014;21(4):2757–72.

47. do Nascimento ES, Pereira ALS, Barros M de O, Barroso MK de A, Lima HLS, Borges M de F, et al. TEMPO oxidation and high-speed blending as a combined approach to disassemble bacterial cellulose. Cellulose. 2019;26(4):2291–302.

48. Luo H, Xiong G, Hu D, Ren K, Yao F, Zhu Y, et al. Characterization of TEMPO-oxidized bacterial cellulose scaffolds for tissue engineering applications. Mater Chem Phys. 2013;143(1):373–9.

49. Klemm D, Kramer F, Moritz S, Lindström T, Ankerfors M, Gray D, et al. Nanocelluloses: A new family of nature-based materials. Vol. 50, Angewandte Chemie - International Edition. John Wiley & Sons, Ltd; 2011 p. 5438–66.

50. Wang J, Tavakoli J, Tang Y. Bacterial cellulose production, properties and applications with different culture methods – A review. Vol. 219, Carbohydrate Polymers. Elsevier Ltd; 2019. p. 63–76.

51. Numata Y, Kono H, Mori A, Kishimoto R, Tajima K. Structural and rheological characterization of bacterial cellulose gels obtained from Gluconacetobacter genus. Food Hydrocoll. 2019;92:233–

9.

52. Jun SH, Park SG, Kang NG. One-pot method of synthesizing TEMPO-oxidized bacterial cellulose nanofibers using immobilized TEMPO for skincare applications. Polymers (Basel). 2019;11(6).

53. Horii F, Hirai A, Yamamoto H. Microstructural analysis of microfibrils of bacterial cellulose. Macromol Symp. 1997;120(1):197–205.

54. Vasconcelos NF, Feitosa JPA, da Gama FMP, Morais JPS, Andrade FK, de Souza Filho M de SM, et al. Bacterial cellulose nanocrystals produced under different hydrolysis conditions: Properties and morphological features. Carbohydr Polym. 2017;155:425–31.

55. Vasconcelos NF, Andrade FK, Vieira L de AP, Vieira RS, Vaz JM, Chevallier P, et al. Oxidized bacterial cellulose membrane as support for enzyme immobilization: properties and morphological features. Cellulose. 2020.

56. Kashcheyeva EI, Gladysheva EK, Skiba EA, Budaeva V V. A study of properties and enzymatic hydrolysis of bacterial cellulose. Cellulose. 2019;26(4):2255–65.

57. Cheng KC, Catchmark JM, Demirci A. Effect of different additives on bacterial cellulose production by Acetobacter xylinum and analysis of material property. Cellulose. 2009;16(6):1033–45.

58. Li J, Wan Y, Li L, Liang H, Wang J. Preparation and characterization of 2,3-dialdehyde bacterial cellulose for potential biodegradable tissue engineering scaffolds. Mater Sci Eng C. 2009;29(5):1635–42.

59. Li H, Wu B, Mu C, Lin W. Concomitant degradation in periodate oxidation of carboxymethyl cellulose. Carbohydr Polym. 2011;84(3):881–6.

60. Peng S, Zheng Y, Wu J, Wu Y, Ma Y, Song W, et al. Preparation and characterization of degradable oxidized bacterial cellulose reacted with nitrogen dioxide. Polym Bull. 2012;68(2):415–23.

61. Dan Dimitrijevich S, Tatarko M, Gracy RW, Linsky CB, Olsen C. Biodegradation of oxidized regenerated cellulose. Carbohydr Res. 1990;195(2):247–56.

62. Wan Y, Chen Y, Xi T, Zheng Y, Zhou L. i>In Vitro Structural Changes of Nano-Bacterial Cellulose Immersed in Phosphate Buffer Solution In Vitro Structural Changes of Nano-Bacterial Cellulose immersed in Phosphate Buffer Solution. Artic J Biomimetics Biomater Tissue Eng. 2011.

63. Shi X, Cui Q, Zheng Y, Peng S, Wang G, Xie Y. Effect of selective oxidation of bacterial cellulose on

degradability in phosphate buffer solution and their affinity for epidermal cell attachment. RSC Adv. 2014;4(105):60749–56.

64. Andrade FK, Moreira SMG, Domingues L, Gama FMP. Improving the affinity of fibroblasts for bacterial cellulose using carbohydrate-binding modules fused to RGD. J Biomed Mater Res - Part A. 2010;92(1):9–17.

65. Sperling C, Fischer M, Maitz MF, Werner C. Blood coagulation on biomaterials requires the combination of distinct activation processes. Biomaterials. 2009;30(27):4447–56.

66. Palta S, Saroa R, Palta A. Overview of the coagulation system. Indian J Anaesth. 2014;58(5):515–23.

67. Zhang S, Li J, Chen S, Zhang X, Ma J, He J. Oxidized cellulose-based hemostatic materials. Vol. 230, Carbohydrate Polymers. Elsevier Ltd; 2020

68. Yuan H, Chen L, Hong FF. A Biodegradable Antibacterial Nanocomposite Based on Oxidized Bacterial Nanocellulose for Rapid Hemostasis and Wound Healing. ACS Appl Mater Interfaces. 2020;12(3):3382–92.

69. De L, Holgado A, Leao A, Rodrigues M, Chaves M, Kinoshita A. Tissue reaction after subcutaneous implantation of a membrane composed of bacterial cellulose embedded with hydroxyapatite.

70. Huang L, Du X, Fan S, Yang G, Shao H, Li D, et al. Bacterial cellulose nanofibers promote stress and fidelity of 3D-printed silk based hydrogel scaffold with hierarchical pores. Carbohydr Polym. 2019;221:146–56.

71. Kumbhar J V., Jadhav SH, Bodas DS, Barhanpurkar-Naik A, Wani MR, Paknikar KM, et al. In vitro and in vivo studies of a novel bacterial cellulose-based acellular bilayer nanocomposite scaffold for the repair of osteochondral defects. Int J Nanomedicine. 2017;12:6437–59.

72. Lima F de MT de, Pinto FCM, Andrade-da-Costa BL da S, Silva JGM da, Campos Júnior O, Aguiar JL de A. Biocompatible bacterial cellulose membrane in dural defect repair of rat. J Mater Sci Mater Med. 2017;28(3).

73. Wang B, Lv X, Chen S, Li Z, Sun X, Feng C, et al. In vitro biodegradability of bacterial cellulose by cellulase in simulated body fluid and compatibility in vivo. Cellulose. 2016;23(5):3187–98.

Chapter 5

Laser patterning of bacterial cellulose membranes surface

An exploratory study was performed intending not only to explore another biomedical application of BC membranes, but also to understand the influence of surface laser patterning on fibroblast adhesion. A CO_2 laser was used, and two different patterns were tested: parallel lines (=) and perpendicular lines (#). When parallel lines were used, the distances between lines were also studied, namely 0.1 and 0.2 mm. The pristine (BC) and laser treated BC (BCL) were analysed by XPS, ATR-FTIR and SEM. The obtained results allowed to conclude that the use of laser did not chemically modify the BC surface and that it is indeed possible to carve the surface of BC using this approach. The effect of surface patterning on cell adhesion was assessed. SEM results showed that fibroblasts were present both surfaces exhibiting its usual phenotype. Furthermore, the metabolic activity did not reveal significant differences between the pristine BC and the patterned surfaces. In general, these preliminary results showed the potential of the laser technology to modify the surface topography opening the room for further studies aiming at improving the performance of BC as an implantable biomaterial.

5.1 - INTRODUCTION

Biomaterials are widely applied in different biomedical fields such as in drug delivery systems, tissue engineering and also as implantable material. In tissue engineering applications, biomaterials provide a three-dimensional (3D) scaffold aiming to mimic the *in vivo* cellular milieu with suitable mechanical, structural and biochemical properties (1). The biocompatibility of biomaterials is related with its surface properties, since this is where the first contact of biomolecules and cells occurs, in the human body. The surface determines the cell-surface communications which are associated to the cell responses such as adhesion, proliferation and differentiation, ultimately determining the foreign body reaction (2). Thus, it is desirable to regulate the cell behavior at the biomaterials surface in a predictable manner, both *in vitro* and *in vivo*.

Bacterial cellulose (BC) is a natural polymer produced by some bacteria that exhibits good biocompatibility, high purity, high crystallinity and improved mechanical properties, a consequence of its nanofibrilar 3D network (3). Although highly biocompatible, BC may be further improved as biomaterial. One example of these limitations concerns the small pores (100 ~ 300 nm in diameter) (4) that restricts its application as tissue engineering scaffold. Since the biomaterial's surface is the first line of interaction between the implant and cells, the topographical features at micro and nanometer scales are crucial for biomedical applications and offer a promising new methodology to control cell-surface interactions. In fact, surface topography is a powerful strategy to regulate cell function, since textured surfaces act as an extracellular physical milieu without involving bioactive molecules (5). Specially, patterned surfaces with micron and sub-micron features may be used to avoid bacterial adhesion. On a patterned surface, the bacteria are surrounded by walls, wells, slopes, slants or other geometric curves. The confined surface structures with pillars of defined geometric shapes limit the attachment, as compared with smooth surfaces. Consequently, the interest in fabricating anti-bacterial surfaces with nanoscale topography has been increasing (6). Another goal of surface patterning concerns the control of the foreign body reaction in implantable materials, in particular, the formation of hypertrophic scar tissue (HST). This is characterized by the abnormal proliferation of fibroblasts and an atypical collagen fiber deposition (7). Since HST causes pain and discomfort to the patients, it is mandatory to developed new strategies to overcome these issues and reduce HST formation during the healing process. One of those strategies is related with the above mentioned patterning of BC-based materials, which affect the fibroblasts adhesion and proliferation with specific influence on HS formation.

In the present study, we aimed to improve the attractive properties of BC membranes for biomedical applications through its surface patterning using a CO_2 laser. This approach has never been reported in the literature, although the use of laser technology to pattern the surface of BC dry membranes have been described (8–10). The modified BC and its interaction with mouse skin fibroblasts (L929) was also analyzed.

5.2 – Materials and Methods

5.2.1 – BC membranes purification

BC membranes (HTK CO., LTD, Ho Chi Minh City, Vietnam) with an initial thickness of 12-15 mm were washed with distilled water and then with 5% (w/v) of sodium dodecyl sulphate (SDS; Sigma-Aldrich, St. Louis, MO, USA), to remove endotoxins, for 5 days (solution renewed everyday), followed by extensive washing with distilled water. All washings were done at room temperature. Afterwards, membranes were pressed between two smooth surface metal plates to a final thickness between 3-6 mm.

5.2.2 – Laser patterning of BC membranes

After purification, the surface of the BC membrane (18 x 6 cm) was patterned using a RedSail M500 CO_2 laser with a power of up to 50 W at the 10.6 μm wavelength in continuous wave regime. In each BC membrane different patterns were designed, consisting of small squares (18 x 18 mm) at a distance between the laser and the BC surface of 1.8 cm. The laser beam is directed through an optical system featuring a moving optical head that allows positioning along the XY plane, achieving a well-focused scribing area of 300 x 500 mm^2 operating at 100 mm/s. Beam diameter at the focal point was ~50 μm.

For cell culture, the patterned squares were cut using a biopsy punch with 13 mm of diameter – which corresponds to the diameter of the wells used for cell culture - and then sterilized by autoclaving at 121°C.

The different used patterns were produced using the same power (23W) for all the samples; the tested conditions are presented in the follow scheme:

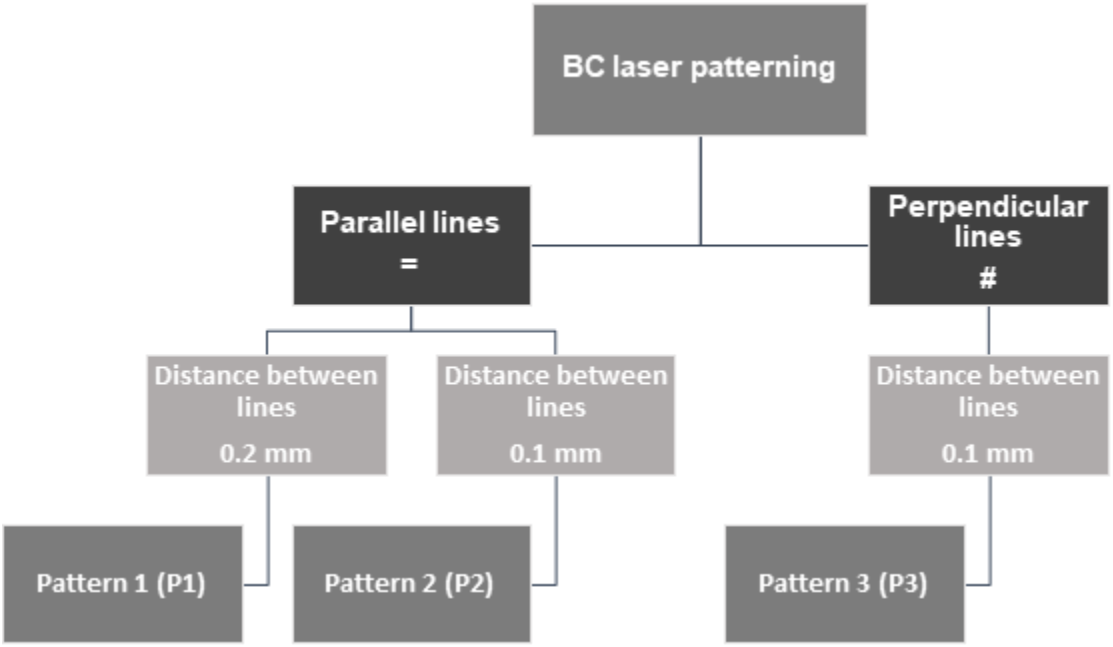

Figure 5.1. The characteristics of the different patterns tested.

5.2.3 – XPS

The influence of laser treatment on the surface chemistry of BC membranes was assessed through XPS analysis. This was performed using a Kratos Axis Ultra HAS with CasaXPS software for data acquisition and analysis. For analysis, a monochromatic Al X-ray source was used, operating at 15 kV (90W). Survey scan spectra were acquired at a pass energy of 160 eV, while for C 1s, O 1s and N 1s individual high-resolution spectra were obtained at a pass energy of 40 and 0.1 eV energy step. Spectra analysis was performed using peak fitting with Gaussian-Lorentzian peak shape and Shirley type background subtraction. The binding energy scales were referenced to the hydrocarbon component (C-C) in the C 1s spectra at 285 eV.

5.2.3 – ATR-FTIR

Prior to analysis both BC (pristine) and BCL (laser treated) samples were dried overnight, in an oven, at 50ºC. Then, the dried samples were analyzed using an ALPHA II- Bruker spectrometer (Ettlingen, Germany) with a diamond-composite attenuated total reflectance (ATR) cell. Data was collected using OPUS software which is integrated on the FTIR equipment. The measurements were recorded with a wavenumber range from 4000 to 400 cm^{-1}, with a resolution of 4 cm^{-1} and 64 scans per sample. The

ATR clamp and platform were cleaned with a cotton swab dampened with isopropyl alcohol and allowed to dry between analysis of each coupon. All assays were done in duplicate for each sample.

5.2.3.1 – Determination of % Iα mass fraction

Through FTIR spectra, hydrogen-bonding vibrational bands are present in the 700-800 cm^{-1} range (11). Allomorphs Iα and Iβ have their bands around 750 cm^{-1} and 710 cm^{-1}, respectively, and they have been used to estimate the ratio of these two allomorphs. The Gaussian function was fitted under the peaks around 750 cm^{-1} and 710 cm^{-1}. The mass fraction of the Iα allomorph was calculated using the following equation (12) (Equation 3):

$$\% I\alpha = 2.55 \times \frac{A_{I\alpha}}{(A_{I\alpha} - A_{I\beta})} - 0.32 \quad (3)$$

where A_{α} and A_{β} are ascribed to the integrated intensities of the contributions from celluloses Iβ and Iα at 710 cm^{-1} and 750 cm^{-1}, respectively. The Iα mass fractions in the celluloses was determined by the Gaussian deconvolution of the peaks, subtracted from a local linear background, and their integration using OriginPro software.

5.2.4 – SEM

The morphology of the samples was evaluated using a desktop SEM. All results were acquired using the ProSuite software. The BC samples were placed on aluminum pin stubs with electrically conductive carbon adhesive tape (PELCO Tabs™). Samples were imaged without coating. The aluminum pin stub was then placed inside a Phenom Standard Sample Holder. The analysis was conducted at 10 kV with intensity map.

5.2.5 – Cell seeding and biocompatibility evaluation

Mouse skin fibroblasts cells (L929) were purchased from American Type Culture Collection (ATCC, Virginia, USA) and used for the *in vitro* cytotoxicity tests. Prior to cell culture, sterilized BC membranes (with and without pattern) were placed in a 24 well-plate in contact with 1 mL of Dulbecco's Eagle's medium (DMEM) (Merck, Germany) during 24h. Sterile Teflon rings who outer diameter fitting the internal diameter of the wells were used to fix the membranes. After swelling, DMEM was rejected and cells were cultivated in fresh DMEM supplemented with 10% fetal bovine serum (FBS) (Sigma-Aldrich, St. Louis, MO,

USA) and 1% of penicillin and streptomycin (PAN-Bioteh, Germany) at 37ºC in humidified atmosphere containing 5% of CO_2. The cells were seeded on BC membranes at a concentration of $1x10^5$cells/well and the cell attachment and viability was evaluated by the 3-(4,5-dimethylthiazol-2-yl)-2,5-diphenyltetrazolium bromide (MTT) assay after 24h and 72h of incubation. Briefly, at each time-point, culture media was removed and 300 µL of 1 mg/mL MTT solution was added in each well and incubated for 2h at 37ºC, protected from light. When cells are metabolically active they are able to reduce the tetrazolium compound forming a colored insoluble formazan product, which was solubilized with isopropanol (1mL/well). The color intensity is proportional to the number of viable cells (13). Absorption was measured using a spectrophotometer (Synergy HT BioTek, Vermont, USA) at 570 nm and cell viability expressed as function of absorbance. The assay was performed in quadruplicate.

The morphology of the cells seeded on BC samples was studied, after 24h and 72h of incubation, by SEM. For this analysis, medium was removed and BC samples were washed twice with PBS in order to remove non-adherent cells. Then, the cells were fixed through the addition of 1 mL of 2.5% glutaraldehyde in PBS in each well and maintained at room temperature for 1h. Afterwards, the membranes were rinsed with distilled water and dehydrated by successive immersion in a series of aqueous ethanol solutions (55, 70, 80, 90, 95 and 100 vol.%) for 30 minutes each. Samples were left at room temperature overnight, in order to evaporate the remaining ethanol.

5.2.6 – Statistical analysis

All quantitative measurements are expressed as means ± standard deviation. The data were analyzed with one-way analysis of variance (ANOVA) followed by the Tukey multiple comparisons test, which was used to evaluate the statistical differences between the groups using GraphPad Prism 5.0 software. The criteria for statistical significance were $*p < 0.05$, $**p < 0.01$ and $***p < 0.001$.

5.3 – RESULTS AND DISCUSSION

Different patterns were laser carved in small squares of 18 x 18 mm (Fig. 5.2).

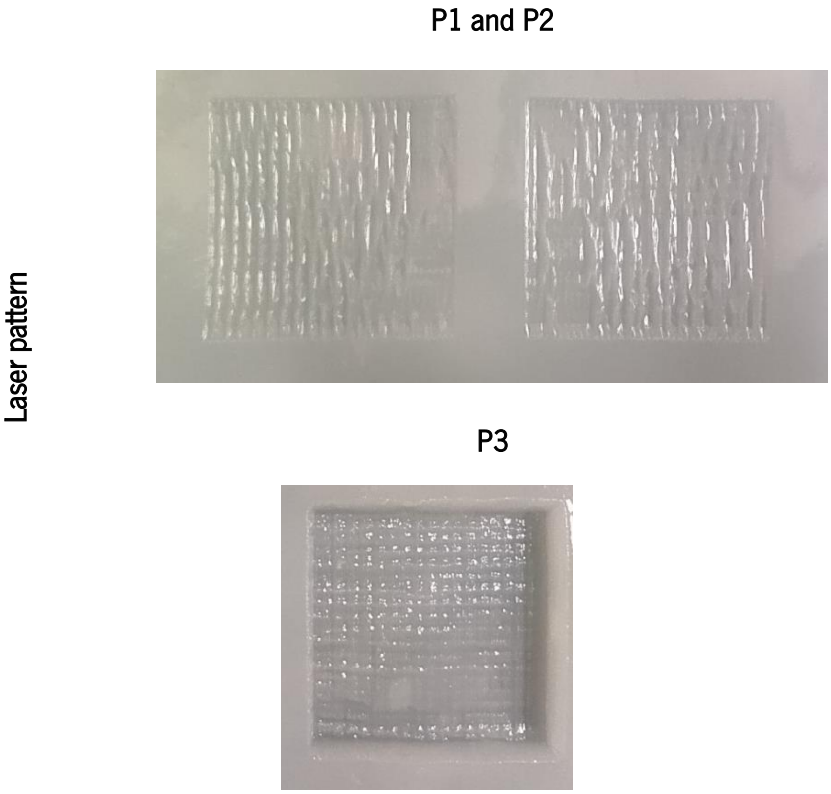

Figure 5. 2. The surface of the wet BC membranes after to laser treatment. P1 and P2 differ only on the distance between lines which is 0.2 and 0.1 mm, respectively.

Figure 5.2 shows the visual appearance of the BCL samples P1, P2 and P3. While in the case of P3 the cardinal pattern is clearly distinguishable, P1 and P2 look alike, the different space between the lines of the two structures being not visually perceptible. This is likely because the long BC "wall" that results from carving two adjacent lines dehydrate and collapse to some instance, filling the space between two adjacent walls. It is also noticeable that the pattern with perpendicular lines (#), obtained by carving all the lines in one direction and then again on the perpendicular direction result in a deeper machining of the BC membrane.

After laser treatment, some samples were dehydrated as described for the cell seeding samples. After dehydration, the pattern can still be identified by optical microscopy, at low magnification, roughly exhibiting lines with the expected inter-space (Fig. 5.3). However, at higher magnification, using SEM, the grooves 0.1 mm apart, although detected, were not clearly distinguishable, which is due to the collapse of the fibers upon drying.

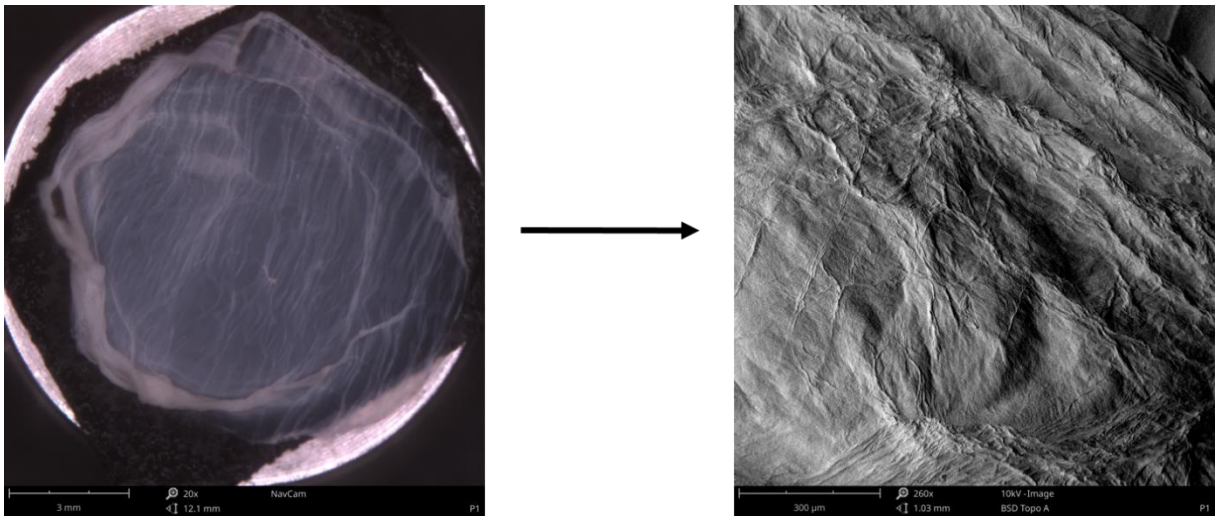

Figure 5.3. The appearance of the patterns after dehydration using SEM equipment.

Shrinkage of the sample upon dehydration is probably responsible for the poor perception of 3D patterning on the SEM images. Because of that, it was hard to measured and confirmed the distance between lines, which should be 0.2 mm and 0.1 mm, for P1 and P2 patterns, respectively. Actually, and despite the freeze-drying process could maintain the morphology of nanoscale materials, this process also weakens the contrast and clarity at the micron scale. Consequently, it was problematic to obtain good and clear SEM images of the produced patterns. In order to circumvent these issues, in forthcoming work the samples will be frozen using liquid nitrogen, which has been shown to better preserve the 3D architecture of the BC membrane through the freeze-drying process. On the other hand, on electronic microscope image (on the right) it was also possible to visualize the lines/patterns on the surface of the BC membranes, bearing the expected in between space. Despite the presence of the patterns, they were not regular and homogeneous as in other works in the literature (7,14,15). In fact, Jin et al. (2018) created patterned BC membranes using PDMS templates at the culture medium-air interface, during the fermentation process, with different size of grooves (50, 30, 10 µm). With this strategy, they were able to produce regular grooves on PDMS templates which were suitably transferred onto BC surface, which had almost the same regular grooves and stripes structure as the PDMS. The authors also tested the effect of pattern surface on fibroblasts (L929) proliferation. They conclude that the patterned surfaces had an inhibitory effect on L929 cells proliferation, especially those with 10 µm stripes, dimensions close to those of the cells. In this work, the produced patterns were bigger compared to the ones in the mentioned reference. Here, the distance between lines were 0.1 and 0.2 mm, one order of magnitude larger.

Nevertheless, the laser technology is rather flexible and can be used to produce different patterning effects, further work being necessary to fully exploit the potential of the technology (7).

5.3.1 – XPS

XPS analysis provides valuable information not only about surface elemental composition but also on its functional groups. BC and BCL membranes were analyzed by XPS in order to study the possible influence of the laser treatment on chemical composition. The laser treatment leads to evaporation of water and combustion of the organic matter (cellulose in this case), residues of the combustion may remain attached to the membrane following the treatment, a possibility that was verified by XPS. The obtained results are present in Fig. 5.4. Also, the relative atomic concentration of C, O and N on the BC and BCL surface is shown on table 5.1.

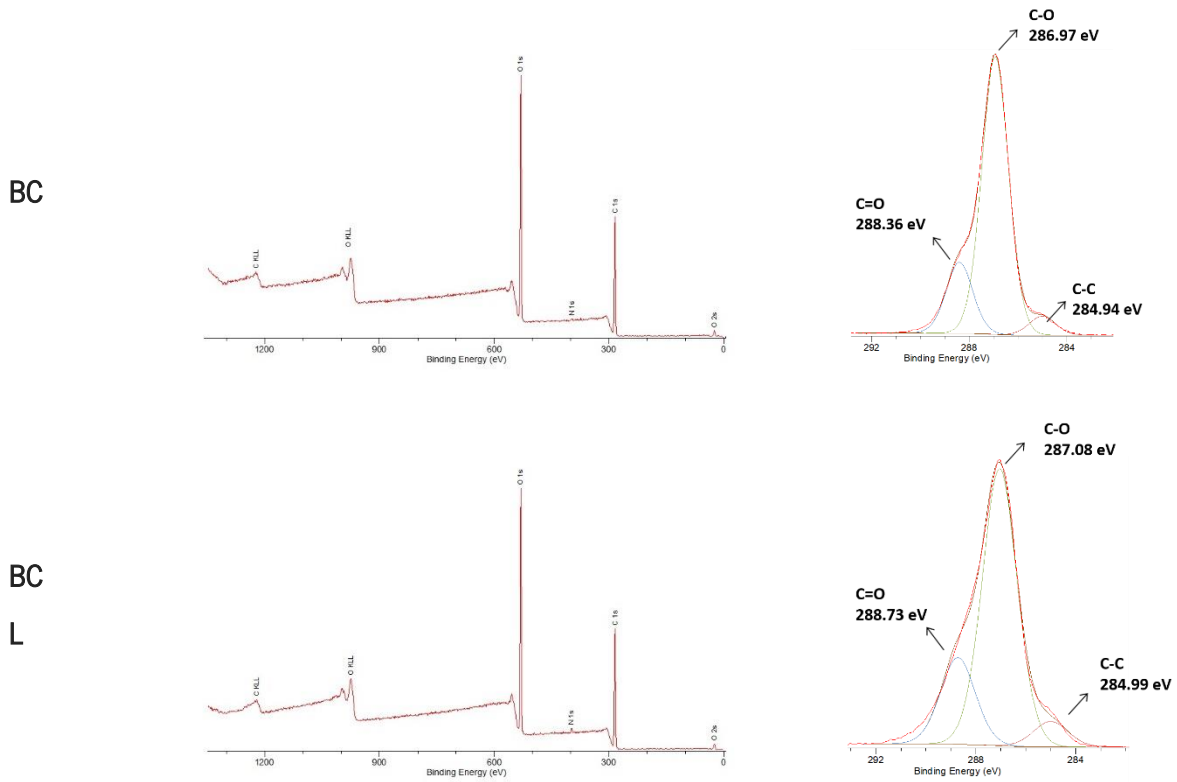

Figure 5.4. XPS survey spectra (left) and the deconvolution of the carbon peak (right) for both BC and BCL samples.

Table 5. 1. Elemental composition of BC and BCL samples analyzed by XPS.

Samples	Carbon (%)	Oxygen (%)	Nitrogen (%)
BC	**57.8**	**41.8**	**0.4**
BCL	**59.2**	**39.9**	**0.9**

As expected, general XPS spectra for both BC and BCL samples revealed that the main elements detected were carbon and oxygen. Beyond these main elements, nitrogen was also detected, in very small amounts, being its presence ascribed to remaining's of the BC biosynthesis process, possibly to some contaminating proteins (16). According to table 5.1, there was a slight decrease on the oxygen concentration on the surface after laser treatment, while a slight increase on carbon and nitrogen concentration was observed. The relative fraction of each element is in agreement with Wang et al. (2020) work and with the survey scan spectra where the most intense peaks are ascribed to carbon (around 283.95 eV) and oxygen (around 531.05 eV) (17). Further information related with surface chemistry can be assessed through deconvolution of the XPS spectra, as depicted on Fig. 5.4. The C 1s peak can be deconvoluted into four components: C1 which corresponds to C-C bonds (around 284 eV); C2, assigned to carbon with one oxygen bond C-O (around 287 eV); C3, where carbon binds with one oxygen through a double bond C=O (around 288 eV). Finally, and although hard to detect in present work, for both BC and BCL samples, C4 is recognized as the carbon linked to two oxygen bonds O-C=O (around 289 eV) (16–20). Since the obtained results for both BC and BCL were very similar, it may be concluded that laser treatment did not induce chemical modifications on the surface of the membranes. Nevertheless, a larger number of samples must be processed in order to confirm whether the difference in the carbon and oxygen content is significant.

5.3.2 – ATR-FTIR

Figure 5.5 shows the ATR-FTIR spectra of bacterial cellulose membranes before and after laser treatment.

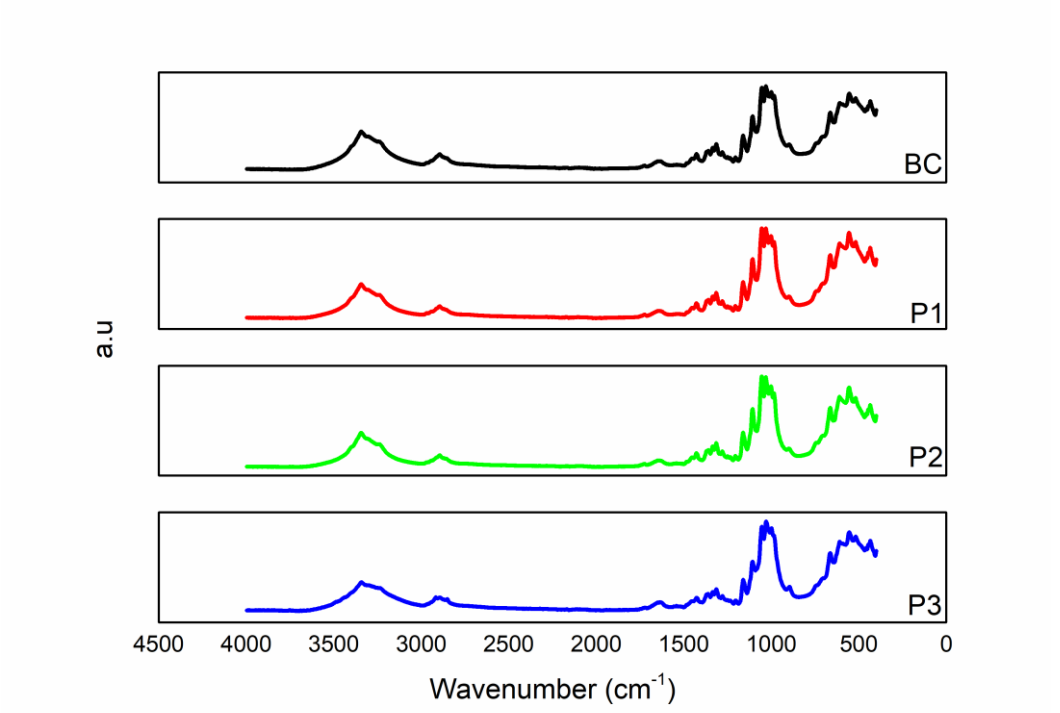

Figure 5.5. FTIR spectra of BC and BCL membranes.

The typical bands ascribed to the structure of cellulosic substrates are observed: O–H symmetrical stretching around 3350 cm^{-1}; C–H stretching around 2900 cm^{-1}; C–O–C stretching around 1162 cm^{-1}; C–O stretching at 1030 cm^{-1} and vibration of amorphous cellulose (stretching of the glucose ring) around 899 cm^{-1} (21–23). As it is possible to observe, the spectra before and after the treatment were indistinguishable which confirms that the samples preserve their chemical structure, being these results consistent with XPS ones. Beyond this, it was also calculated the Iα mass fraction through Gaussian deconvolution of the peaks and the obtained results are present in the following figure.

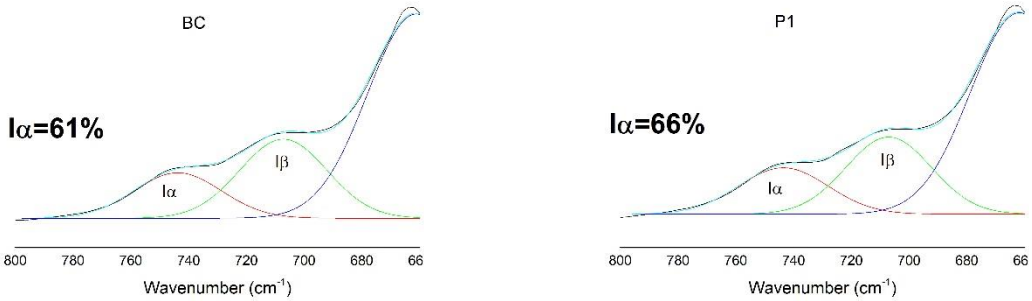

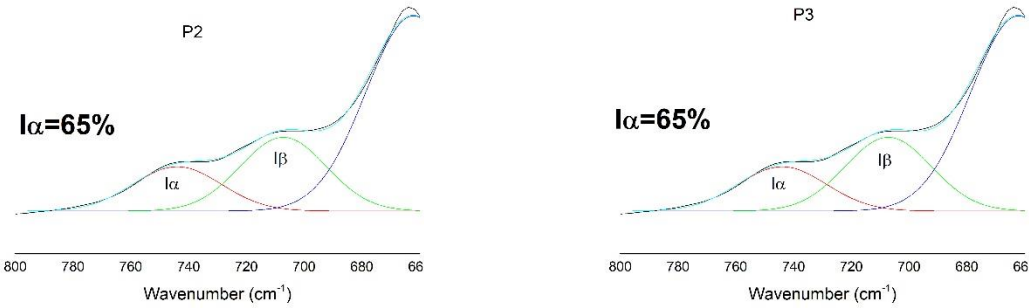

Figure 5.6. The deconvoluted absorption peaks attributed to the Iα (750 cm-1) and Iβ (719 cm-1) crystalline forms of cellulose obtained by ATR-FTIR.

Figure 5.6 exhibits the typical bands attributed to both allomorphs Iα (at 750 cm^{-1}) and Iβ (at 710 cm^{-1}) of the celluloses in which the absorbance bands at 3240 cm^{-1} and 3270 cm^{-1} are ascribed to Iα and Iβ, respectively (24). Despite a slight increase on the Iα values from 61% at ~65% after laser treatment, in general, the obtained values were very similar. Moreover, these high values on Iα mass fraction is in accordance to the literature (25–27).

5.3.3 – Cell viability

To assess the *in vitro* differential cell affinity, mouse fibroblasts L929 cells were cultured in direct contact with BC and BCL samples and the cell viability was measured using MTT assay. Figure 5.7 shows the relative viability of L929 cells after an incubation period of 24h and 72h.

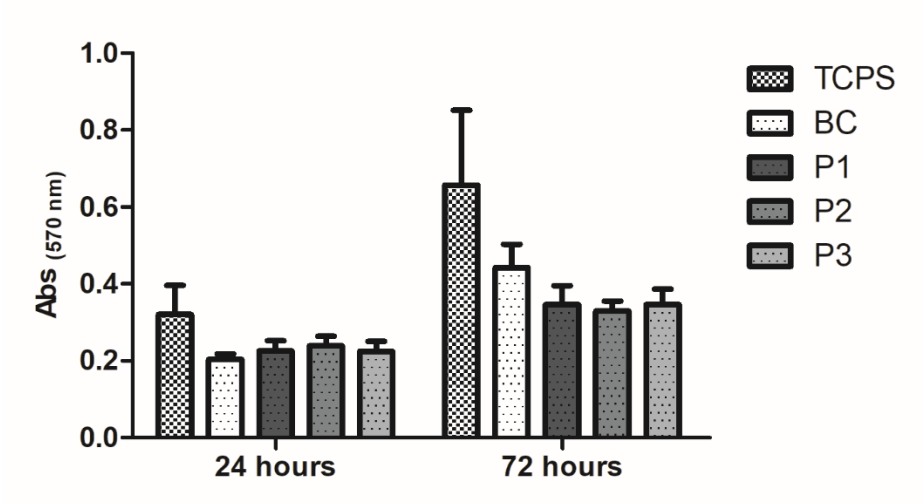

Figure 5.7. Cell viability quantified by MTT assay after 24h and 72h of incubation. Significant differences are indicated as follow: * P<0.05, **P<0.01 and *** P<0.001.

It was shown that there were no significant differences between BC-based surfaces and TCPS demonstrating that they were not cytotoxic. Furthermore, metabolic activity increased from 24h to 72h of culture in all groups, more expressively on Tissue Culture Polystyrene (TCPS). Besides, the obtained cell density on TCPS act as reference to evaluate if the cells are proliferating normally (2). Cell viability was similar on BC and BCL surfaces, suggesting that the surface patterning did not affect significantly the cell affinity of the material, but it suggests a trend towards a lower cell proliferation. According to Robotti et al. (2018) a decrease on cell density along of the culture time was expected. In fact, the authors observed a maximal reduction of 65% of cell density on patterned surfaces when compared to the flat control, after 72h of incubation. The authors tested hexagonal and square patterns featuring pits with 3 μm < *d* < 10 μm and 6 μm < *i* < 20 μm which are the ones imparting PDMS surfaces showing the most efficient anti-adhesive properties (15). Furthermore, the decrease on cell density was also observed by Jin et al. (2018) where the patterned surfaces having an inhibitory effect on L929 cells proliferation *in vitro*. The *in vivo* results showed that the modified surface also inhibited inflammatory response, decreased the accumulation of fibroblasts with consequent decreasing on HST effect (7). In contrast, the results presented by Kurniawan et al. (2012) revealed that the treatment of BC membranes with different plasmas was able to enhance cell affinity. Their results indicated that fibroblast adhesion and proliferation was significantly enhanced by the plasma treatment highlighting the great potential of this surface treatment on the improvement of BC biocompatibility. However, when using plasma treatment both the

chemistry and the topography of the material are modified, thus these results are not comparable to those obtained using laser technology (2).

5.3.4 – SEM

The surface morphology of the BC and BCL membranes after cell culture and the morphology of the cells were examined by SEM and the results are presented on Fig. 5.8.

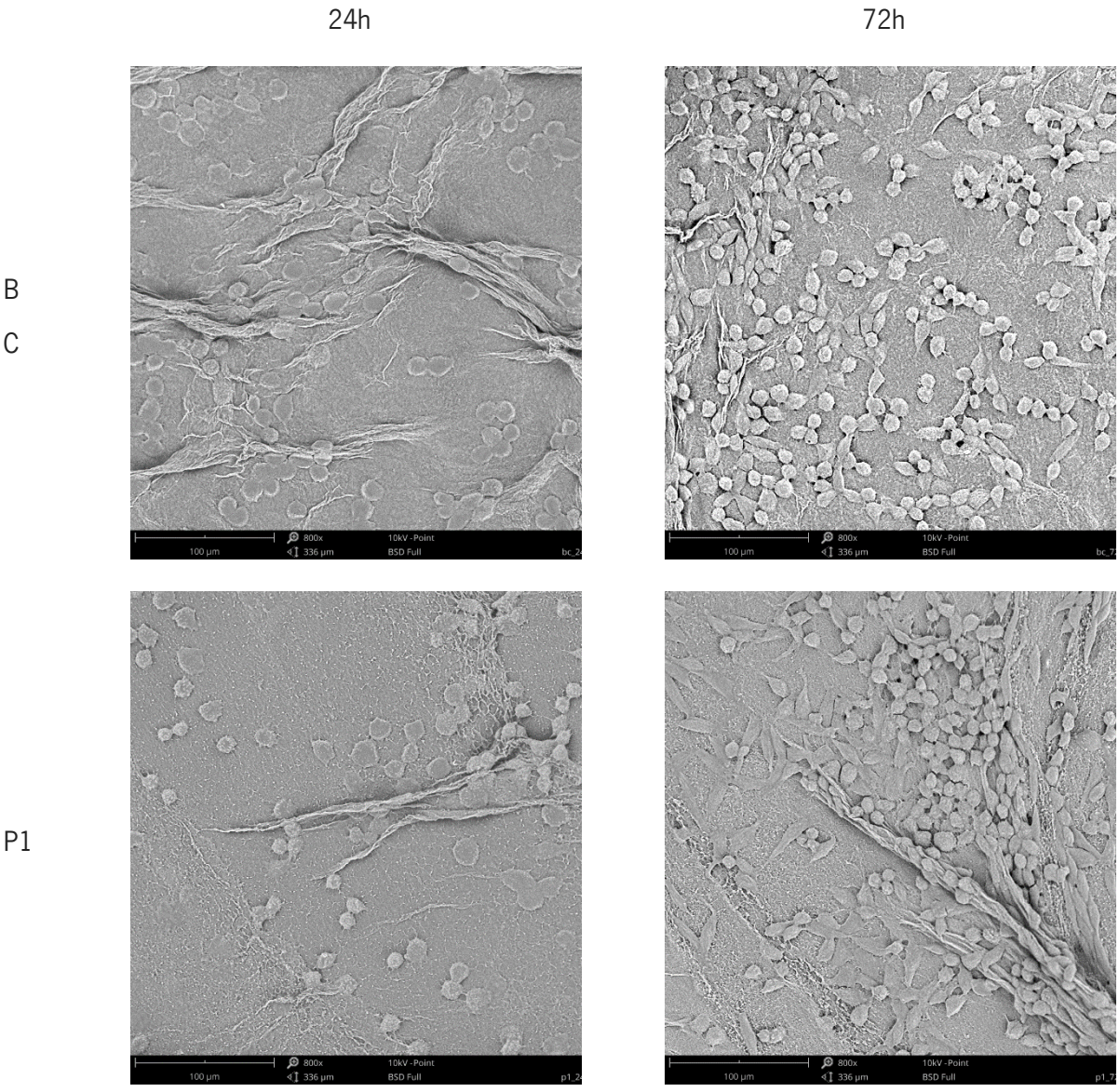

P2

P3

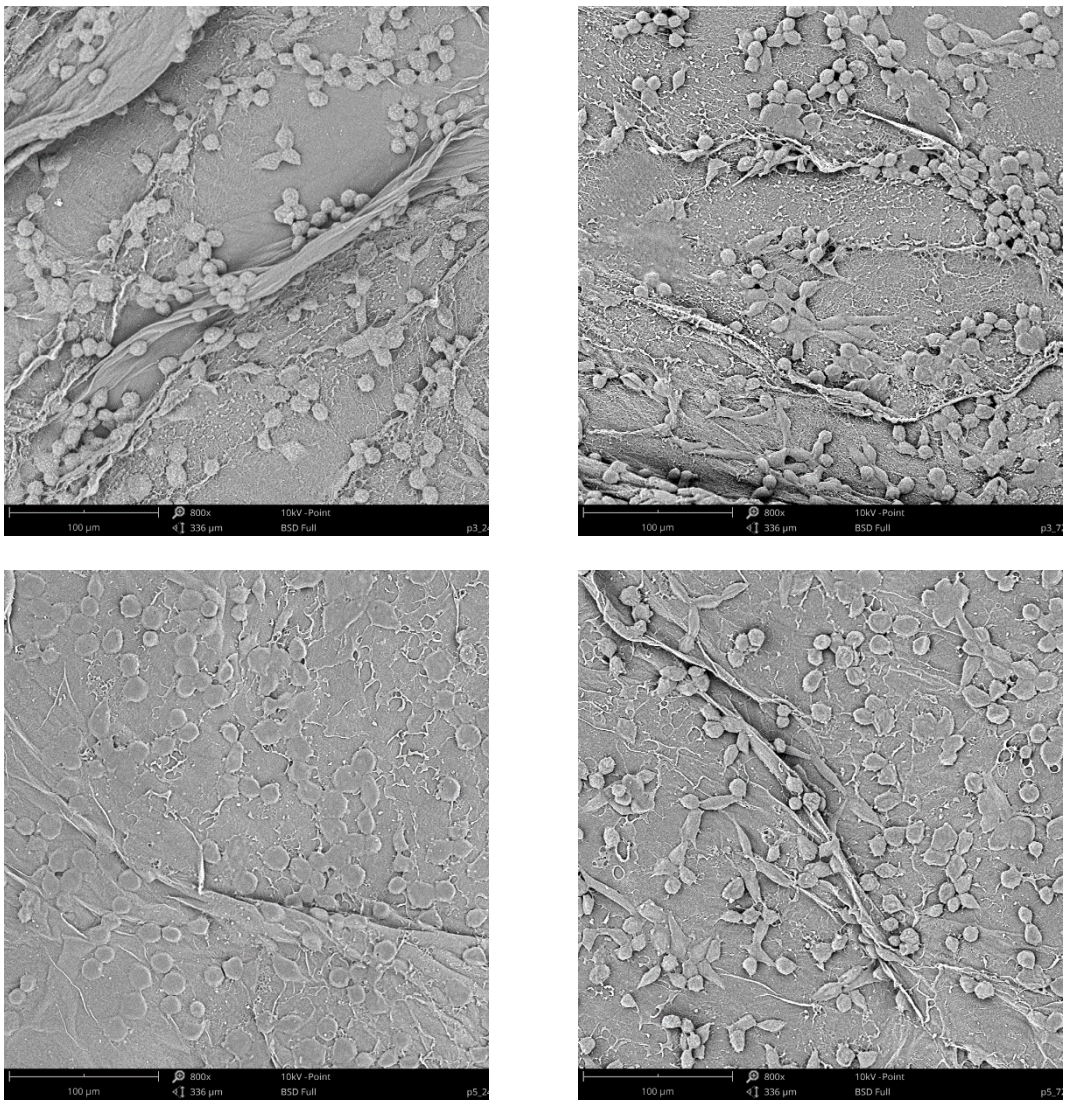

Figure 5.8. L929 morphology after 24h and 72h of incubation (Magnification: 800x).

In all the conditions, membranes exhibited a dense network where it was very hard to observe the individual cellulose fibers. Furthermore, it was possible to observe the presence of cells showing their adhesion on the biomaterial surface. The BC surface thus supports the adhesion of fibroblasts and enabled their proliferation. The *in vitro* adhesion of cells involves different phases: i) sedimentation where the initial attachment is related with the adherence of the round cell body to the surface; ii) cell attachment, where cells acquire flattened shape and spread onto the surface, increasing the contact area and iii) cell spreading and stable adhesion, where cells fully spread onto the surface through reorganization and distribution of the actin skeleton, to increase adhesion strength (28). Figure 5.8 showed that L929 cells were able to attach and spread on BC surfaces with and without surface

patterning. There was an increase on cell number in every surfaces along the time, being this increase difficult to compare in quantitative terms. Furthermore, the growing fibroblasts cells onto BC and BCL samples exhibited the typical cell morphology with usual spindle shape and spread covering the material surface (15,28–30). This behavior was more evident after 72h of culture since a higher number of elongated cells was present demonstrating that at 24h of culture, the cells were on the first stage of adhesion.

5.4 – Conclusions

This exploratory work intended to enhanced the properties of BC membranes for biomedical applications through its surface patterning using a CO_2 laser. Contrarily to other works where the BC producing bacteria were cultured on microstructured PDMS molds, yielding BC membranes with the desired topographical shape, in this work the patterns were designed directly on the BC membranes. In fact, it was possible to draw the pattern after BC production, but we had some difficulties on keeping those patterns upon drying. However, it is important to pattern the surface on wet membranes since the cell culture must be performed in this environment. This issue may be overcome by freezing the BC in liquid nitrogen. According to XPS and FTIR results, the use of laser technology did not chemically modify the BC chemistry and structure. The biocompatibility of the BC and BCL membranes were evaluated using mouse skin fibroblasts cells (L929). SEM results showed that fibroblasts were present both in BC and BCL membranes exhibiting the usual phenotype of these cells. Furthermore, the metabolic activity did not reveal significant differences between the pristine BC and the pattern surfaces, but seems to suggest a trend towards lower adhesion on the patterned surfaces, as expected taking in account other works. Further work is necessary to exploit the potential of this promising approach for the surface modification of BC membranes.

5.5 – References

1. Modulevsky DJ, Cuerrier CM, Pelling AE. Biocompatibility of Subcutaneously Implanted Plant-Derived Cellulose Biomaterials. PLoS One. 2016;11(6):e0157894.
2. Kurniawan H, Lai JT, Wang MJ. Biofunctionalized bacterial cellulose membranes by cold plasmas. Cellulose. 2012;19(6):1975–88.
3. Carvalho T, Guedes G, Sousa FL, Freire CSR, Santos HA. Latest Advances on Bacterial Cellulose-Based Materials for Wound Healing, Delivery Systems, and Tissue Engineering. Biotechnol J.

2019;14(12):1900059.

4. Hutchens SA, Benson RS, Evans BR, O'Neill HM, Rawn CJ. Biomimetic synthesis of calcium-deficient hydroxyapatite in a natural hydrogel. Biomaterials. 2006;27(26):4661–70.

5. Jung YL, Donahue HJ. Cell sensing and response to micro- and nanostructured surfaces produced by chemical and topographic patterning. Vol. 13, Tissue Engineering. Tissue Eng; 2007. p. 1879–91.

6. Tran KTM, Nguyen TD. Lithography-based methods to manufacture biomaterials at small scales. Vol. 2, Journal of Science: Advanced Materials and Devices. Elsevier B.V.; 2017. p. 1–14.

7. Jin M, Chen W, Li Z, Zhang Y, Zhang M, Chen S. Patterned bacterial cellulose wound dressing for hypertrophic scar inhibition behavior. Cellulose. 2018;25(11):6705–17.

8. Jing W, Chunxi Y, Yizao W, Honglin L, Fang H, Kerong D, et al. Laser Patterning of Bacterial Cellulose Hydrogel and its Modification With Gelatin and Hydroxyapatite for Bone Tissue Engineering.. 2013;11(2):173–80.

9. Xiong G, Luo H, Zhang C, Zhu Y, Wan Y. Enhanced biological behavior of bacterial cellulose scaffold by creation of macropores and surface immobilization of collagen. Macromol Res 2015 238. 2015;23(8):734–40.

10. Hu Y, Liu H, Zhou X, Pan H, Wu X, Abidi N, et al. Surface engineering of spongy bacterial cellulose via constructing crossed groove/column micropattern by low-energy CO2 laser photolithography toward scar-free wound healing. Mater Sci Eng C. 2019;99:333–43.

11. Szymańska-Chargot M, Cybulska J, Zdunek A. Sensing the structural differences in cellulose from apple and bacterial cell wall materials by Raman and FT-IR Spectroscopy. Vol. 11, Sensors. 2011 p. 5543–60.

12. Yamamoto H, Horii F, Hirai A. In situ crystallization of bacterial cellulose II. Influences of different polymeric additives on the formation of celluloses Iα and Iβ at the early stage of incubation. Cellulose. 1996;3(1):229–42.

13. Mosmann T. Rapid colorimetric assay for cellular growth and survival: Application to proliferation and cytotoxicity assays. J Immunol Methods. 1983;65(1–2):55–63.

14. Geisel N, Clasohm J, Shi X, Lamboni L, Yang J, Mattern K, et al. Microstructured Multilevel Bacterial Cellulose Allows the Guided Growth of Neural Stem Cells. Small. 2016;12(39):5407–

13.

15. Robotti F, Bottan S, Fraschetti F, Mallone A, Pellegrini G, Lindenblatt N, et al. A micron-scale surface topography design reducing cell adhesion to implanted materials. Sci Rep. 2018;8(1):10887.

16. Panaitescu DM, Vizireanu S, Nicolae CA, Frone AN, Casarica A, Carpen LG, et al. Treatment of nanocellulose by submerged liquid plasma for surface functionalization. Nanomaterials. 2018;8(7).

17. Wang Q, Xie D, Chen J, Liu G, Yu M. Superhydrophobic paper fabricated via nanostructured titanium dioxide-functionalized wood cellulose fibers. J Mater Sci. 2020;55(16):7084–94.

18. Li J, Wan Y, Li L, Liang H, Wang J. Preparation and characterization of 2,3-dialdehyde bacterial cellulose for potential biodegradable tissue engineering scaffolds. Mater Sci Eng C. 2009;29(5):1635–42.

19. Pertile RAN, Andrade FK, Alves C, Gama M. Surface modification of bacterial cellulose by nitrogen-containing plasma for improved interaction with cells. Carbohydr Polym. 2010;82(3):692–8.

20. Kuzmenko V, Wang N, Haque M, Naboka O, Flygare M, Svensson K, et al. Cellulose-derived carbon nanofibers/graphene composite electrodes for powerful compact supercapacitors. RSC Adv. 2017;7(73):45968–77.

21. do Nascimento ES, Pereira ALS, Barros M de O, Barroso MK de A, Lima HLS, Borges M de F, et al. TEMPO oxidation and high-speed blending as a combined approach to disassemble bacterial cellulose. Cellulose. 2019;26(4):2291–302.

22. Favi PM, Ospina SP, Kachole M, Gao M, Atehortua L, Webster TJ. Preparation and characterization of biodegradable nano hydroxyapatite–bacterial cellulose composites with well-defined honeycomb pore arrays for bone tissue engineering applications. Cellulose. 2016;23(2):1263–82.

23. Pacheco G, de Mello CV, Chiari-Andréo BG, Isaac VLB, Ribeiro SJL, Pecoraro É, et al. Bacterial cellulose skin masks—Properties and sensory tests. J Cosmet Dermatol. 2018;17(5):840–7.

24. Imai T, Sugiyama J. Nanodomains of Iα and Iβ cellulose in algal microfibrils. Macromolecules. 1998;31(18):6275–9.

25. Supian NNI, Zakaria J, Amin KNM, Mohamad S, Mohamad SFS. Effect of fermentation period on

bacterial cellulose production from oil palm frond (OPF) juice. IOP Conf Ser Mater Sci Eng. 2021;1092(1):012048.

26. van Zyl EM, Coburn JM. Hierarchical structure of bacterial-derived cellulose and its impact on biomedical applications. Curr Opin Chem Eng. 2019;24:122–30.

27. Chen S-Q, Mikkelsen D, Lopez-Sanchez P, Wang D, Martinez-Sanz M, Gilbert EP, et al. Characterisation of bacterial cellulose from diverse Komagataeibacter strains and their application to construct plant cell wall analogues. Cellul 2017 243. 2017;24(3):1211–26.

28. Kummala R, Soto Véliz D, Fang Z, Xu W, Abitbol T, Xu C, et al. Human Dermal Fibroblast Viability and Adhesion on Cellulose Nanomaterial Coatings: Influence of Surface Characteristics. Biomacromolecules. 2020;21(4):1560–7.

29. Chiaoprakobkij N, Sanchavanakit N, Subbalekha K, Pavasant P, Phisalaphong M. Characterization and biocompatibility of bacterial cellulose/alginate composite sponges with human keratinocytes and gingival fibroblasts. Carbohydr Polym. 2011;85(3):548–53.

30. Volova TG, Prudnikova S V., Sukovatyi AG, Shishatskaya EI. Production and properties of bacterial cellulose by the strain Komagataeibacter xylinus B-12068. Appl Microbiol Biotechnol. 2018;102(17):7417–28.

Chapter 6

Conclusions and Future Work

This last chapter presents an overview of the main achievements of the present thesis, as well as the general conclusions. Some suggestions are outlined for continuing the work with the aim of exploring the potential of BC in biomedical field.

CONCLUSIONS

BC is an excellent raw material with impressive intrinsic properties that make it suitable to be applied in several different fields. This doctoral project intended to explore some of the multiple BC applications on biomedical area.

Prior to studying possible biomedical applications of BC, the fermentation conditions and its influence on BC's properties were also evaluated. Both ATCC 53582 and ATCC700718 strains were tested, and two distinct culture media was used (HS and MOL). Furthermore, studying the influence of different types of culture was also aimed, namely of the static and agitated culture. In general, the obtained results revealed only slight differences between static and agitated conditions concerning to BC properties. However, it is important to mention that it seemed to occur a slight decrease on degree of polymerization and BC's crystallinity on agitated samples. The ATR-FTIR results showed that the chemical structure of obtained BC using both fermentation methods was comparable to those obtained for all the tested times of culture, since the mass fraction of Iα was higher and similar to all the obtained samples.

The first attempt to develop a BC-based medical device concerns mimicking Surgicel®, a bio-absorbable hemostatic material widely applied to prevent surgery-derived adhesions, while attempting to overcome the critical issues associated to this material. With this work, it was possible to produce oxidized BC membranes using electrochemical methods, with hemostatic properties and partially degradable. Both oxidized and non-oxidized BC were characterized by FTIR, NMR, SEM, XRD and their degree of polymerization was also determined. Both FTIR and NMR analysis allowed to conclude that the oxidation reaction occurred mainly at the surface layer of the cellulose fibers. According to XRD results, after oxidation, there was a slight decrease on crystallinity of around 4%, even for the samples with a higher oxidation degree (pristine BC had approximately 92% and oxidized BC had around 88%). Both *in vitro* degradability of the oxidized membranes and their hemostatic potential were evaluated using Surgicel® as a control. The obtained results demonstrated that the oxidized BC exhibited higher hemostatic activity than the pristine material, although not as effective as that of Surgicel®. *In vivo* assays aimed to evaluate the degradability of oxidized BC membranes and also its biocompatibility, through subcutaneous implantation of the membranes in the rat during 3, 14 and 56 days. The obtained results showed a highly biocompatible behavior, triggering only a mild inflammation process. Still, both oxidized and non-oxidized BC membranes were detected at the implantation site even after 56 days of culture.

Finally, the enhancement of the properties of BC membranes through its surface patterning using a CO_2 laser was attempted. Two distinct patterns were designed: parallel (=) and perpendicular lines (#). Two distances between lines being used in the former case: 0.1 and 0.2 mm. With the propose technique it was possible to pattern the surface on wet BC membranes, which is crucial since the cell culture is performed in this environment. Pristine BC and laser BC (BCL) were analyzed by XPS, ATR-FTIR, SEM and the fibroblasts adhesion to the surfaces was also assessed. Both XPS and ATR-FTIR analysis showed that the chemical structure of BC was maintained, even after laser treatment. Once again, BC and BCL surfaces showed good biocompatibility with no significant differences between them in what concerns metabolic activity of the cultivated cells. Also, SEM results displayed fibroblasts in both surfaces exhibiting its usual phenotype.

FUTURE WORK

The work carried out and discussed in the present dissertation focused on the important BC properties and its application on biomedical field. Considering all the results and conclusions drawn from this work, it will be interesting to further exploit the following topics:

- Undertaking a more comprehensively study the physical-chemical properties of BC obtained by different strains using different cultivation methods. The results suggest that slightly different DPs and crystallinities were found and, the assessment of porosity is another property that should be considered. The universe of strains and experimental conditions analyzed should be enlarged;
- Improving the electrochemical cell design in order to increase the dimension of the oxidized BC membrane; at the same time, attempting to develop ways to oxidized BC homogeneously, and not just superficially, potentially achieving a fully biodegradable membrane. This would also make possible to understand whether it is possible to obtain such material with suitable mechanical properties;
- Set different BC patterns more comprehensively characterized;
- To produce BC topographies that allow a better control of the interaction with cells, improving the *in vivo* biocompatibility, specially allowing a better control of the foreign body reaction.